Evaluation and Calibration of Pedestrian Bridge Standards for Vibration Serviceability

by

Pampa Dey

A thesis
presented to the University of Waterloo
in fulfillment of the
thesis requirement for the degree of
Doctor of Philospphy
in
Civil Engineering

Waterloo, Ontario, Canada, 2017

Examining Committee Membership

The following served on the Examining Committee for this thesis. The decision of the Examining Committee is by majority vote.

External Examiner:	Mustafa Gul Associate professor, Dept. of Civil and Environmental Engg., University of Alberta
Supervisor(s):	Sriram Narasimhan Associate professor, Dept. of Civil and Environmental Engg., University of Waterloo Scott Walbridge Associate professor, Dept. of Civil and Environmental Engg., University of Waterloo
Internal Member:	Giovanni Cascante Professor, Dept. of Civil and Environmental Engg., University of Waterloo Mahesh Pandey Professor, Dept. of Civil and Environmental Engg., University of Waterloo
Internal-External Member:	Stephen D. Prentice Associate professor, Dept. of Kinesiology, University of Waterloo

I hereby declare that I am the sole author of this thesis. This is a true copy of the thesis, including any required final revisions, as accepted by my examiners.

I understand that my thesis may be made electronically available to the public.

Abstract

An increase in the use of lightweight materials and emphasis on architecturally appealing designs has resulted in lively pedestrian bridges. A prominent example for this is the serviceability failure of the London Millenium Bridge in 2001, where excessive vibrations from inauguration crowds resulted in shutting down the structure. While the bridge was subsequently retrofitted with damping devices, this incident brought often overlooked and poorly understood issues on pedestrian bridges to the fore. Various load models and design procedures have since been proposed to assess the serviceability of pedestrian bridges under walking-induced loads, load modelling being the one that has attracted the most attention in the recent years. In general, all of the existing design provisions employ a Fourier series approach to modelling the foot-fall force due to a single pedestrian and extrapolate this to groups through multiplication factors. Despite two decades of use, there are significant discrepancies amongst the provisions and little has been done in terms of evaluating them, especially using experimental data.

The main objectives of this thesis are two-fold: first, a comprehensive evaluation of existing standards is undertaken to understand the performance of the existing design provisions in predicting the actual performance of lively pedestrian bridges; next, changes are recommended based on such experiments to key factors used in the provisions to better align the observations with the predictions. In the current study, design provisions currently being used in North America and Europe are evaluated, including ISO 10137, Eurocode 5, the British National Annex to Eurocode 1, and SÉTRA. The experimental program was undertaken on three full-scale aluminum pedestrian bridges; one in the field and two in the laboratory. Aluminum structures provide a high strength-to-weight ratio, are corrosion resistant, and aesthetically pleasing. Due to their relative light weight, they can be built in a laboratory environment to full-scale and still produce lively structures that can be excited with relatively lower actuation compared to comparable steel or concrete structures. The current experimental study focuses on such cases where there is the possibility of resonance with the higher harmonics of the walking frequency, not just the fundamental frequency. The test bridges were instrumented and subjected to a range of modal and pedestrian walking tests of varying traffic sizes. The comparison results between the predicted and measured responses show that commonly employed load models for single pedestrian walking can sometimes be un-conservative. Moreover, the outcomes from the serviceability assessment under crowd-induced loading show significant differences in the predicted responses by the guidelines with respect to the measurements, which are mainly attributable to differences in the dynamic load factors adopted in the guidelines, and lack of guidance on the appropriate walking speeds in crowd loading conditions and the factor

scaling the individual pedestrian load to multiple pedestrians. Additionally, the guidelines are evaluated in a reliability-based framework to incorporate the potential uncertainties associated with the walking loads, structural properties, and occupant comfort limits. The key results point towards calibrating the current design provisions to a higher reliability index for the design events in order to achieve sufficiency during the non-frequent or rare loading events.

Hence, an attempt is made towards to improving the predictions by the guidelines. Several recommendations are proposed to harmonize the design provisions with each other and with measurements. The recommended modifications lead to a substantial improvement in the predicted responses by the guidelines. In the next step, the design provisions are calibrated for higher reliability to achieve acceptable performance during the design as well as non-frequent (rare) heavy traffic loading events. For this purpose, the reliability level required for the calibration process is estimated and corresponding partial factors for the calibrated design are reported. The study also suggests adopting comfort limits based on the frequency of occurrence of the traffic event and the pedestrian bridge class in order to yield economic designs.

Acknowledgements

I would like to take this opportunity to express my sincere gratitude to all those who have provided me with guidance and support in various ways through my journey as a Doctoral student.

First and foremost, I would like to express my deepest gratitude to my advisors, Dr. Sriram Narasimhan and Dr. Scott Walbridge for giving me the chance to pursue my Doctoral studies. Both have been great mentors and instilled confidence in me throughout my PhD candidature by providing the perfect balance of independence and guidance in my research. I am grateful to Dr. Mustafa Gul, Dr. Stephen Prentice, Dr. Giovanni Cascante, Dr. Mahesh Pandey, and Dr. Dipanjan Basu for serving as my committee members and their time in reviewing my work.

I want to thank Dr. Stephen Prentice for allowing me to use their Biomechanics laboratory to perform walking force measurements. I have also been fortunate to have Dr. Arndt Goldack from TU Berlin visiting University of Waterloo during the course of the experimental studies. His insights during the experimental work have played a significant role in improving some aspects of the laboratory bridge specimen.

I would also like to take this opportunity to acknowledge the Most Advanced Aluminium Design and Inspection (MAADI) Group and the Aluminium Association of Canada for supporting us with the experimental set-up, including the full scale Make-A-Bridge aluminium pedestrian bridge lab specimen.

I would like to say a big Thank You to Ann Sychterz for her collaboration on the experimental studies. I want to extend my sincere gratitude to the technicians of the Structures laboratory, Richard Morrison, Michael Burgetz and Rob Sluban, for their help and support in building the bridges and designing instrumentation, which has been very monumental for my thesis. I am also thankful to all the volunteers and undergraduate research assistants who were part of the walking tests on the laboratory bridge specimens, with my special acknowledgment to Kevin, Rajdip, Rakesh, Guru, Roya, Stan, Shilpa, Ben, Amr, Laura, and Melissa.

Any attempt to thank my parents, sisters and brother-in-law: Baba, Ma, Didi, Jiju, and Mithu, would fall short. Their love, support, and encouragement have been my primary motivation. Last but not least, I owe my deepest gratitude to my dear husband Satya for being by my side throughout the roller coaster journey. Your unconditional love and trust has always been a source of support and encouragement to continue my passion.

Dedication

To Baba, Ma, Didi, Jiju, Mithu, and Satya

Table of Contents

List of Tables

List of Figures

Chapter 1

Introduction

1.1 General Introduction

Structural designs are traditionally governed by their strength or load carrying capacity, which is known as the ultimate limit state design (ULS). However, recent design trends towards high-strength and light-weight construction materials, especially in pedestrian bridges, have made them more susceptible to vibration serviceability problems under walking service loads. Furthermore, compared to ULS failure events, serviceability failures occur more frequently. While the cost of individual serviceability failure events can be less, the cumulative economic impact of serviceability failures can be significant. Previous surveys have shown that considerable costs can be incurred due to serviceability failures, rather than strength, and thus serviceability issues cannot be underestimated (Stewart, 1996). Therefore, vibration serviceability has become a dominant criterion in structural design over the last two decades (Allen and Murray, 1993; Willford et al., 2006) and has since been increasingly the focus of researchers worldwide.

Issues related to vibration serviceability of structures under human activities have been identified since the 19^{th} century (Tredgold, 1890). However, the possibility of resonance has been ignored in their design until recently. Pedestrian bridges (PBs) are prone to vibrations due to one or more natural frequencies falling within the range of typical human activities such as walking, running, bouncing or jumping. Among all these activities, walking is the most frequently occurring one and thus is the primary source of excitation in PBs. Some of the well publicized incidents of serviceability failures of PBs under walking-induced excitations include the London Millennium bridge (Dallard et al., 2001), the Pont du Solferino in Paris (Danbon and Grillaud, 2005) and the T-Bridge in Japan (Fujino et al.,

1993). These bridges experienced large amplitude vibrations due to the resonance between the structural vibration modes and the periodicity of pedestrian walking forces. These high profile incidents have prompted investigation into the behaviour of low-frequency bridges under crowd loading conditions and a large volume of research activity aimed at investigating vibration serviceability design in guidelines and standards has since taken place, and continuing to take place. Despite this volume of activity, there still exists considerable uncertainty regarding how to reliably quantify force due to walking, and to properly verify and calibrate load models using experimental observations.

Early research into quantifying the vibration response of PBs for design purposes dates back to the seventies, starting with the seminal work of Blanchard et al. (1977) to develop design guidelines for the assessment of human-induced vertical vibrations of PBs. His work was later incorporated into several international bridge design codes such as the BS 5400 (BS 5400, 1978) and the Canadian Highway Bridge Design Code (CAN/CSA S6, 2011). These design codes are based on the forces induced by a single pedestrian under resonant conditions. Although the effect of pedestrian crowds on PBs was studied at that time (Matsumoto et al., 1978; Wheeler, 1982), only a simplified single pedestrian load scenario was incorporated into the aforementioned standards. More recently, vibration assessment of PBs has advanced from the deterministic approach towards a more comprehensive probabilistic approach focused on groups of pedestrians characterized by probability distributions of arrival time, pacing frequency, step length, and force magnitude (Živanović, 2006; Butz, 2008; Pedersen and Frier, 2010; Racic and Brownjohn, 2011). These concepts have been incorporated into some guidelines (EN 1995-2, 2004; NA to BS EN 1991-2, 2003; SÉTRA, 2006; HIVOSS, 2008; FIB, 2005), by allowing to estimate the structural response due to crowds of different densities using the resonant response obtained from a single pedestrian. However, the Canadian, AASHTO LRFD and Australian standards (CAN/CSA S6, 2011; AASHTHO LRFD, 2007; AS 5100, 2004) still lag behind considerably, especially in dealing with crowd loading in both the lateral and vertical directions.

There exist very few studies that evaluate the current guidelines (referred to collectively as guidelines) for lightweight bridges under pedestrian induced loads in any systematic fashion (Roos, 2009; Van Nimmen et al., 2014; Salgado et al., 2014; Živanović et al., 2010). While Salgado et al. (2014) compared the measured and predicted responses using various guidelines under single-pedestrian walking loads, Živanović et al. (2010) performed a comparison between the existing design procedures based on experiments on two full-scale bridges under groups of pedestrians. All of these comparison studies conducted so far are based on low frequency PBs with vibration modes near the first harmonic of walking frequency. However, lightweight PBs, such as aluminum PBs, results in relatively high-frequency structures, i.e. their fundamental frequency is outside the range of nor-

mal walking frequency. Hence, they have thus far not attracted much attention in the literature. However, their relative light weight and low intrinsic damping often results in resonance with the higher harmonics of walking frequency and not with the first harmonic, which could lead to significant serviceability issues. Evaluation and comparison of design provisions for such lightweight PBs with the potential risk of resonance with the higher harmonics of walking frequencies, is lacking. On the other hand, none of these guidelines have been evaluated in a reliability-based framework incorporating uncertainties arising from pedestrian loads, the structure, and comfort limits for the pedestrians. Moreover, despite significant disagreement observed between measurements and predictions by the design guidelines in resonance (mostly with the first harmonics of walking frequency), no attempts have been made yet to better align observations with predictions by the guidelines, at the same time ensuring reliable and economical designs. Hence, the main motivation for this work is to evaluate, and subsequently improve the existing vibration serviceability design guidelines using extensive experimental tests on full-scale pedestrian bridges.

1.2 Objectives of the research

The overarching objectives of the proposed research are summarized as follows:

- Evaluate the most popular design guidelines in both deterministic and reliability-based frameworks in predicting the performance of lively pedestrian bridges under walking-induced excitations through experimental study conducted on full-scale pedestrian bridges that resonate with the higher harmonics of walking frequency.
- Improve the vibration serviceability design provisions for PBs, in order to ensure more reliable and economical designs, at the same time reconciling the inconsistencies within the existing guidelines and between the guidelines and the observations.

1.3 Organization of the thesis

The thesis contains 6 chapters and is organized as follows:

- **Chapter 1** provides a brief introduction to the problem of vibration serviceability evaluation of pedestrian bridges and a summary of research objectives.

- A detailed background on the widely used pedestrian load models is presented in **Chapter 2**. First, the conventional deterministic periodic load model is reviewed, followed by the probabilistic and biomechanical load models. Crowd-induced excitation and resulting structural response is also discussed. Next, the existing design guidelines for serviceability assessment of PBs are briefly reviewed along with the methodology to estimate the structural response through the design load models.

- **Chapter 3** presents the experimental program involving full-scale aluminum PBs, both in the field and laboratory, with a brief description of the structures followed by the instrumentation used and the test matrix. The performance of the periodic load model in predicting the response of PBs in the vertical direction is assessed through measurements, followed by evaluating the existing design provisions in predicting the serviceability of these pedestrian bridges under crowd-induced excitation.

- **Chapter 4** presents an overview of all possible sources of uncertainties in the design equations by the existing guidelines, followed by evaluation of the design provisions for sufficient and uniform reliability under all possible traffic conditions in the design life of the structure.

- **Chapter 5** demonstrates key design recommendations proposed in order to reconcile the design guidelines with measurements. Moreover, the design provisions are calibrated in order to achieve sufficient reliability under all possible traffic conditions on the bridge.

- Finally, a number of conclusions resulting from the presented work are discussed in **Chapter 6**. Several recommendations for future study are also discussed, followed by a summary of the significant contributions of the current work.

Chapter 2

Background

A review of the background on the walking load models is presented first, including the time-domain periodic load model and current trends using the biomechanics principles of walking. Existing design guidelines in the context of serviceability assessment of PBs under walking-induced excitation are then reviewed, followed by a methodology to predict the bridge responses. Finally, a brief review on the full-scale studies of PBs under pedestrian-induced walking loads is presented.

2.1 Pedestrian-induced walking loads

2.1.1 Basics of walking

According to Whittle (2003), normal human walking is the gait used by humans when they walk at low speeds. A complete gait cycle is the time period between two identical events during the walking process, and consists of two phases: stance and swing (Perry, 1992). Alternatively, a complete gait cycle can also be represented by right and left steps. An illustration for a complete gait cycle is shown in Figure 2.1. The stance phase refers to the period during which the foot is in contact with the ground while the swing phase refers to the period when the foot is off the ground. The stance phase starts with the heel striking the ground, known as initial contact, and ends with the toe off the ground. At the same time, the human body passes through two stages during the walking process, the double- and the single-support stages. In the double-support stage, both feet are in contact with the ground, while single-support occurs with the contact of only one leg. In

general, a walking process is described through temporal and spatial parameters. While walking speed, pacing rate or walking frequency, and the gait cycle time are typically the temporal parameters, spatial parameters are step length, step width, and stride length.

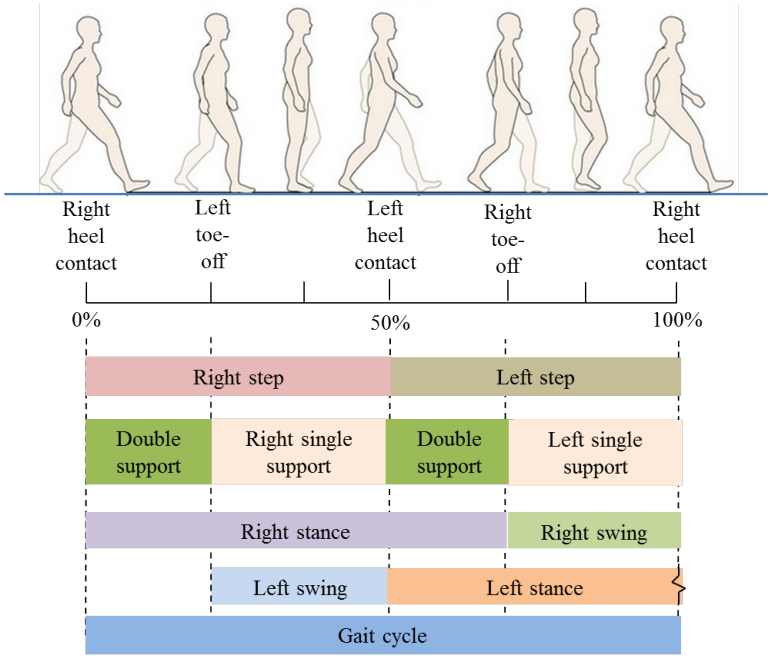

Figure 2.1: Schematic diagram of a complete gait cycle during normal walking (reproduced from Simoneau (2002))

During walking, the acceleration and deceleration movement of body's centre of mass (COM) generates ground reaction forces (GRF), which transfer to the ground through contact of each foot during the stance phase of gait. The principal directions of GRFs are vertical, lateral, and longitudinal. Of these the vertical and lateral are of primary interest for the vibration study of PBs. In Figure 2.2, a typical GRF of a person weighing 65 kg as projected onto vertical and lateral directions is shown, both for a single step (left and right leg) as well as for continuous walking, alongside their Fourier spectra. The GRF measurements were collected by the author from force plates at the Biomechanical Laboratory at the University of Waterloo.

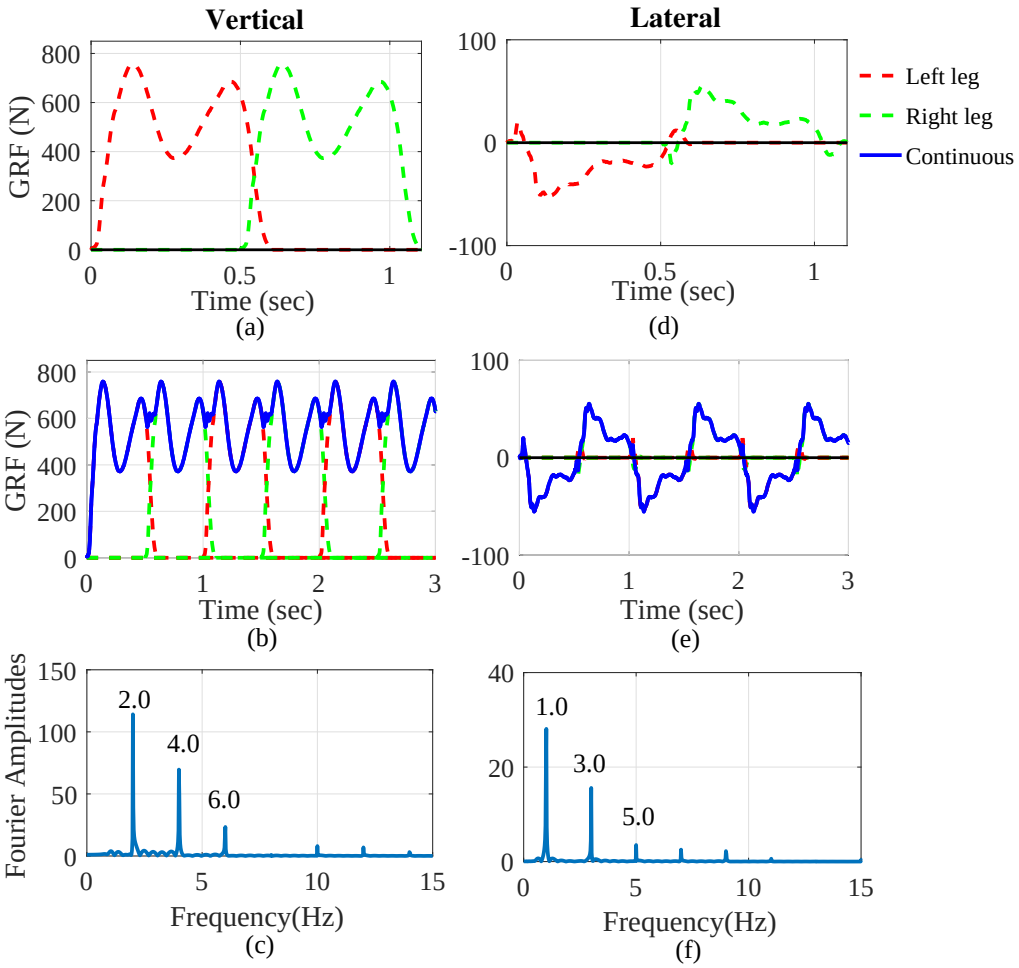

Figure 2.2: (a) GRF of a single step in the vertical direction; (b) GRF for continuous walking in the vertical direction; (c) Fourier spectrum of the GRF in the vertical direction; (d) GRF of a single step in the lateral direction; (e) GRF for continuous walking in the lateral direction, and (f) Fourier spectrum of the GRF in the lateral direction, by a person walking at 2 Hz

2.1.2 Walking force measurements

There have been numerous attempts to measure the GRFs induced by a single pedestrian. Gait cycle tests have been performed on several types of surfaces, including transducer-equipped floor surface or short walkways (Blanchard et al., 1977; Rainer et al., 1988) and instrumented treadmills (Dierick et al., 2004; Riley et al., 2007). One of the earliest measurements of walking forces from a single step was conducted by Elftman (1938) using a force plate. Following this work, several single-step measurements were carried out by other researchers (Harper, 1962; Galbraith and Barton, 1970; Wheeler, 1982; Kerr, 1998) using force plates. However, as the forces from two steps are not always identical, extending single step force measurements may not be a correct representation of continuous walking forces. Hence, more advanced measurements of continuous walking forces comprising several consecutive steps were carried out by several researchers. While Blanchard et al. (1977) designed a "gait machine" to continuously measure walking forces, Rainer et al. (1988) employed a floor strip with known dynamic properties to measure GRFs from consecutive steps. Subsequently, several researchers (Ebrahimpour et al., 1994; Gard et al., 2004) utilized short instrumented walkways with multiple force plates to capture forces from several steps. In all these studies, it was observed that the measured time histories were approximately periodic. However, there are some associated downsides of using floor-mounted force plates for measurement of GRFs. Force plate measurements are usually time consuming and require mounting multiple force plates on walkways or floors. Moreover, deliberately targeting the force plates while walking trials can alter the natural walking pattern (Perry, 1992).

In order to overcome the shortcomings from force plate measurements, instrumented treadmills have been used for quick collection of continuous GRFs over a wide range of steady-state gait speeds (Dierick et al., 2004). Recently, Riley et al. (2007) conducted a series of experiments on an advanced treadmill system and compared the two modes of measurements of walking forces (force plates and treadmill). They concluded that treadmill gait is qualitatively and quantitatively very similar to that through measurements from force plates or transducer-equipped surfaces. Among instrumented treadmill studies, Brownjohn et al. (2004b) conducted one of the first treadmill tests for measuring continuous walking forces, in the civil engineering context. Their work reported the effect of random imperfections in human walking on the structural response. More recent work on characterizing the randomness in the gait parameters data was presented by Pachi and Ji (2005) and Sahnaci and Kasperski (2005). However, a sufficiently large database of GRFs for statistically reliable application of human-induced forces in a civil engineering context with continuously recorded time series for single and multiple pedestrians walking over

both rigid and perceptibly moving surfaces, is still lacking. Recently there is a growing trend in monitoring pedestrian behaviour from a bio-mechanical standpoint using novel technologies such as the motion capture technology (Racic et al., 2008; Zheng et al., 2016) for civil engineering applications. However, there is still a great deal of research needed towards understanding human-induced walking forces on civil engineering structures.

2.1.3 Walking load models

Modelling of human-induced walking forces is challenging due to high inter- and intra-subject variabilities. As a result, the dynamic walking force induced by an individual is a random process and thus difficult to characterize precisely. Nevertheless, numerous attempts have been made towards modelling walking forces induced by a single person by employing simplifying assumptions. Conventionally, walking forces are modelled either in the time or the frequency domain, the time-domain load models being the favourite choice for design guidelines. Hence, the current background study is focused on the time-domain load models. Generally, two classes of time-domain models have been proposed in the literature: deterministic (Blanchard et al., 1977; Bachmann and Ammann, 1987; Rainer et al., 1988; Young, 2001; SÉTRA, 2006) and probabilistic (Brownjohn et al., 2004b; Živanović et al., 2007). The deterministic type has focused on establishing one general force model for each type of human activity without directly considering variability. On the other hand, probabilistic models take into account the random nature of of walking and hence the human activity force. In the following sections, the time-domain force models are presented in detail.

The deterministic load model

The deterministic force model is based on the assumption that walking is perfectly periodic and both legs produce identical forces. The continuous walking force of a pedestrian in the vertical and lateral directions are shown in Figures 2.2 (b) and (e) for a person walking at 2 Hz step frequency. As seen from the Fourier spectrum of the vertical GRF in Figure 2.2(c), the vertical force contains significant contributions from even harmonics corresponding to step frequency of 2 Hz i.e., 2 Hz, 4 Hz, 6 Hz and so on. In the lateral direction, Figure 2.2(f) shows the contribution from the odd harmonics of lateral step frequency of 1 Hz, i.e., 1 Hz, 3 Hz, 5 Hz and so on. The continuous walking forces in the vertical and lateral directions are represented using the following Fourier series expansion of a periodic force

(Blanchard et al., 1977):

$$P(t) = \begin{cases} G + \sum_{i=1}^{n} G\alpha_{v,i} \sin(i2\pi f_s t + \phi_{v,i})) \\ \sum_{i=1}^{n} G\alpha_{l,i} \sin(i2\pi t \frac{f_s}{2} + \phi_{l,i})) \end{cases} \tag{2.1}$$

where, $P(t)$ is the human-induced continuous ground reaction force, G is the pedestrian weight, $\alpha_{v,i}$ and $\alpha_{l,i}$ are the dynamic load factors (DLF) of the i^{th} harmonic in the vertical (v) and lateral (l) directions respectively, and f_s is the pedestrian step-frequency (Hz). $\phi_{v,i}$ and $\phi_{l,i}$ are the phases of the i^{th} harmonic in the respective directions.

Over time, many researchers have attempted to quantify DLFs based on direct or indirect force measurements. The earliest work on this aspect was by Blanchard et al. (1977). The authors proposed a model with one harmonic term in Equation 2.1 for the vertical direction, with the DLF of value 0.257 based on a resonant condition assuming a pedestrian of weight G equal to 700N. This work is extensively used by the Canadian Highway Bridge code (CAN/CSA S6, 2011) and the British Standard (BS 5400, 1978) to design PBs. Their model considered that resonance would occur in the first vibration mode due to the first harmonic of the dynamic load. This DLF was applied to PBs with vertical frequencies upto 4 Hz, and reduction factors were applied to this value for bridges with frequencies in the range of 4 Hz to 5 Hz. Later on, Bachmann and Ammann (1987) proposed five and two harmonics, respectively, to model the vertical and lateral walking forces. They proposed DLF values for the first harmonic of the vertical force ranging between 0.4 at frequency 2.0 Hz and 0.5 at 2.4 Hz, with linear interpolation for other frequencies within this range. They also suggested identical DLFs for the second and third harmonics equal to 0.1, for step frequencies near 2 Hz. They proposed a DLF value of 0.1 for the first two harmonics in the lateral direction. In 1988, Rainer et al. (1988) confirmed the strong dependency of DLFs on the walking frequency based on measured continuous forces for a single pedestrian. They proposed values for the first four DLFs as shown in Figure 2.3. However, this work lacked statistical reliability due to the limited number of test subjects and trials. Kerr Kerr (1998) attempted to overcome these shortcomings and proposed similar values for DLF based on 1000 force measurements on 40 test subjects.Following these works, Young (2001) proposed statistical mean values for DLFs for the four harmonics of the vertical force as a function of the walking frequency f_s as follows:

$$\begin{aligned} \alpha_1 &= 0.37(f_s - 0.95) \leq 0.5 \\ \alpha_2 &= 0.054 + 0.0044 f_s \\ \alpha_3 &= 0.026 + 0.0050 f_s \\ \alpha_4 &= 0.010 + 0.0051 f_s \\ \phi_i &= 0 \end{aligned} \tag{2.2}$$

where, α_1 to α_4 are the first four harmonics and ϕ_i is the phase for the ith harmonic. This is the first work where the stochastic behaviour of human walking has been taken into account in the estimation of DLFs. A brief outline of these efforts in estimating the values of DLF values is presented in Table 2.1 and Figure 2.4.

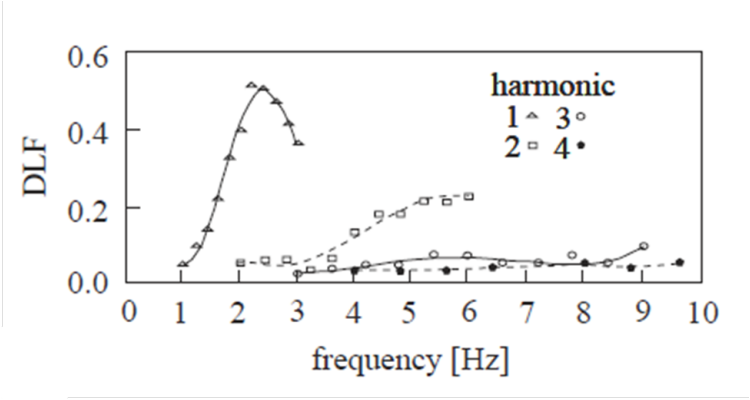

Figure 2.3: Dynamic load factors (DLFs) for first four harmonics of walking (taken from Rainer et al. (1988))

It should be stressed that the DLFs were obtained by direct or indirect force measurements on rigid surfaces. However, in the context of civil engineering applications, the flexibility of the walking surface has impact on the walking force and hence the DLF values. Pimentel (1997) found from measurements of structural responses on two full-scale PBs that the first and second resonant vertical harmonics were lower than those given in literature, which was probably due to human-structure interaction. It should also be stressed that all of the aforementioned studies deal with a single pedestrian. It is impractical to measure the walking-induced loads for groups of people through the experimental set-ups used. Very few studies on quantifying the effect of crowd on the DLF values exist in the literature. Ellis (2003) found through the measured structural responses on a floor under a group of pedestrians that DLF values decrease as the size of the group increases. Pernica (1990) also reported similar phenomena. These studies point towards imperfect synchronization within the group leading to a dynamic decrease in the DLF values. The effect of multiple pedestrians or crowd and corresponding synchronization phenomena are discussed later on.

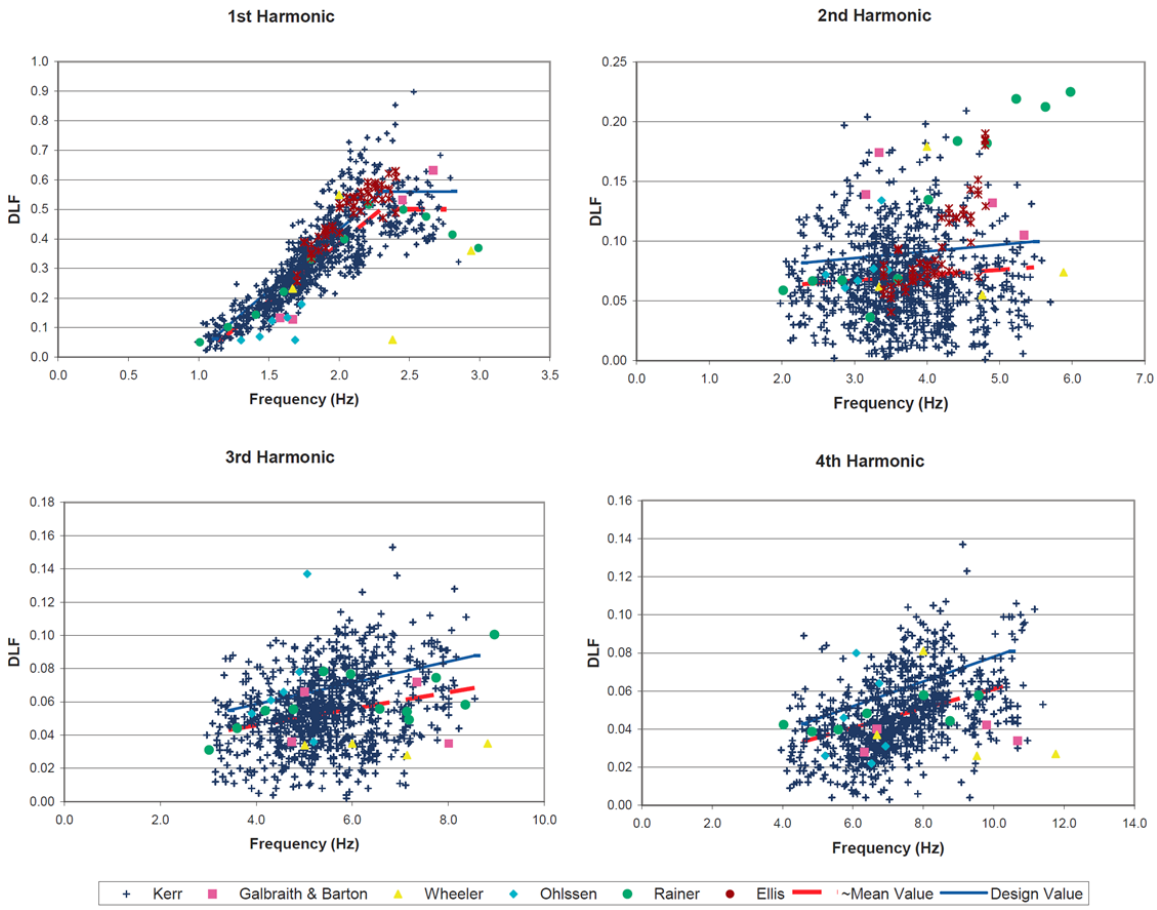

Figure 2.4: Dynamic load factors (DLFs) reported in the literature (taken from Willford et al. (2006))

Table 2.1: Summary of proposed DLF values reported in the literature

Researchers	DLF	Direction	Step frequency (Hz)
Blanchard et al. (1977)	$\alpha_1 = 0.257$	Vertical	< 4
Bachmann and Ammann (1987)	$\alpha_1 = 0.4 - 0.5$, $\alpha_2 = \alpha_3 = 0.1$	Vertical	$2.0 - 2.4$
Schulze (1980) (after Bachmann and Ammann (1987))	$\alpha_1 = 0.37$,$\alpha_2 = 0.10$, $\alpha_3 = 0.12$, $\alpha_4 = 0.04$, $\alpha_5 = 0.08$	Vertical	2.0
	$\alpha_1 = 0.039$, $\alpha_2 = 0.010$, $\alpha_3 = 0.043$, $\alpha_4 = 0.012$, $\alpha_5 = 0.015$	Lateral	
Rainer et al. (1988)	Figure 2.3	Vertical	
Allen and Murray (1993)	$\alpha_1 = 0.50$, $\alpha_2 = 0.20$, $\alpha_3 = 0.10$, $\alpha_4 = 0.05$	Vertical	$1.6 - 2.4$
Bachmann et al. (1995)	$\alpha_1 = 0.4/0.5$, $\alpha_2 = 0.10$		2.0
	$\alpha_3 = 0.10$	Vertical	2.0
	$\alpha_1 = 0.10$	Lateral	
Kerr (1998)	α_1 in Figure 2.4	Vertical	
	$\alpha_2 = 0.07$, $\alpha_2 = 0.10$		
Young (2001)	Equation 2.2	Vertical	$1 - 2.8$

Probabilistic descriptions for load model parameters

It is unlikely for a person to produce exactly the same walking force in repeated trials, which is known as intra-subject variability. This is even more unlikely for multiple persons, which is known as inter-subject variability. Therefore a probability based approach to model walking force is more appropriate than a deterministic approach. Uncertainties can be incorporated into the periodic load model in Equation 2.1 through probability distributions for force amplitude, time-frequency parameters of walking and time delay between several persons walking. This section reviews the existing probability distributions for step frequency, walking velocity and step length.

The work by Matsumoto et al. (1978) was the earliest one to report the statistics of step frequencies based on a sample of 505 persons walking at self-selected speeds. They recommended a normal distribution for step frequency with a mean and standard deviation of 1.99 Hz and 0.173 Hz, respectively. Later on, similar research towards estimating

the statistics of step frequencies yielded varying statistics, as listed in Table 2.2 (Kramer and Kebe, 1980; Kerr, 1998; Pachi and Ji, 2005; Živanović, 2006; Kasperski and Sahnaci, 2007). Figure 2.5 shows the normal density function proposed by different authors for step frequency. Živanović (2006) explained these discrepancies arising due to a wide ranging factors including gender. In their work, Pachi and Ji (2005) found a linear relationship between walking speed and step frequency from 800 measurements for 100 men and 100 women:

$$v = L_s f_s \tag{2.3}$$

where v is the walking speed of the person, f_s is the step frequency and L_s is the average step length of 0.71 m. Based on the data collected by Pachi and Ji (2005), Živanović (2006) showed that the walking velocities follow normal distribution at a specific frequency of walking as shown in Figure 2.6. In the study by Živanović et al. (2007), the step length of the people crossing the bridge was also measured and found to be normally distributed with a mean value of 0.71 m and a standard deviation of 0.071 m. Furthermore, they found that the step length was independent of step frequency, which is contrary to one of the earliest findings by Wheeler (1982) on the correlation between step length and frequency. In order to investigate the relationship between walking parameters such as speed, step length, and stance period, a comprehensive biomechanical study by taking gender into consideration was undertaken by Yamasaki et al. (1991). They reported a nonlinear relationship between walking speed and step length, which adds to the confusion from previous studies.

Table 2.2: Statistics os step frequency by different researchers

Authors	Mean (Hz)	Standard Deviation (Hz)
Matsumoto et al. (1978)	1.99	0.173
Kerr (1998)	1.9	—
Kramer and Kebe (1980)	2.2	0.3
Pachi and Ji (2005)	1.8	0.13
Živanović (2006)	1.87	0.186
Kasperski and Sahnaci (2007)	1.82	0.12

Besides the time-frequency parameters for walking, force amplitude is also another important parameter to model. When modelling the human walking force in the time-domain, the force amplitude ($G\alpha_m$) is usually defined as the portion of pedestrian's weight i.e., product of dynamic load factor (DLF or α_m) and pedestrian's body weight (G). Generally, the weight of the pedestrian is treated as a random variable. Wheeler (1982) assumed

a distribution of weights obtained for the Australian population. In their probabilistic modeling framework, Živanović et al. (2007) did not consider any uncertainties from G. Later on, Pedersen (2012) conducted a parametric study to investigate the sensitivity of the 95^{th} percentile response of a bridge to a stochastic model of pedestrian weight. They reported that the response is not very sensitive to whether a stochastic or deterministic model is assumed for G, however, it is sensitive to the mean value of the weight used.

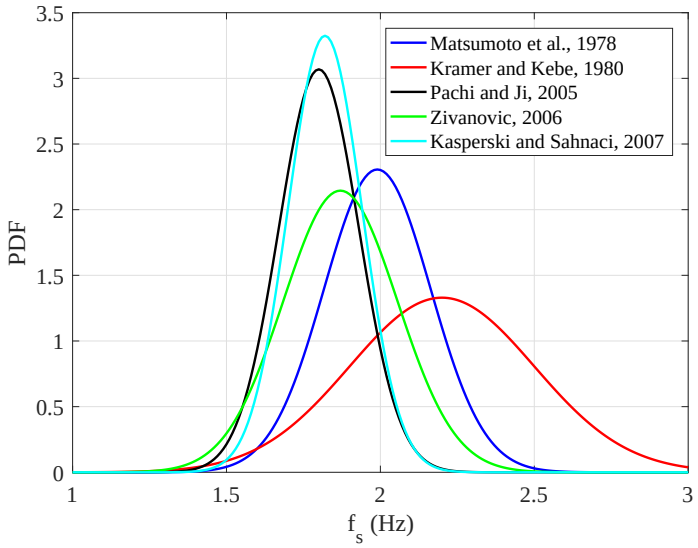

Figure 2.5: Distribution of step frequency for normal walking

Apart from the weight of pedestrian, significant scatter is also found in the DLF values. The most extensive research to statistically characterize the DLF was conducted by Kerr Kerr (1998). From 1000 force records on 40 test subjects, the mean DLF for the first harmonic as a function of step frequency is given by:

$$\mu_\alpha = -0.2649 f_s^3 + 1.3206 f_s^2 - 1.7597 f_s + 0.7613 \tag{2.4}$$

Under the assumption that the DLFs are normally distributed around their mean value (for a certain walking frequency), the COV was found to be 0.16 (Živanović, 2006). Kerr observed large scatter in the DLF values corresponding to higher harmonics, with a COV of 0.40. Galbraith and Barton (1970) showed an interdependence between G and α_m, however, they could not quantify this dependency and assumed that the two variables are independent.

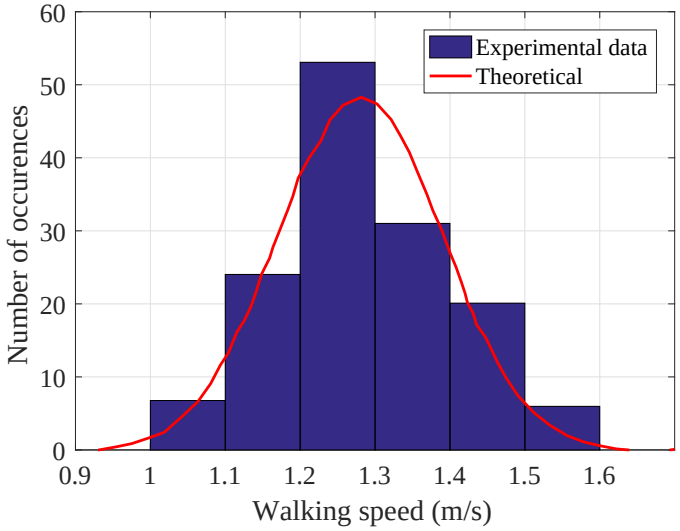

Figure 2.6: Distribution of walking speeds at 1.8 Hz (reproduced from Živanović (2006))

These probability density functions of the loading parameters can be used in a probability-based framework to predict a certain level of vibration response. The work by Ebrahimpour et al. (1996) was one of the earliest to include this randomness into modelling forces. They included the probability distribution function of the time delay between several pedestrians and determined the DLF for the first harmonic under groups of pedestrians. However, they did not provide a comprehensive force model that can be used to predict the structural response. The first work on estimating the vertical response of a PB through incorporating the probability density functions of the loading parameters in a novel probabilistic framework was proposed by Živanović (2006). However, the methodology is only limited to a single harmonic. Later on, Živanović et al. (2007) extended this probability-based model to cover not only the main harmonics of the walking force, but also the sub-harmonics, which appear in the frequency domain. A more advanced stochastic load model in the vertical direction was proposed by Racic and Brownjohn (2011) through a comprehensive database of measured continuous vertical walking loads from an instrumented treadmill. Their procedure can simulate random walking force signal from a given step frequency and walking period.

Although the probabilistic framework incorporates the intra-and inter-subject variabilities in walking forces, the main shortcoming of this modelling approach is that it is numerically cumbersome. As a result, it has not been adopted by practitioners, who still

resort to the simplified deterministic load model.

Biomechanical load model

An emerging trend is to model the dynamics and biomechanics of walking, which could potentially allow for better characterization of the dynamic forces induced and also to quantify human-structure interaction (Willford, 2002; Brownjohn et al., 2004b; Živanović et al., 2010). In this context, mainly two classes of models have been proposed in the literature. The first category is linear oscillator-based, with single or multiple lumped masses connected together with linear springs and dampers. Such models are known as the spring-mass damper (SMD) models. The second category are biomechanically-inspired models, which were developed originally to simulate walking gait, realistically.

Archbold et al. (2005) used an single-degree-of-freedom (SDOF) SMD model of a single pedestrian walking across a PB by using parameters selected from the biomechanics literature, which were developed for standing and running actions. Kim et al. (2008) adopted a two-degree-of-freedom SMD model for simulating a single pedestrian walking on a 99 m long cable-stayed PB (Figure 2.7(a)). Caprani et al. (2011) developed the SDOF SMD model by adding a contact force to the model. They reported that their model response estimates were considerably lower compared to force-only simulations near resonant conditions. However, their work lacks experimental validation. A few attempts have been made since then to identify the bio-dynamic parameters in the context of civil engineering applications. The work of Silva and Pimentel (2011) is one such example, where the parameters of a SDOF SMD walking human model were identified through analyzing the correlation of walking force and accelerations of the human body centre of mass (CoM) recorded at the waist of the subject. Later on, da Silva et al. (2013) developed this model for multi-person traffic and reported a reduction in the natural frequency of the structure along with an increase in damping, which also intensified with an increase in the traffic size.

Inverted-pendulum models from the biomechanics literature have also been used extensively to simulate the interaction of walking pedestrians with PBs. In such models, the two lower limbs of a human are modelled, known as bipedalism. Bocian et al. (2012) proposed a bipedal model in which human walk is modelled using an inverted pendulum (Figure 2.7(b)) and the bridge motion perturbed the gait in the lateral direction. Later on, this work was extended to a vertically oscillating bridge Bocian et al. (2013), where the motion of the bridge modified the passive motion of the pedestrian's centre of mass. However, the inverted pendulum cannot model the double-support phase of walking and ignores the compliant leg behaviour. Furthermore, their model also did not provide experimental validation, specifically in adequately capturing the GRF on a flexible platform. Qin et al.

(2013) adopted a bipedal walking model with damped compliant legs to simulate walking on a vibrating beam as shown in Figure 2.7(c). The dynamic analysis could incorporate human-structure interaction as well as bipedal mechanism of walking. However, too many parameters makes this model overly complex. Their research, moreover, did not include any experimental validation studies to support their modelling assumptions.

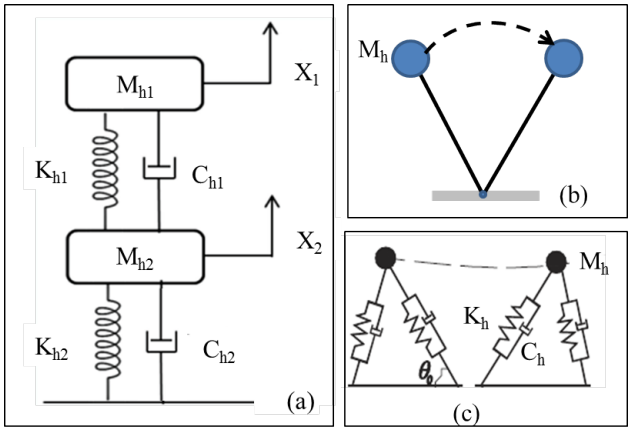

Figure 2.7: (a)Two degree of freedom SMD model as adopted by Kim et al. (2008), (b) inverted pendulum model as adopted by Bocian et al. (2012) and (c) bipedal-walking model as adopted by Qin et al. (2013)

Modelling crowd effect

Since the serviceability problems of PBs are exacerbated by groups of pedestrians or crowds, quantifying crowd-induced loads is essential for vibration serviceability assessment of PBs. All of the aforementioned studies on modelling walking load from measurements using force plates or instrumented treadmills deal with a single pedestrian. Similar studies for groups of people do not exist. Modelling crowd effect has been conducted so far by extrapolating the effect of single pedestrian through a multiplication factor. The first attempt at modelling random loads induced by a group of N pedestrians was conducted by Matsumoto et al. (1978). Assuming pedestrian arrival at the bridge follows a Poisson distribution, they stochastically superimposed individual responses to predict the total response. It was found that the total response can be obtained by multiplying a single pedestrian response by a multiplication factor, $\sqrt{N}$ or λT_0, where λ is the mean arrival rate of pedestrians (number of pedestrians/second/width), and T_0 stands for the elapsed time to cross the

bridge. But, this method did not take into account synchronization of pedestrians. For a perfect synchronization, this multiplication factor will be N (Živanović et al., 2005). In reality, perfectly synchronized crowd or no synchronization is unlikely and thus the factor will lie between these two bounds. There have been attempts to stochastically simulate crowd loading from bio-dynamic models of walking (Caprani et al., 2012; da Silva et al., 2013). Caprani et al. (2012) proposed enhancement factors for estimating crowd-induced vibrations of PBs for different levels of synchronization amongst the pedestrians. The current design guidelines also apply a multiplication factor to estimate the response under groups of pedestrians. However, due to the complicated synchronization phenomenon, modelling crowd loads still has many open questions.

The main difficulty in modelling the effect of crowd is in determining the degree of synchronization. Synchronization can happen either among the pedestrians or between the crowd and the structure. Although different in nature, these occur simultaneously and significantly influence the GRF generated by the crowd. Hence, synchronization is an important aspect of human-structure interaction affecting structural response, which is still being extensively studied. There is little documented evidence of vertical synchronization in a crowd (Willford, 2002). However, pedestrians are very sensitive to even small amplitudes of lateral vibration, and there has been documented evidence of synchronization in the lateral direction (Fujino et al., 1993). It was only after the serviceability failure of the London Millennium bridge (LMB) that researchers started considering the possibility of synchronization between people in a dense crowd. Lateral vibration disturbs the lateral balance of pedestrians while walking and as a result, pedestrians tend to adapt their gait to the lateral motion of the bridges in order to control their balance, leading to synchronization. The amplitude of vibration increases with the number of pedestrians in sync with the bridge, as observed by an experimental study by Willford (2002) on the LMB. Several measurements have been carried out on different full-scale bridges to understand the lateral synchronization phenomena under crowd excitations (Dallard et al., 2001; Brownjohn et al., 2004a). From a controlled crowd test on the LMB, it was observed that there was a critical number of pedestrians, which caused the responses to amplify excessively. This hypothesis has since been pursued by many to quantify this critical number based on full-scale measurements (Dallard et al., 2001; Caetano and Cunha, 2002; Macdonald, 2008). The basic idea suggested in these works is that the pedestrian loading can be modelled as a function of velocity, and equivalently can be represented as a negative damping applied to the structure. Bocian et al. (2012) presented a simplified inverted pendulum model combined with lateral balance control law to verify this equivalent negative damping concept. The results of this study showed the independency of the model on the human-structure phase of synchronization. However, due to uncertainties in the phenomenon of lateral syn-

chronization, more experimental results from real case studies are required to verify these hypotheses.

2.1.4 Limitations of existing walking load models

Despite numerous attempts to characterize and model pedestrian-induced walking forces, as discussed in the previous sections, there are clear shortcomings in the existing walking load models, which are summarized below:

- In general, nearly all walking load models are based on force measurements, obtained from either force plates on rigid ground or instrumented treadmills in artificial laboratory conditions. However, in the context of civil engineering applications, the flexibility of the walking surface has an effect on the induced force due to human-structure interaction. Although several attempts have been made recently to monitor walking behaviour through novel technologies such as the motion capture technology for civil engineering applications, conclusive results are still not available. Thus, a great deal of research needs to be dedicated towards understanding human-induced walking forces on flexible structures.

- The traditional deterministic load models do not take into account intra-subject variability. Although, the probabilistic models incorporate both intra-and inter-subject variabilities in walking forces, the main shortcoming of this modelling approach is that it is computationally intensive. As a result, probabilistic models have not yet been adopted by practitioners, who rely on simplified deterministic load models.

- Although the bio-mechanical models attempt to account for human structure interaction, too many model parameters and the absence of generally applicable values of biodynamic properties of human body model make these models difficult to apply in design situations. Moreover, experimental studies employing these models are lacking.

- The difficulty in characterizing crowd-induced walking excitation is in determining the degree of synchronization within the pedestrians as well as between the structure and the pedestrians. Due to uncertainties in the phenomenon of synchronization, experimental results from real case studies are required to investigate and quantify this phenomenon.

2.2 Vibration serviceability design of PBs

In the serviceability-based design of PBs, a simple predictive model of the pedestrian-induced walking force, the dynamic properties of the structures, and the desired acceleration limits for human comfort are the key required elements. Early research into vibration serviceability of PBs dates back to the seventies, with the work of Blanchard et al. (1977) to define design guidelines for the assessment of human-induced vertical vibrations of PBs. His work was later incorporated into several international bridge design codes (BS 5400, 1978; CAN/CSA S6, 2011). Although the effect of multiple pedestrians has been well appreciated in the seventies (Matsumoto et al., 1978; Wheeler, 1982), only a simplified single pedestrian load scenario was included in the standards. Over the years, several codes and guidelines has been developed to calculate the vibration response to multi-person traffic by multiplying the response due to a single person excitation with a factor. This approach originated from the work of Matsumoto et al. (1978) and is adopted by the existing design guidelines due to its simplicity. However, most of the design guidelines consider a range of multiplicative factors, not the values originally suggested by Matsumoto et al. (1978). As the serviceability issues of PBs is exacerbated in crowd scenarios and generally governs the design case, the current study is limited to the vibration serviceability design under group/crowd loading conditions, which covers ISO 10137, Eurocode 5, British national Annex to Eurocode 1 and SÉTRA. The four design guidelines (see Table 2.3) are discussed in detail in the following sections.

2.2.1 A two-step approach

In general, all the design guidelines ensure serviceability in a two-step approach. In the first step, the structural frequency is checked to see if it falls outside a critical frequency ranges, prescribed by the guidelines. If the structural frequency falls above the prescribed critical values, the structure is deemed to automatically satisfy the serviceability requirements. However, if the structural frequency falls below these critical values, the serviceability is met through limiting the structural vibrations to specified acceleration levels. For this purpose, a detailed dynamic analysis should be performed, following which the predicted acceleration response is compared with the vibration limit in order to ensure desired comfort to the pedestrians on the bridge.

In the first step, restricting the structural frequency outside the critical frequency limits ensures that the serviceability requirements are satisfied. These frequency limits are proposed by the guidelines in order to take care of the walking harmonics potentially resonating

with the dominant structural modes of vibration. Keeping the structural frequency outside the critical ranges avoids the possibility of excessive vibrations under resonant conditions. Table 2.3 lists the critical values of frequency suggested by the guidelines. As shown in the table, these frequency ranges are not consistent across provisions. Some criteria limit the frequency in the vertical direction to 5 Hz (EN 1995-2, 2004; SÉTRA, 2006), which considers the possibility of resonance up to the second harmonic of the walking frequency (≈4.8 Hz). Only the British National Annex considers up to three harmonics by assuming the critical frequency limit at 8 Hz. Although ISO 10137 explicitly does not provide any limit on the frequency, it considers up to five harmonics of walking frequency and thus, implicitly defines a critical range of 1.2 Hz to 12 Hz. Similarly in the lateral direction, the frequency limit is 2.5 Hz in most of the guidelines, aimed at capturing up to two harmonics, except the British National Annex which limits to 1.5 Hz.

Table 2.3: Limiting frequencies proposed by different design guidelines

Code	*Limit frequency in Hz*	
	Vertical	lateral
ISO 10137 (implicit)	$1.2 - 12$	1.2
Eurocode 5	< 5	< 2.5
British Annex to Eurocode 1	< 8	< 1.5
SÉTRA	$1 - 5$	$0.3 - 2.5$

In the second step of serviceability assessment, it is ensured that the bridge responses estimated through a dynamic analysis meet the desired comfort limits. The comfort limits for pedestrians are generally specified in terms of peak acceleration, except for ISO 10137, which uses the root mean square (RMS) value (1 second average) of accelerations. ISO 10137 provides base curves as shown in Figure 2.8, which are multiplied by a factor of 60 for the RMS acceleration in both the vertical and lateral directions. It is worth noting that the acceleration limit in the lateral direction does not extend below 1 Hz, while a lateral fundamental frequency below 1 Hz could also be important, as evidenced by the LMB. The peak acceleration limits specified by other guidelines are listed in Table 2.4. While Eurocode 5 and ISO 10137 propose a single comfort limit, other codes have proposed different limits based on site usage, height of the structure, traffic class or the level of comfort. The British National Annex proposes the following acceleration limit:

$$a_{lim} = 1.0 k_1 k_2 k_3 k_4 \text{ with } 0.5 \leq a_{lim} \leq 2.0 \text{ m/s}^2 \tag{2.5}$$

where, k_1 is the site usage factor with values ranging between 0.6 to 1.6 based on the intended bridge function; k_2 is the route redundancy factor with values ranging from 0.7

to 1.3; k_3 is the height factor with values from 0.7 to 1.1; k_4 is the exposure factor and is taken as 1.0 unless specified. The limits proposed by ISO 10137 are frequency dependent, while others are independent of frequency. This implies that the limits are applicable only within the specified frequency range in Table 2.3, as specified by the respective guidelines. With the exception of ISO 10137, which offers guidance on the limits until 80 Hz, others do not offer guidance for structural frequencies above 5 or 8 Hz.

Table 2.4: Acceleration limits specified in guidelines

Codes	*Limit acceleration in* m/s^2	
	Vertical	Lateral
Eurocode 5	0.70	0.20 for single pedestrian, 0.4 for crowd loading
British National Annex to Eurocode 1	$0.5 - 2.0$ (Equation 2.5) depending on site usage, route redundancy and height of structure	–
SÉTRA		
Maximum comfort:	< 0.5 (Limit I)	< 0.1 (Limit I)
Average comfort:	0.5 (Limit I) $-$ 1.0 (Limit II)	0.1 (Limit I) $-$ 0.3 (Limit II)
Minimum comfort:	1.0 (Limit II) $-$ 2.5 (Limit III)	0.3 (Limit II) $-$ 0.8 (Limit III)
Unacceptable:	> 2.5 (Limit III)	> 0.8 (Limit III)

2.2.2 Dynamic analysis

In the second step of the serviceability assessment, a dynamic analysis may be required for PBs with natural frequencies (vertical or lateral) within the critical values listed in Table 2.6. For this analysis, the design guidelines assume resonant conditions, where the structure is assumed to be excited at its natural frequency by the pedestrians. Either the SDOF (single degree of freedom) approach for simple structures or the finite element method for complex systems are recommended for response prediction by the guidelines. A detail review of the response prediction by the guidelines is presented below.

ISO 10137

The ISO 101317 (ISO 10137, 2007) guideline is published by the International Organisation for Standardization, and can be used for vibration serviceability design of buildings and

pedestrian walkways. This guideline provides some scenarios to consider during such an assessment:

- one person walking across the bridge;
- average pedestrian flow for groups of between 8 and 15 people;
- streams of pedestrians for groups of significantly more than 15 people, and
- the occasional festive or choreographic event if relevant.

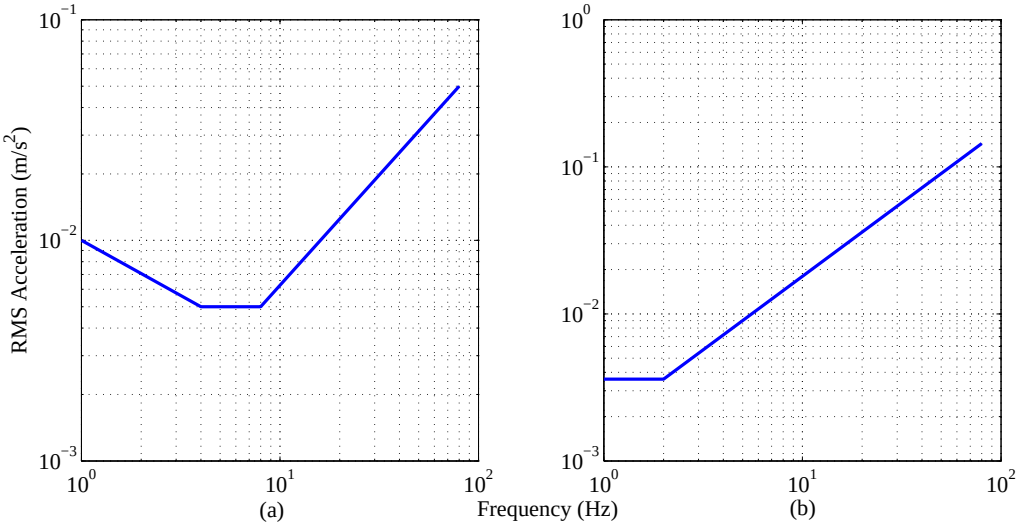

Figure 2.8: Base curves in accordance to ISO 10137 for (a) vertical and (b) lateral directions

ISO 10137 describes the dynamic actions of one or more people by the use of a time-domain moving load model, which is expressed using a Fourier series approximation. The force due to a single pedestrian in both the lateral and vertical directions can be written as (Allen and Murray, 1993):

$$F_d(t) = Q(1 + \sum_{m=1}^{k} \alpha_{m,d} \sin(2\pi m f_d t + \phi_{m,d})) \tag{2.6}$$

where, $\alpha_{m,d}$ and $\phi_{m,d}$ are, respectively, the dynamic load factor (DLF) and the phase angle corresponding to the m^{th} harmonic in the direction under consideration (the subscript d

stands for direction, vertical or lateral). Q is the total static load of the participating pedestrians and f_d is the frequency of walking in the direction under consideration. The lateral frequency is one-half of the vertical frequency. Other design parameters such as the step frequency and DLF to estimate the forces due to one person are listed in Table 2.5.

Table 2.5: Design parameters for moving forces due to one person according to ISO 10137.2007

Harmonic number, n	*Range of frequency,* f	*Numerical coefficient*	
		$\alpha_{n,v}$	$\alpha_{n,h}$
1	1.2 to 2.4	$0.37(f - 1.0)$	0.1
2	2.4 to 4.8	0.1	
3	3.6 to 7.2	0.06	
4	4.8 to 9.6	0.06	
5	6.0 to 12.0	0.06	

ISO 10137 states that the dynamic actions of group of pedestrians depends primarily on the weight of the participants, the maximum density of persons per unit floor area, and on the degree of coordination among the pedestrians. The coordination is taken into account by applying a coordination factor, $C(N)$, to the forcing function in Equation 2.6:

$$F(t)_N = F_d(t)C(N) \tag{2.7}$$

If the movement of the group is uncoordinated, the coordination factor is $\sqrt{N}/N$. It is easy to see the similarity between this coordination factor and the $\sqrt{N}$ multiplier in (Matsumoto et al., 1978) if we think of Q in Equation 2.6 as a product of N and the average weight of the pedestrians in a group (G). A conservative approach for the phase angle is obtained by introducing a phase shift of 90° for harmonic contributions below resonance.

Eurocode 5

Eurocode 5 (EN 1995-2, 2004) was developed in the U.K. in 2004, specifically for the design of timber bridges. However, the response model defined is not specific to any material and therefore, could be used for PBs in general. Moreover, this code assumes the PB to be a simply supported beam or a truss system. Unlike ISO 10137, it provides the equation to estimate the maximum acceleration response of PBs under N pedestrians. A value of $N = 13$ for distinct groups and $0.6A$ for a continuous stream of pedestrians is suggested for design, where A is the bridge deck area in m^2. According to this standard, the vertical

acceleration of the bridge due to N pedestrians, $a_{v,n}$ in m/s^2, is given by:

$$a_{v,n} = 0.23 a_{v,1} N k_{vert} \tag{2.8}$$

where $a_{v,1}$ is the response under single pedestrian and given by,

$$a_{v,1} = \begin{cases} \frac{200}{M\zeta} & \text{for } f_v \leq 2.5 \\ \frac{100}{M\zeta} & \text{for } 2.5 < f_v \leq 5.0 \end{cases} \tag{2.9}$$

Similarly, the lateral acceleration $a_{h,n}$ in m/s^2 is calculated using:

$$a_{h,n} = 0.18 a_{h,1} N k_{hor} \tag{2.10}$$

where, $a_{h,1}$ is the lateral acceleration in m/s^2 for one person crossing the bridge and calculated using:

$$a_{h,1} = \frac{50}{M\zeta} \quad \text{for } 0.5 \leq f_h \leq 2.5 \tag{2.11}$$

In these equations, M is the total mass of the bridge, ζ is the damping ratio, f_v and f_h are the vertical and lateral natural frequencies of the structure, respectively, and k_{vert} and k_{hor} are coefficients according to Figure 2.9 (a) and (b) and N is the number of pedestrians. Although this guideline uses a response based model as opposed to a force model, equations 2.9 and 2.11 are in fact a result of the basic moving load model (Equation 2.1) under resonant condition, while using different values for the dynamic load factor (Butz, 2008). These formulae given are based on the following parameters:

- the weight of the pedestrian is 700 N;
- the DLF in the vertical directions are 0.45 and 0.22 respectively for first and second harmonics and 0.10 in the lateral direction for the first two harmonics, and
- a reduction factor of 0.63 is applied to take care of the reduction due to the pedestrian's movement in the longitudinal space.

The factor 0.23 in Equation 2.8 accounts for the synchronization probability of the group of pedestrians crossing the bridge, and the factor 0.18 in Equation 2.10 accounts for the horizontal lock-in probability for the group of pedestrians crossing the bridge. The coefficients k_{vert} and k_{hor} account for the risk of resonance that the step frequencies coincide with the natural frequency of the bridge.

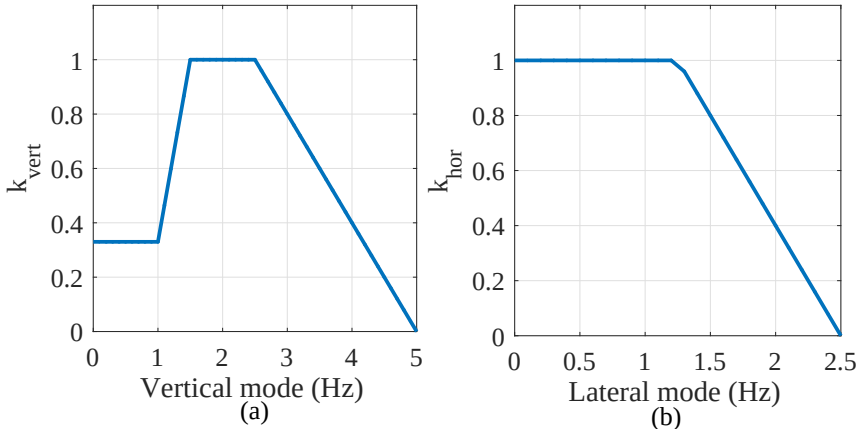

Figure 2.9: (a) Vertical and (b) lateral response reduction factors in accordance with Eurocode 5

British National Annex to Eurocode 1

The British National Annex (NA to BS EN 1991-2, 2003) classifies PBs into four categories:

- Class A: rural locations, which are seldomly used (2 P or 0 P/m^2);
- Class B: location with occasional variations in the pedestrian loading intensity (4 P or 0.4 P/m^2);
- Class C: urban routes subject to significant variation in the daily usage (8 P or 0.8 P/m^2);
- Class D: primary access to major public assembly (16 P or 1.5 P/m^2).

Three load models are proposed based on these classifications. Two of these models consider the vertical direction, while the third considers the lateral direction. The maximum vertical acceleration under a group of N pedestrians walking is estimated by assuming a moving vertical force (F in N) at constant speed, which is given by:

$$F = F_0 k(f_v)\sqrt{1+\gamma(N-1)}\sin(2\pi f_v t) \tag{2.12}$$

where, F_0 is the moving force amplitude of 280 N for a pedestrian weight of 700 N; $k(f_v)$, which is a function of the vertical natural frequency (f_v) in Figure 2.10(a) is a combination

factor to deal with: (a) the effect of more realistic pedestrian population, i.e., equivalent number of pedestrians, (b) harmonic response, and (c) relative weighting of pedestrian sensitivity to response; γ is a factor to allow for the unsynchronized combination of actions in a pedestrian group and is obtained from Figure 2.10(b); N is the number of pedestrians who are assumed to cross the bridge together in a group. With force amplitude F_0 being 280 N, it is clear that this guideline considers a uniform DLF of 0.4 for all the first three harmonics. The reduction in response due to second and third harmonics (α_2 and α_3) is accounted through $k(f_v)$ in Figure 2.10(a). The DLFs for these higher harmonics can be obtained through the function $k(f_v)$ by normalizing the maximum value of $k(f_v)$ in the second ($2.8 \leq f_v < 5.6$) and third harmonic regions ($5.6 \leq f_v < 8.0$) to 1.0. The α_2 and α_3 values so obtained are, respectively, 0.14 and 0.051 with normalized $k(f_v)$, denoted by $k'(f_v)$

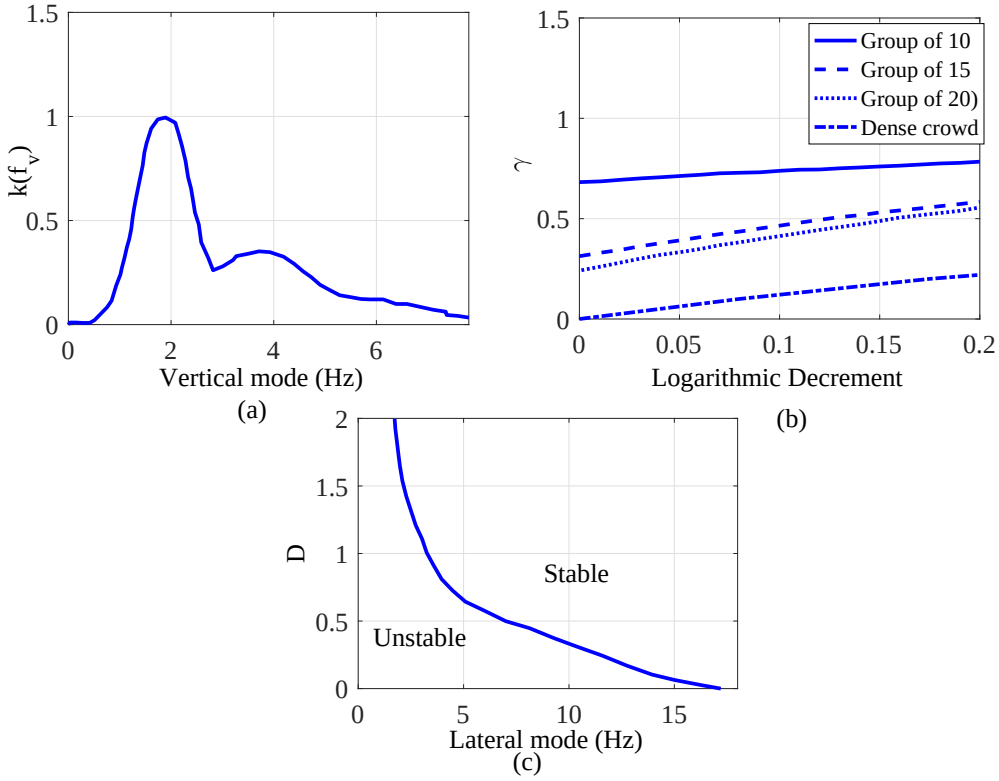

Figure 2.10: (a) Vertical response reduction factor, (b) reduction factor γ as a function of the logarithmic decrement, and (c) the damping factor as a function of the lateral mode by the British National Annex

The second modelling approach is based on the assumption of continuous flow, where the pedestrians are on the bridge for a sufficient amount of time such that steady state conditions are achieved. In such a scenario, the load is distributed over the entire span and is given by:

$$w = 1.8\frac{F_0}{A}k(f_v)\sqrt{\frac{\gamma N}{\lambda}}\sin(2\pi f_v t) \tag{2.13}$$

where, w is the distributed load in N/m^2; A is the area of deck in m^2; N is the number of pedestrians in the group, given by ρA; ρ is the crowd density per m^2; λ is a factor that reduces the effective number of pedestrians in proportion to the enclosed area of the mode of interest (for the first mode shape of a simply supported beam, this is equal to 0.634).

This standard does not require a dynamic analysis to assess serviceability in the lateral direction. This involves calculating the damping parameter D using:

$$D = \frac{m_{bridge}\zeta}{m_{pedestrian}} \tag{2.14}$$

where, m_{bridge} is the mass per unit length of the bridge and $m_{pedestrian}$ is the mass per unit length of pedestrians for the relevant crowd density. The serviceability in the lateral direction is determined through comparing the parameter D with the stability envelope as defined in Figure 2.10(c). Instability will occur when the this damping parameter falls below the indicated envelope.

SÉTRA

The SÉTRA guideline (SÉTRA, 2006) of the Technical Department for Transport, Roads and Bridges Engineering and Road Safety of France (2006) adopts different ranges of frequencies and traffic classes in its design methodology. It has presented three load cases for pedestrian walking loads: Case 1 for sparse and dense crowd with densities ranging from 0.5 - 0.8 pedestrians (P)/m^2 ; Case 2 for very dense crowd with densities $\geq$ 1.0 P/m^2; and Case 3 to consider second harmonic effect for an evenly distributed crowd. These load cases are developed based on four classes of PBs depending on the level of traffic they are expected to experience:

- Class I: urban PB subjected to very heavy traffic frequently (1.0 P/m^2)
- Class II: urban PB with heavy traffic (0.8 P/m^2)
- Class III: PB with moderate traffic (0.5 P/m^2)

- Class IV: PB with low level of traffic (< 0.5 P/m^2)

SÉTRA also proposes four classes of frequency ranges depending on the expected risk of resonance as reported in Table 2.6. Table 2.7 lists the proposed load cases to consider based on the traffic dependent bridge classes and frequency ranges.

Table 2.6: Frequency ranges for vertical and lateral vibrations

Ranges of frequency	Vertical frequency (Hz)	Lateral frequency (Hz)
Range 1	1.7-2.1	0.5-1.1
Range 2	1-1.7; 2.1-2.6	0.3-0.5; 1.1-1.3
Range 3	2.6-5.0	1.3-2.5

Table 2.7: Load cases considered for different fundamental frequency ranges

Bridge class	Range 1	Range 2	Range 3
Class I	Case 2	Case 2	Case 3
Class II	Case 1	Case 1	Case 3
Class III	Case 1	—	—

Random loads due to a stream of N pedestrians corresponding to a specific crowd density (d) are simplified to deterministic loads under equivalent number of pedestrians (n_{eq}), which is given by:

$$n_{eq} = \begin{cases} 10.8\sqrt{\zeta_i N} & \text{for } d < 1.0 \\ 1.85\sqrt{N} & \text{for } d \geq 1.0 \end{cases} \tag{2.15}$$

Here, ζ_i is the i^{th} modal damping factor. To estimate response, the load due to n_{eq} pedestrians is assumed to be uniformly distributed on the deck. The distributed load per unit area (A) in any direction (vertical or lateral) is defined as:

$$p = \frac{\alpha G \psi n_{eq}}{A} \cos(2\pi f t) \tag{2.16}$$

where G is the average weight of the group of pedestrians and α is the DLF, which is 0.4 and 0.1 for the first and second harmonics in the vertical direction, respectively and 0.05 and 0.01 for the first and second harmonics in the lateral direction, respectively. ψ is the reduction factor, which is a function of the structural frequency (Figure 2.11(a) and (b)) and denoted by ψ_v and ψ_l in the vertical and lateral directions respectively. f is the excitation frequency and equals to the structural frequency as the analysis is performed

under resonant condition. The uniformly distributed load is applied to the entire bridge. The direction of application of the load is the same as the direction of the mode shape. The SÉTRA guideline considers the possibility of resonance in the first and second harmonics of walking through the factor ψ. The loads are distributed according to the corresponding mode shape to obtain the design response.

SÉTRA explicitly takes into account the effect of pedestrian weight on the structural frequency and predicts two bounds for the peak response; one considers the effect on an empty bridge, while the other is calculated based on the modified structural frequency due to the weight of pedestrians (uniformly distributed on the deck). The modified frequency is estimated as:

$$f'_n = \frac{f_n}{\rho} \tag{2.17}$$

where ρ is the influence factor for additional pedestrian mass given by,

$$\rho = \sqrt{\frac{\mu_D + \mu_p}{\mu_D}} \tag{2.18}$$

with μ_D and μ_p are the bridge deck and pedestrian mass per unit length of bridge, respectively.

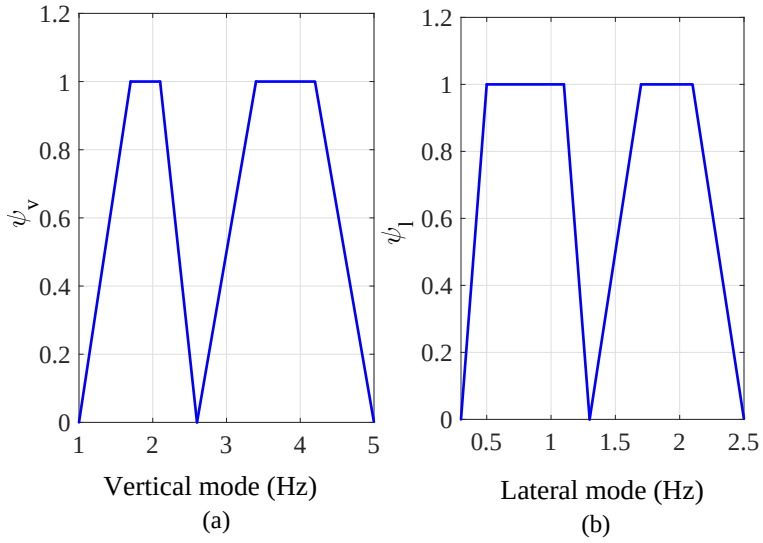

Figure 2.11: Response reduction factor (ψ) in the (a) vertical and (b) lateral directions accordance with SÉTRA guideline

2.3 Structural response simulation under walking loads

A PB can be modelled in terms of mass, damping, stiffness of the bridge, and possible human-structure interaction for the purposes of response simulations. Traditionally, a combination of modal testing and finite element analysis is conducted to estimate the mass, damping, and stiffness of bridges. Knowing the modal properties and modelling the source or the walking force as discussed in the previous section, the well known equation of motion of a multiple-degree-of-freedom (MDOF) system can be formulated as:

$$\mathbf{M}\ddot{\mathbf{x}}(t) + \mathbf{C}\dot{\mathbf{x}}(t) + \mathbf{K}\mathbf{x}(t) = \mathbf{f}(t) \tag{2.19}$$

where $\mathbf{M}$, $\mathbf{C}$ and $\mathbf{K}$ are the mass, damping, and stiffness matrices respectively of $n \times n$, where n is the degrees of freedom of the structure. $\ddot{\mathbf{x}}(t)$, $\dot{\mathbf{x}}(t)$, $\mathbf{x}(t)$, and $\mathbf{f}(t)$ are vectors of size n corresponding to acceleration, velocity, displacement, and the force induced by the pedestrian. Assuming that the system is linear and proportionally damped, the given equation of motion can be written in the modal domain as n uncoupled equations representing n equivalent single-degree-of freedom systems:

$$M_n\ddot{Y_n} + C_n\dot{Y_n} + K_nY_n = f_n(t) \tag{2.20}$$

where, $Y_n(t)$ is the n^{th} modal displacement response of the system at the time instant t and its first and second derivative represent the velocity and acceleration of the bridge due to the excitation. M_n, C_n, K_n, and $f_n(t)$ represent the n^{th} modal mass, damping, stiffness, and force of the bridge. For response simulation using the periodic load models, the pedestrian is assumed to be moving with an uniform walking speed (Figure 2.12). The modal force $f_n(t)$ is given by:

$$f_n(t) = \int_0^L \delta(x - vt)\phi_n(x)P(t)dx \tag{2.21}$$

where $P(t)$ is continuous walking force by a pedestrian while walking at speed of v. $\phi_n(x)$ is the mode shape of the bridge deck. If the bridge deck acts as a simply supported beam of length L, the mode shape of the beam is given by:

$$\phi_n(x) = \sin(\frac{n\pi x}{L}) \tag{2.22}$$

where $x = vt$ is the position of moving load at any time t on the beam. v is the walking speed and can be calculated as a function of the pacing frequency using the relation (Živanović, 2012):

$$v = 0.714f_s + 0.055 \tag{2.23}$$

Hence, the equation of motion in Equation 2.20 for mode n can be rewritten after substituting the modal load $f_n(t)$ as:

$$M_n\ddot{Y_n} + C_n\dot{Y_n} + K_nY_n = (G + \sum_{i=1}^{m} G\alpha_i \sin(i2\pi f_s)) \sin(\frac{n\pi vt}{L}) \tag{2.24}$$

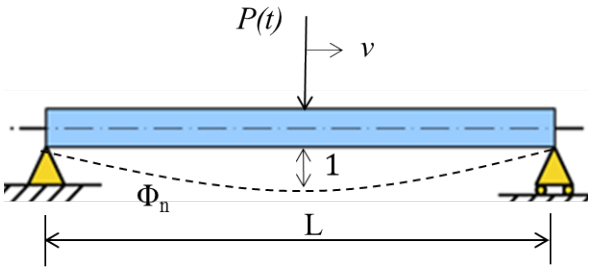

Figure 2.12: Moving load on a simply supported PB

In the case of PBs, the forced phase, i.e., when the pedestrian is on the bridge, alone is important for serviceability. For the forced phase, the response is simulated from the time the pedestrian steps onto the bridge to the instant the pedestrian leaves the bridge at the other end. Hence the total duration required to cross the bridge is $T = L/v$. The response of the bridge at the mid-span can the be estimated numerically or analytically (see Appendix A). Generally, the most popular method for establishing and solving Equation 2.24 is the finite element (FE) method. However, when one mode dominates, which often happens in PBs, the response can be estimated sufficiently accurately using an SDOF modal equation for the appropriate mode. This is very often implemented in practice when checking PB vibration serviceability using the design guidelines.

2.4 Full-scale experiments on PBs

There have been several full-scale studies on PBs conducted for their performance assessment under pedestrian-induced excitations. One of the most extensive experimental campaign was carried out on the LMB following the large amplitude motions, which occurred during its inauguration day (Dallard et al., 2001), leading to a shutdown. The LMB is a steel suspension bridge with a total span of 332 m and the largest individual span being at the centre, 144 m in length. It has natural frequencies at 0.48 Hz, 0.78 Hz, 0.95 Hz, and 1.05 Hz in the lateral direction and thus falls within the critical ranges of frequencies in

the lateral direction with risks of resonance at the first harmonic. It was observed that for a certain number of pedestrians, the bridge response was limited, whereas a small increase in the number of pedestrians (beyond a critical number) often resulted in excessive lateral response (Dallard et al., 2001) causing instability to the pedestrians. In 2002, Willford (2002) reported an increase in the damping of the LMB under walking load in the vertical direction. Subsequently, several other bridges were subjected to field tests for dynamic performance assessment, most notably, the M-Bridge in Japan (Nakamura, 2003), the steel bridge at Changi airport in Singapore, (Brownjohn et al., 2004a), the Clifton Suspension Bridge in England (Macdonald, 2008), and the Pedro e Inês bridge in Portugal (Caetano et al., 2010).

The M-Bridge is a suspension bridge with a main span of 320 m, which consists of a reinforced concrete tower supporting a deck with H-girders, sway bracing, and steel grating. The critical frequencies were found to be the third mode at 0.88 Hz and the fourth mode at 1.02 Hz, both in the lateral direction (Nakamura, 2003). The Changi Mezzanine Bridge is a 140 m span flat arch bridge constructed from welded tubular steel sections inside a tunnel that connects two passenger terminals at the Changi Airport in Singapore. The modes that can be easily excited by pedestrian movements are: the lateral mode at approximately 0.9 Hz and the torsional mode at 1.64 Hz. Macdonald (2008) investigated the Clifton Suspension Bridge in England. The main span, between centre lines of the piers, is approximately 214 m, with chain side spans each of 59 m. Footways on either side of the deck, outside the girders, result in a total deck width of 9.46 m between the centre lines of parapets. The deck is comparatively light, being made of timber with wrought iron lattice cross-girders in line with each pair of suspension rods. A total of 27 modes under 3 Hz were identified, with most of those modes being either vertical or torsional. The 274 m long Pedro e Inês bridge in Portugal is formed by a central parabolic arch with approximately 9 m rise and 110 m chord. The deck has a width of 4m and is formed by a L-shaped box cross section, whose top flange is a composite steel-concrete slab. This bridge mostly results in very complex mode shapes, which have coupled lateral and vertical displacements. Caetano et al. (2010) identified a total 10 vibration modes below 3 Hz, which are in the range of pedestrian excitable frequencies. All of these bridges are mostly prone to potential resonance with the first harmonic of the walking frequencies. The experimental studies on theses bridges consisted of modal testing using accelerometers as well as walking tests with groups of pedestrians. Mostly, the results from the experiments pointed towards the synchronization phenomenon due to human-structure interaction leading to changes in their modal properties.

Besides these studies, several attempts have been made in the literature to evaluate the design guidelines through experimental studies on in-service PBs. Pimentel (1997)

conducted modal as well as walking tests on three PBs: a single span composite PB with first vertical mode at 3.67 Hz, a single span stressed ribbon concrete PB with first two vertical modes at 2.3 Hz and 3.6 Hz, and a three span ACM cable-stayed PB with first two vertical modes at 1.92 Hz and 2.59 Hz. The results from the study highlighted that the deterministic load models overestimate the response under resonant conditions. Salgado et al. (2014) conducted single pedestrian walking tests on the timber Góis PB in Portugal with first lateral vibration mode at 2.46 Hz and concluded that the current codes are not fully applicable to all kind of PBs, particularly when they have frequencies near those, which are considered to have vibration problems. Živanović et al. (2010) performed a comparison between the existing design procedures for groups of pedestrians based on experiments on two full-scale bridges: Reykjavik City pedestrian bridge and Podgorica bridge. The 160 m long Reykjavik City bridge was built as a continuous post tensioned concrete beam. The first two critical vertical modes of the bridge are at 2.08 Hz and 2.33 Hz. The Podgorica bridge of length 104 m is a steel box girder pedestrian bridge with critical vertical frequency at 2.04 Hz. All these comparison studies conducted so far are based on low-frequency PBs with risk of resonance with the lower harmonics of walking frequency. Experimental studies to assess the performance of bridges with different dynamic properties, specifically having risk of resonance with the higher harmonics of walking frequencies, are still lacking in the literature. Moreover, these full-scale studies are based on in-service PBs, where it is was not possible to conduct repetitive walking tests with different traffic conditions due to usage restrictions. While there are a few laboratory platforms involving prototype bridge specimens, no full-scale studies on lively PBs have been conducted to the author's knowledge in a controlled laboratory environment, with the exception of this work.

2.5 Gap areas in existing research on vibration serviceability of PBs

For PBs, a large amount of research, as discussed in the previous sections, has been published in recent years, which broadly focuses on analyzing vertical and lateral pedestrian-induced vibrations. However, several important issues related to their design methodologies and performance assessment remain unaddressed, or only partially addressed in the literature. A summary of the gap areas in the existing research on vibration serviceability of PBs is described here under and presents the motivation for the current study:

- Evaluating and improving existing design models for vibration serviceability assess-

ment of PBs relies on the availability of experimental data from full-scale PBs with a range of dynamic characteristics. Although several experimental studies on full-scale PBs under walking-induced excitation have been performed, at the moment a comprehensive experimental data set of walking tests under different traffic conditions on lively PBs that exhibit a potential for resonance with the higher harmonics of walking frequency, is not available. Moreover, most of the laboratory experimental studies were conducted on short walkways instrumented to characterize the walking-induced GRFs. This may not represent walking on a flexible bridge. Aside from a lack of experimental database, there is limited evidence of real case studies to investigate the human-structure interaction phenomena. Hence developing a comprehensive experimental data base from lively structures, on which the interaction phenomena is most likely to occur, would significantly contribute in understanding and modelling this phenomena.

- All design guidelines adopt the periodic moving load model. Although the performance of such models has been evaluated for resonant cases (with respect to the first harmonic of the walking frequency), there is still a need to validate these models for structures that do not resonate with the first harmonic, but with higher harmonics of walking. Although counter-intuitive at first, such an investigation is important, as the results might show that the design guidelines are un-conservative for the non-resonant cases. Moreover, the frequency characteristics of the simulated response, i.e., contributions from the harmonics of walking frequency as well as the structural frequency (transient) have also not been investigated yet.

- Although significant disagreement is observed between measurements and predictions by the design guidelines in resonance (mostly with the first harmonics of walking frequency), no attempts have been made yet in reconciling the shortcomings of the design provisions. To be clear, it is to be expected that the serviceability assessment outcomes using the guidelines should yield conservative values, but they should also be balanced so that they are economical.

- Uncertainties in the arrival time, pacing frequency, step length, and weight have already been accounted for in developing design provisions such as SÉTRA and the British National Annex to Eurocode 1. However, the sensitivity of various serviceability assessment methodologies to the uncertainties from the structural properties or the human perception levels to structural motion have not yet been studied. Moreover, none of the existing guidelines have been evaluated in a reliability-based framework.

2.6 Specific objectives

Based on the identified gaps in the literature, the specific objectives of this thesis are the following:

- develop a comprehensive experimental test program on full-scale pedestrian bridges encompassing different dynamic characteristics with particular focus on PBs that resonate with the higher harmonics of walking frequency;
- assess the performance of the conventional load model adopted by all the existing design guidelines in predicting the structural response under single-pedestrian walking for resonant as well as non-resonant scenarios through the experimental study;
- evaluate the most popular design guidelines for serviceability under groups of pedestrians;
- evaluate the guidelines in a reliability-based framework taking into account the potential sources of uncertainties arising from the pedestrian excitations, the structural properties, and pedestrian's sensitivity to structural vibration; and
- propose recommendations to improve and reconcile these guidelines both within the existing deterministic as well as a new probabilistic framework to better align the observations with the predictions, while at the same time ensuring reliable and economic designs.

Chapter 3

Experimental evaluation of design provisions using tests on full-scale bridges

In this chapter, popular design guidelines are evaluated using a comprehensive experimental database of walking trials on full-scale aluminum pedestrian bridges. First, the performance of the periodic load models adopted by the existing guidelines for single pedestrian walking are validated through measurements under resonant and non-resonant conditions. Next, the guidelines are evaluated for vibration serviceability under groups of pedestrians and key observations from the serviceability assessment are summarized.

3.1 Experimental program

Aluminum has a track record of good performance in vehicular bridge applications dating back nearly eight decades Sanders and Abendroth (1995); Mader and Pieper (2006); Siwowski (2006). The positive attributes of aluminum structures include light weight, high corrosion resistance, and extrudability. Of particular importance to this thesis, their relative lightweight and low intrinsic damping results in resonance with the higher harmonics of walking and not just the fundamental pacing frequency, which means they can be used to build near full-scale vibration susceptible structures that still fit within laboratory spaces. The current study focuses on investigating the effect of higher harmonics of walking on the vibration serviceability of PBs, as the effect of walking resonating with the fundamental frequency has already been well studied in the literature. The experimental program

was carried out on three pony-truss aluminum bridges, constructed out of aluminum by MAADI group.

One of the test beds was an in-service bridge, the Daigneault Creek Bridge in Brossard, Quebec. The laboratory experiments were conducted on two modular bridges, assembled in the Structures laboratory at the University of Waterloo. Multiple trials of pedestrian walking tests were performed on the bridges under different traffic conditions. The details of the structural characteristics, instrumentation, and the test matrix are discussed in the following sections.

3.1.1 Description of the bridges

The Daigneault Creek Bridge has been in active service since 2012, connecting a new subdivision from Rue Claudel to a transportation hub and commercial area on Rue Grande Alle in Brossard, Quebec (Figure 3.1(a)). It has a clear span of 43.7 m, a height of 2.8 m and width of approximately 4.4 m. This bridge is Canada's longest aluminium pony truss bridge. The cross section of top and bottom girders are HSS 254x254 mm. The deck purlins are HSS 203.2x203.2 mm and the deck diagonal bracings are HSS 152.4x152.4 mm. The modular bridges were fabricated with bolted connections solely for research purposes from a patented modular bridge product called Make-A-Bridge® by MAADI Group. The specimens can be assembled in various lengths ranging from 3 m to 22.9 m with 1.35 m in width, and 1.140 m in height. For this study, two spans were tested: 22.9 m and 12.2 m (Figures 3.1(b) and (c)). There are six main components to the Make-A-Bridge design, which are all fabricated from extruded T6061 aluminum through updated assembly in patent CA 268813 (Figure 3.2): top chord, bottom chord, diagonal, transversal, deck stringers, and decking. The top and bottom chord sections are joined by tubular diagonal members. Tubular transversal sections connect the bottom chords and provide the connection locations for the anti-slip surface deck plates. The bottom chord, transversal, and lower end of the diagonals were fitted with neoprene sleeves and bolted into a patented cast join (patent number CA 2607711). The 12.2 m span weighed 982 kg and the 22.9 m span weighed 1,735 kg.

3.1.2 Instrumentation

Both the field and laboratory bridges were instrumented with twelve low-frequency, high-sensitivity accelerometers of model number 393B31 manufactured by PCB Piezotronics®. They were installed on the bottom chords at quarter and mid-points along the length of

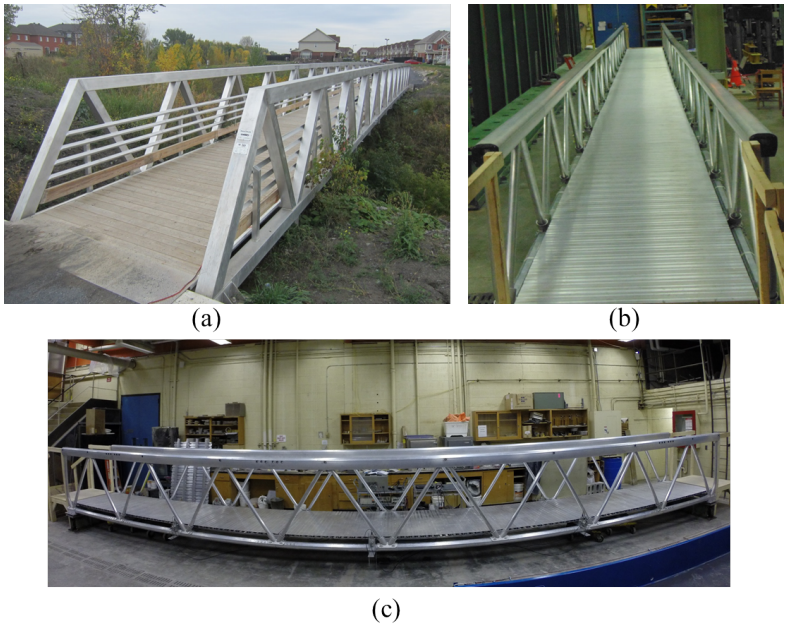

Figure 3.1: (a) Daigneault Creek Bridge of span 43.7 m, (b) Modular aluminum bridge of span 22.9 m, and (c) Modular aluminum bridge of span 12.2 m

the bridges. The accelerometers were attached to six mounting blocks, three on each side of the bridges, as shown in Figure 3.3 (a). Each mounting block carried an accelerometer in the lateral and vertical directions (Figure 3.3 (b)). The operable frequency range of the accelerometer is 0.1 Hz to 200 Hz. The acceleration measurements were acquired using three 4-channel A/D data acquisition modules (daisy-chained) of model no. DT9837A manufactured by Data Translation (Figure 3.3(c)). In addition to the accelerometers, the supports of the modular bridges were instrumented using triaxial load cells of model no. TR3D-B-4K from Michigan Scientific® as shown in Figure 3.3(a) and (d). Three string potentiometers were installed at the mid-span to measure the vertical and lateral displacements as shown in Figure 3.3 (a) and (e). The data from the load cells and string potentiometers (after appropriate signal conditioning) was acquired using a 16-bit 12-channel A/D DAQ, model DT9836 also manufactured by DataTranslation.

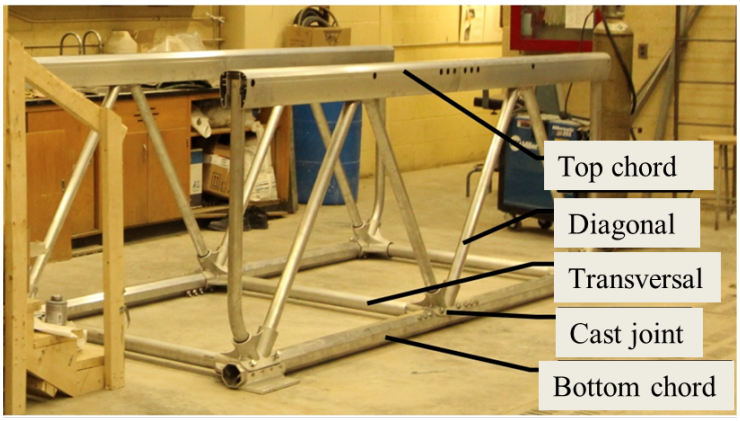

Figure 3.2: Basic assembly of Make-A-Bridge® specimen

3.1.3 Testing program

Prior to the start of walking tests, the modal characteristics for the bridges were obtained experimentally through modal testing. Heel drop tests were conducted on the Daigneault Creek Bridge in order to estimate its modal properties. Impact loading tests, i.e., hammer drop were employed on the laboratory bridge specimens for modal identification in the vertical as well as the lateral directions. Impact hammer and pull-then-release tests using a custom pulley system, were employed on the laboratory bridge specimens for modal identification in the vertical as well as the lateral directions. The modal properties of the structures are described in the next section, under dynamic characteristics.

Besides modal testing, a suite of pedestrian tests were conducted on the three bridges. While only individual walking at prescribed rates controlled using a metronome were conducted on the field bridge, two people walking synchronously and asynchronously, and crowds of varying densities in addition to individual walking tests at different walking frequencies were performed on the laboratory bridges. All tests consisted of multiple trials in order to achieve statistical significance. For the Daigneault Creek Bridge, five test subjects (Table 3.1) were involved. With the exception of subject P5, all the test subjects walked at their normal walking frequencies tabulated in Table 3.1. These frequencies were arrived at through multiple trials and interviewing test subjects subsequent to the tests regarding their perception of the walking rate undertaken. Subject P5 performed 30 trials in nine different frequencies ranging from 1.67 Hz to 2.33 Hz with an interval of 0.083 Hz.

For the laboratory specimens, considerably more repetitions were performed in terms of both inter and intra subject variability. For the 12.2 m bridge, single pedestrian tests

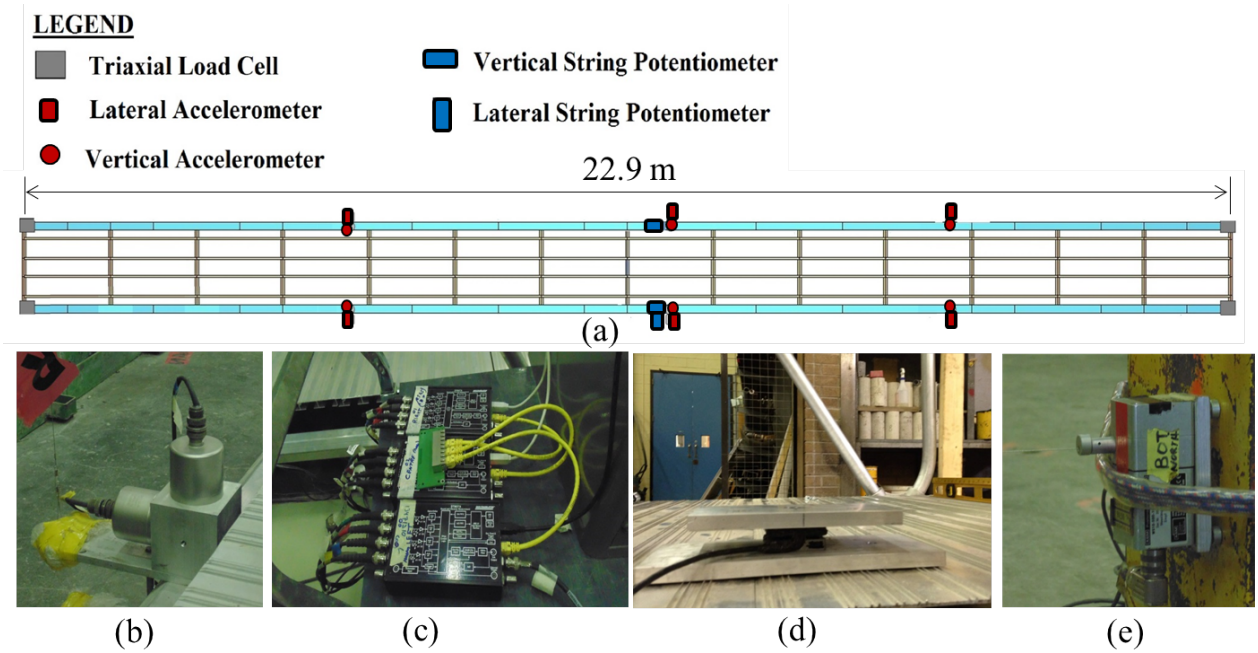

Figure 3.3: (a)Plan view of the bridge of length 22.9 m with locations for the instrumentation showing (b) accelerometers, (c) vibration data collection system (d) load cells, (e) displacement transducer

were conducted using three male and three female subjects (to minimize gender bias in walking characteristics). Their weights are listed in Table 3.2. All the tests were repeated 30 times for 5 sets of frequencies ranging from 1.67 Hz to 2.33 Hz with an interval of 0.167 Hz. Each test subject walked a total distance of 1.83 km during the course of testing. For the 22.9 m bridge, seven male and four female subjects participated in the walking tests. Their weights and the number of tests are listed in Table 3.3 for 5 sets of frequencies (1.67 Hz to 2.33 Hz with a interval of 0.167 Hz). Each test subject walked a total distance of 1.15 km to 3.4 km, depending on the number of trials completed.

Group walking tests on the two laboratory bridges included two people walking synchronously and asynchronously, and crowds of varying densities. The test matrices are reported in Tables 3.4 and 3.5 along with the average weights of the pedestrians who participated in this study. Each set of tests was repeated 30 times for the 12.2 m bridge while 10 to 30 trials of tests for each case were performed for the 22.9 m bridge specimen. Crowd densities of 0.2, 0.5, and 1.0 pedestrians per unit of deck area (P/m^2) were adopted for the tests on the 12.2 m bridge. However, the 22.9 m bridge specimen was not loaded beyond

Table 3.1: Physical and gait parameters of test subjects in the Daigneault Creek Bridge study

Test subject	Mass (kg)	Gender	Normal step frequency (Hz)
$P1$	97	Male	1.80
$P2$	89	Male	1.76
$P3$	72	Male	1.95
$P4$	68	Female	2.00
$P5$	65	Female	1.99

Table 3.2: Physical and gait parameters of test subjects in the 12.2 m bridge study

Test Subject	Mass (kg)	Gender	Number of Sets×Trials
$Q1$	89	Male	5×30
$Q2$	70	Male	5×30
$Q3$	65	Male	5×30
$Q4$	65	Female	5×30
$Q5$	64	Female	5×30
$Q6$	54	Female	5×30

0.7 P/m^2 crowd density due to excessive amplitude motions. In addition to uncontrolled walking tests (where pedestrians walked normally), controlled tests for two pedestrians around 2.0 Hz for the 12.2 m bridge and approximately 2.3 Hz for the 22.9 m bridge specimen were conducted in an effort to induce resonant conditions (with higher harmonics). Figure 3.4 shows example results from the walking tests on the 22.9 m bridge specimen during the experimental study.

3.1.4 Dynamic properties of the bridges

The modal parameters were extracted through a combination of modal testing and finite element analysis in SOFiSTiK® (Sychterz, 2014). The average natural frequencies were obtained using FFT of the free vibration responses for the bridges (Figure 3.5), by repeating the impact tests five times. Table 3.6 summarizes the first two vertical and lateral vibration modes predicted by modal analysis using free vibration testing (in brackets) and finite element models for the three bridge specimens. The mode shapes from the finite element models are shown in Figures B.1 to B.5 in Appendix B. It can be seen that for most of the cases the results from the experimental tests match the results from the finite element

Table 3.3: Physical and gait parameters of test subjects in the 22.9 m bridge study

Test Subject	Mass (kg)	Gender	Number of Sets×Trials
$R1$	125	Male	5×30
$R2$	106	Male	5×10
$R3$	86	Male	5×10
$R4$	77	Male	5×10
$R5$	70	Male	5×30
$R6$	70	Male	5×30
$R7$	70	Male	5×10
$R8$	64	Female	5×15
$R9$	60	Female	5×10
$R10$	59	Female	5×10
$R11$	45	Female	5×30

Table 3.4: Test matrix for 12.2 m pedestrian bridge

Tests	*Weights of pedestrians (kg)*			
	Mean	Standard deviation	Maximum	Minimum
Two persons	66.5	2.1	68	65
Crowd density of 0.2 P/m^2	69	14	89	53
Crowd density of 0.5 P/m^2	67	9.0	89	60
Crowd density of 1.0 P/m^2	68	14	90	41

analysis relatively well (see Table 3.6). The differences mainly arise due to the modelling assumptions (e.g. joint fixity) and the contributions to the overall stiffness from the deck, which was not included in the finite element models. For the current study, the first vertical and lateral frequencies from the modal tests are used for all of the bridges, as in all cases the lower order harmonics of walking only resonate with the fundamental frequency and the contributions from higher order modes are neglected.

Besides the modal frequencies and mode shapes, the damping ratio is an important parameter in order to estimate the response of the structure under pedestrian loading. For the 12.2 m and 22.9 m laboratory specimens, damping is estimated from impact tests using the simple free decay method (Humar, 2012) for the first vertical and lateral modes, as only these modes are important from a serviceability assessment standpoint. The details of the methods to estimate damping ratio are presented in Appendix C. The average damping ratios estimated for the bridge specimens are listed in Table 3.7. For the current analysis

Table 3.5: Test matrix for 22.9 m pedestrian bridge

Tests	*Weights of pedestrians (kg)*			
	Mean	Standard deviation	Maximum	Minimum
Two persons	67.5	3.5	70	65
Four persons	65	4.1	70	60
Crowd density of 0.2 P/m^2	72	7.5	82	65
Crowd density of 0.3 P/m^2	70	11.8	82	45
Crowd density of 0.5 P/m^2	71	10.8	82	45
Crowd density of 0.7 P/m^2	68	12.4	100	45

half of the total mass is assumed to participate in the first modes of vibration.

Table 3.6: Natural frequencies and mode shapes for the bridges through finite element analysis and modal testing

Daigneault Creek Bridge		*12.2 m Bridge*		*22.9 m Bridge*	
f_n(Hz)	Mode Shape	f_n(Hz)	Mode Shape	f_n(Hz)	Mode Shape
3.34(3.43)	Vertical	2.3(2.3)	Lateral	1.0(1.29)	Lateral
6.8(6.9)	Lateral	6.1(4.9)	Lateral	2.6(2.3)	Lateral
9.5(9.4)	Lateral	13.0(11.8)	Vertical	4.4(4.58)	Vertical
10.9(10.3)	Vertical	35.1(32.6)	Vertical	14.7(12.8)	Vertical

*Note: FE result is given along with result based on modal testing in brackets ()

Table 3.7: Damping ratio for the bridges through modal testing

Bridge	Vertical	Lateral
Daigneault Creek bridge	0.01	0.01
22.9 m lab specimen	0.008	0.033
12.2 m lab specimen	0.012	0.030

3.2 Performance of design guidelines

All of the design guidelines reviewed in the current study adopt a two-step approach as discussed in Section 2.2. When structural frequency is within the critical frequency

(a) (b)

Figure 3.4: (a) One pedestrian and (b) groups of pedestrians walking on the 22.9 m bridge specimen during the experimental study carried out in the Structures Laboratory at the University of Waterloo

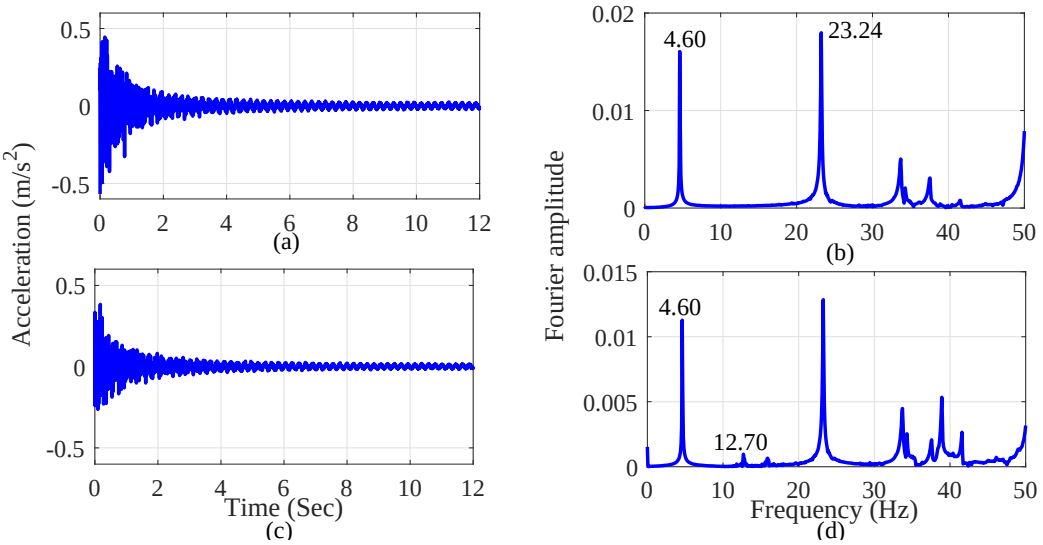

Figure 3.5: Acceleration time history ((a) and (c)) and corresponding Fourier spectrum ((b) and (d)) of impact testing at centre ((a) and (b)) and quarter (((c) and (d))) spans of the 22.9 m bridge specimen

ranges in Table 2.3, dynamic analysis is required to assess the serviceability of the bridges. Despite different functional forms used by these guidelines, the dynamic analysis is based on a common underlying idea that estimates of the response under N pedestrians (a_N) is obtained by multiplying the response due to a single pedestrian (a_s) with a multiplication factor (S_N):

$$a_N = S_N \times a_s \tag{3.1}$$

The multiplication factors S_N are summarized in Table 3.8. All the parameters in Table 3.8 are already defined in Section 2.2.

The structural response due to a single pedestrian a_s, is estimated from a moving concentrated force (P_{mov}) or a uniformly distributed force $p(x)$, which can be equivalently represented as a concentrated load of $p(x)L$. The periodic walking load is represented using Equation 2.1. The DLFs prescribed by the guidelines are summarized in Table 3.9. In this section, performance of the four guidelines, ISO 10137, Eurocode 5, British National Annex to Eurocode 1, and SÉTRA, are evaluated. First, this periodic load model is validated under single pedestrian walking trials employing the DLF values from Table 3.9. Next, the performance of the design methodologies are assessed in terms of serviceability assessment of the bridges as well as response predictions under groups of walking pedestrians.

Table 3.8: Multiplication factors for crowd loading used by existing guidelines

Codes	Vertical	Lateral
ISO 10137	$\sqrt{N}$	$\sqrt{N}$
Eurocode 5	$0.23k_{vert}N$	$0.18k_{hor}N$
British National Annex	$k(f_v)\sqrt{1+\gamma(N-1)}$ (Group)	–
	or $1.8k(f_v)\sqrt{\frac{\gamma N}{\lambda}}$ (Crowd)	–
SÉTRA	$10.8\sqrt{\zeta_n N}\psi_v$ for $d < 1.0$	$10.8\sqrt{\zeta_n N}\psi_l$ for $d < 1.0$
	$1.85\sqrt{N}\psi_v$ for $d \geq 1.0$	$1.85\sqrt{N}\psi_l$ for $d \geq 1.0$

3.2.1 Single pedestrian load model

Response simulation

This section focuses on evaluating the moving periodic models for single pedestrian walking on PBs. The performance study is restricted only to vertical vibration of the PBs and considers both resonant and non-resonant scenarios. In order to simplify the analytical

determination of the response, the pedestrian is assumed to walk on the structure at a uniform walking speed. Moreover, the structure is assumed to be linearly elastic. Hence, the modal equation of motion for the bridge response in Equation 2.24 corresponding to mode of vibration under consideration is employed. For the present study, the analytical solution, derived in Appendix A, based on the works by Abu-Hilal and Mohsen (2000) and Hilal and Zibdeh (2000), is adopted through employing the principle of superposition of responses from a constant moving load G and the harmonic loading terms $G\alpha_m \sin(m2\pi f_s)$ for m^{th} harmonic in Equation 2.24:

$$Y_n = X_n + \sum_{i=1}^{m} X_{mn} \tag{3.2}$$

where X_n and X_{mn} are the displacement response of the simply supported beam in Figure 2.12 under respectively constant and harmonic moving loads as derived in Appendix A. The acceleration response history $\ddot{Y}_n$ is then estimated by employing a second order derivation on Y_n.

Table 3.9: Dynamic load factors adopted by guidelines and standards

Codes	*vertical*	*Lateral*
ISO 10137	$\alpha_1 = 0.37f_s - 1.0$	$\alpha_1 = 0.10$
	$\alpha_2 = 0.1$	
	$\alpha_3 = \alpha_4 = \alpha_5 = 0.06$	
Eurocode 5	$\alpha_1 = 0.4$	$\alpha_1 = 0.1$
	$\alpha_2 = 0.2$	
British Annex to Eurocode 1	$\alpha_1 = 0.4$	$- - -$
	$\alpha_2 = 0.14^*$	
	$\alpha_3 = 0.051^*$	
SÉTRA	$\alpha_1 = 0.4$	$\alpha_1 = 0.05$
	$\alpha_2 = 0.1$	$\alpha_2 = 0.01$

*Note: The DLF values are corresponding to $k'(f_v)$

Response data processing

In order to evaluate the performance of the design walking load models in predicting the response of the PBs, only the modal response corresponding to the first mode of vibration of the bridge is considered. The measurements were first truncated to the forced vibration

phase only, and then low-pass filtered (with a cut-off frequency of 10 Hz in the case of the Daigneault Creek bridge and 15 Hz in the case of laboratory bridge specimens) in order to filter out the contributions of second and higher modes of vibrations. Then the measured and simulated acceleration time histories were converted to the frequency domain through Fourier transform (FFT). Figures 3.6 to 3.9 show the comparison of the acceleration time histories and corresponding Fourier spectra of the time histories at the centre of the Daigneault Creek Bridge for non-resonant (2 Hz) and near-resonant (1.75 Hz) conditions.

It can be seen from Figure 3.6 that the predictions overestimate the measurements both in terms of maximum and root mean square of acceleration. Furthermore, the guidelines are not consistent due to the different number of harmonics taken into consideration, as well as the different DLF values used. The Fourier spectra in Figure 3.7 show that the simulated response from the design models only contains contributions from the walking harmonics with negligible contributions from the transients (natural frequency of the structure). However, the response measurements contain contributions from both the transient and the excitation harmonics. In order to simulate the bridge responses, the walking load is assumed to be moving over the entire span of the bridge at constant speed and the transient part of the total response has sufficient time to decay, which leads to negligible contributions from the transients in the predicted response. But, in reality, the heel impacts the ground at the beginning of every step, leading to insufficient time to decay of the transients and hence significant contributions from the transients in the measured response. It is certain that the Fourier spectra are dominated by the resonating harmonic (second) for the near-resonant case, and the frequency characteristics of the predicted response by the design models in such cases agrees with the measurements. However, all the models overestimate the measurements in near-resonant conditions (Figure 3.8), which is expected for conservative design.

It is clear that application of the periodic load model results in the excitation harmonics (steady-state solution) dominating the response, with negligible contributions from the transient response. However, in all the three bridges tested in this study, it was observed that the transients are of the same order of magnitude or sometimes larger than the steady-state components. Since the bridges tested here were non-resonant (in their fundamental mode) with the the excitation frequency, a significant portion of the response must have been contributed by the transients. Hence, the response data was filtered to separate the contributions from various frequency components in the spectra after truncating to the forced vibration phase only, and then low-pass filtered, as discussed before. In order to enable a comparison between the simulated and measured responses, individual contributions from the harmonics (both natural frequency as well as excitation) are extracted from

the total response. For this purpose, the filtered response signal is assumed to contain a finite number of damped sinusoids and the modified Prony method based on total least squares approach (known as TLS-Prony) (Rahman and Yu, 1987) is used to estimate the magnitude, frequency, phase, and damping of the individual sinusoids. This method is more robust with respect to measurement noise as compared to the native form of the Prony's method (Hildebrand, 1956), and allows a better approximation of the response using damped sinusoids compared to the basic FFT approximation. The basic idea of the TLS-Prony method (Hildebrand, 1956; Rahman and Yu, 1987) is discussed in the following paragraph.

Assume that $x[n]$ is a sampled version of a equally-spaced time-series (e.g. acceleration). The Prony approximation consisting of M damped harmonics can be written as Hildebrand (1956):

$$y[n] = \sum_{k=1}^{M} h_k z_k^n \tag{3.3}$$

where, $h_k = A_k e^{j\psi_k}$ and $z_k = e^{(\alpha_k + j2\pi f_k)T_s}$. T_s is the sample time, f_k is the frequency in cycles per second, ψ_k is the phase of the k^{th} component, and α_k is the damping coefficient of the k^{th} component. The M-length vector A represents the amplitude of the damped sinusoids, yielding k^{th} contributions from the excitation and transient harmonics in the measured signals. These amplitudes directly yield the contributions from the harmonics of interest. The key steps in estimating these coefficients along with the frequencies, phase and damping coefficients are summarized in Appendix D.

As mentioned earlier, none of the three specimens are resonant in their lowest vertical mode with the first harmonic of pedestrian pacing frequency. However, they are in resonance, or nearly resonant, with the higher harmonics of the excitation frequency. The Daigneault Creek Bridge is nearly resonant (3.43 Hz) with the second harmonic of the walking frequency at 1.67 Hz and 1.75 Hz (slow walking), while the fundamental frequency of the 12.2 m bridge specimen (11.81 Hz) is close to resonance with the sixth and fifth harmonics of 2 Hz and 2.33 Hz walking frequencies, respectively. Similarly, the natural frequency of the 22.9 m bridge specimen (4.58 Hz) is close to the second harmonic of the walking frequency at 2.33 Hz (fast walking). While all three bridges would be considered as being relatively insensitive to pedestrian forces from a vertical flexural response standpoint, the peak vertical acceleration responses at the centre recorded during single pedestrian tests reached 0.5, 1.2, and 3.6 m/s^2 for the three bridges respectively (maximum for all tests conducted).

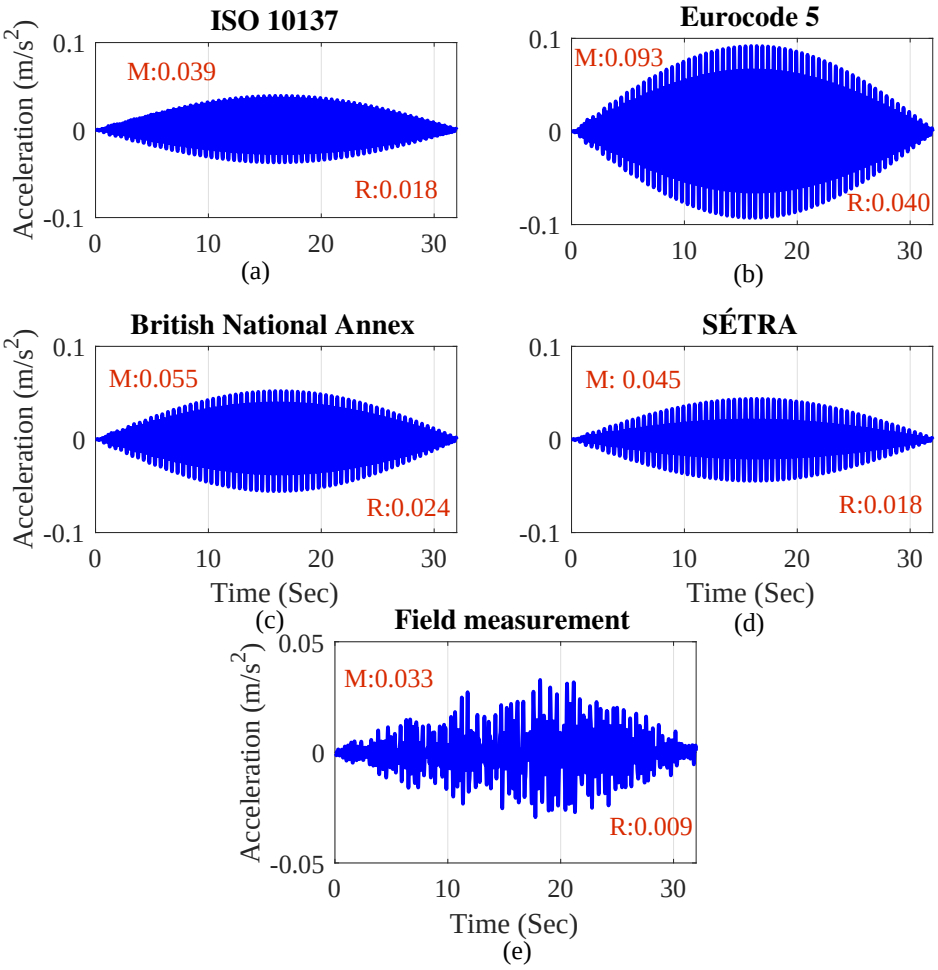

Figure 3.6: The acceleration time history at the centre of the Daigneault Creek Bridge for walking at 2.0 Hz in the case of simulated response using (a) ISO 10137, (b) Eurocode 5, (c) British National Annex, and (d) SÉTRA models and (e) field measurements (Here, M are R represents respectively the maximum and RMS accelerations)

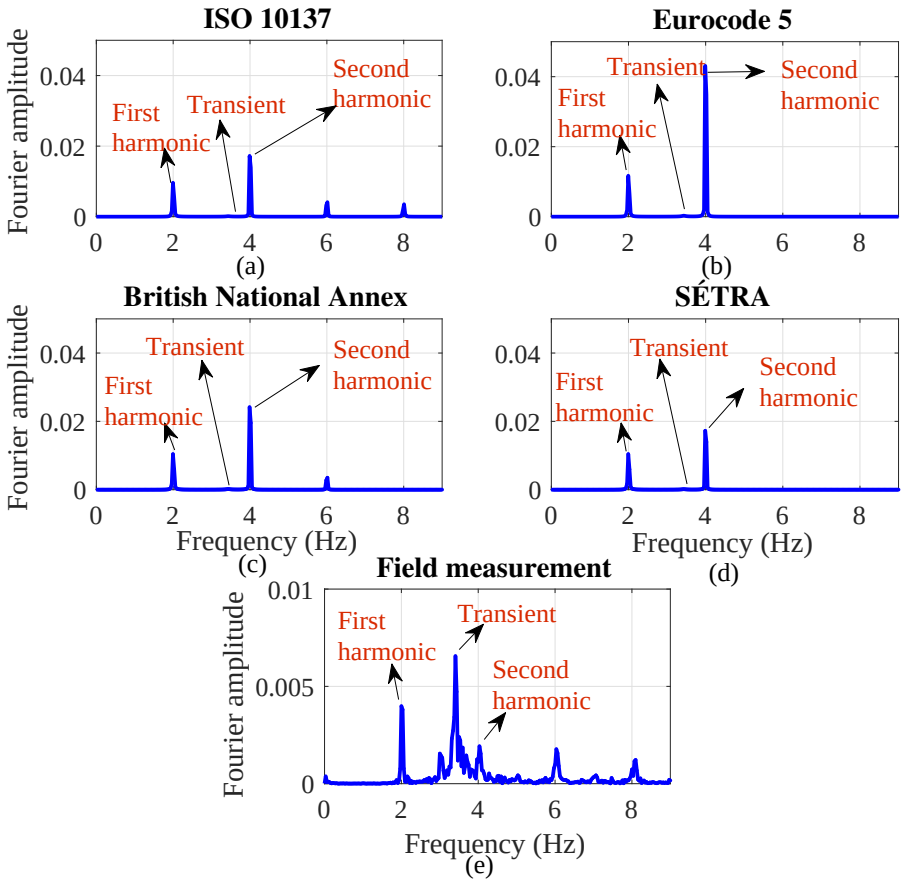

Figure 3.7: Fourier spectra of the acceleration response at the centre of the Daigneault Creek Bridge for walking at 2.0 Hz in the case of simulated response using (a) ISO 10137, (b) Eurocode 5, (c) British National Annex, and (d) SÉTRA models and (e) field measurements

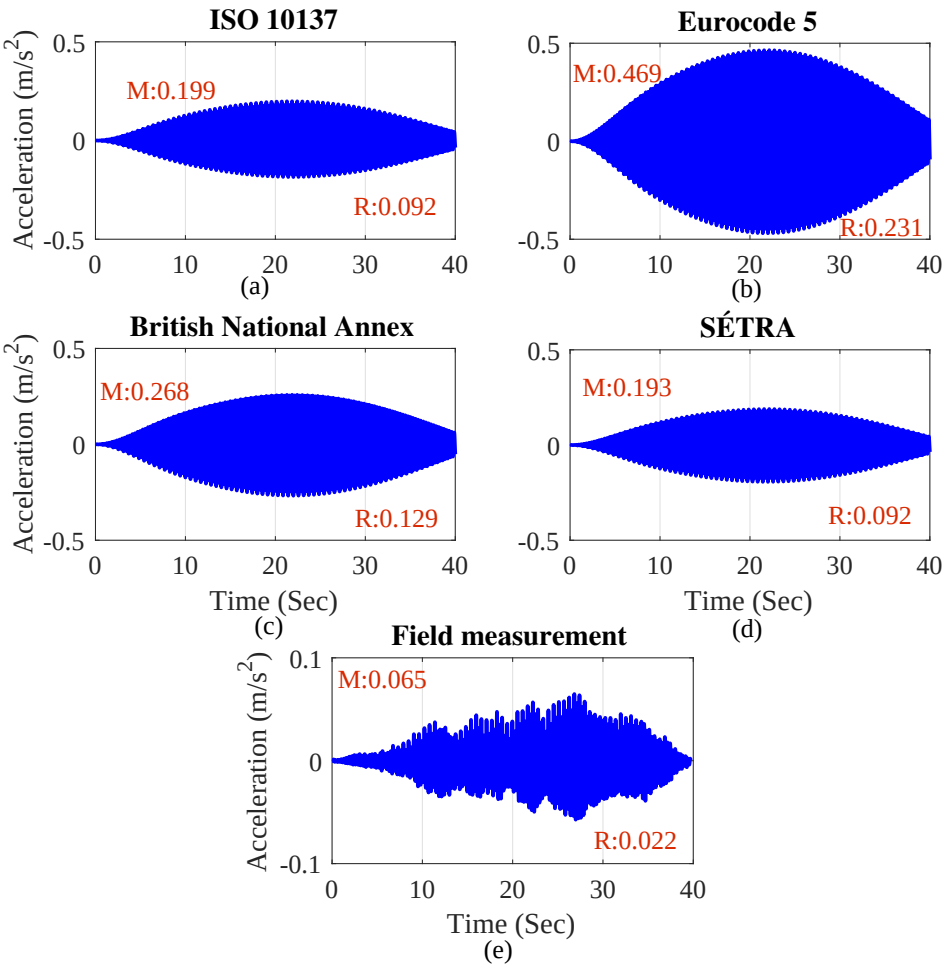

Figure 3.8: The acceleration time history at the centre of the Daigneault Creek Bridge for walking at 1.75 Hz in the case of simulated response using (a) ISO 10137, (b) Eurocode 5, (c) British National Annex, and (d) SÉTRA models and (e) field measurements (Here, M are R represents respectively the maximum and RMS accelerations)

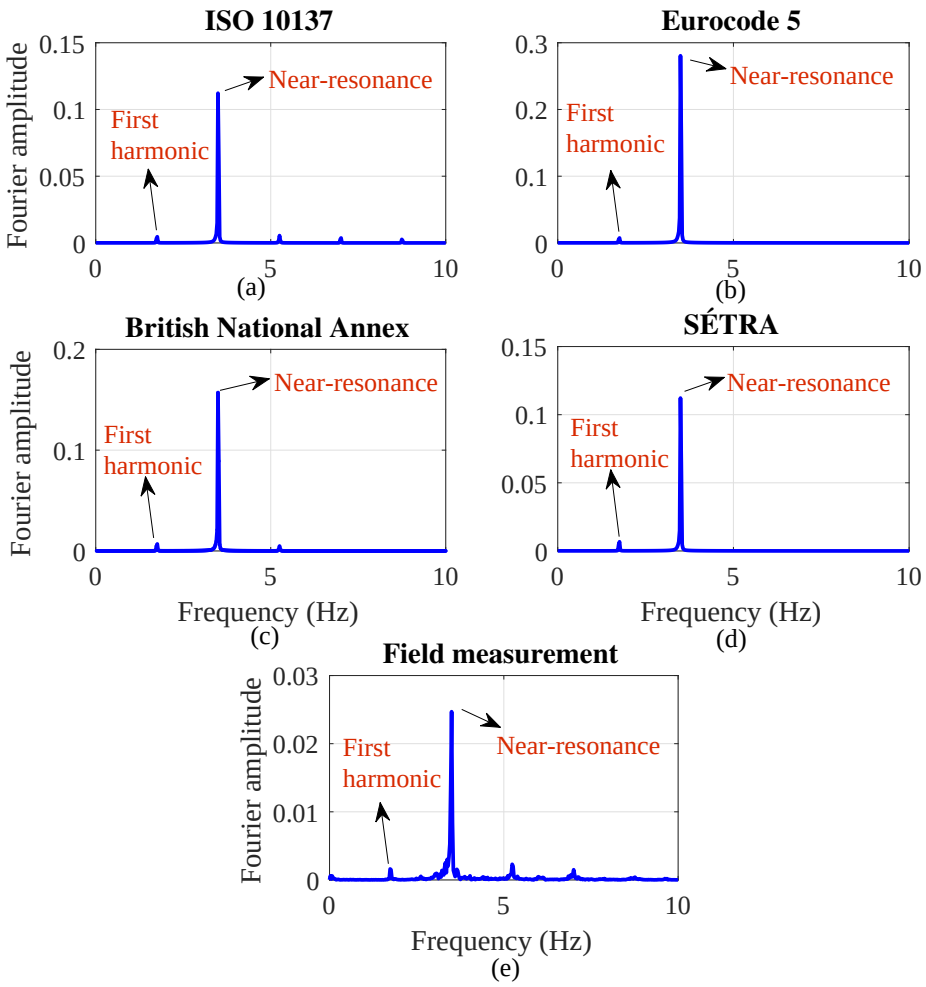

Figure 3.9: Fourier spectra of the acceleration response at the centre of the Daigneault Creek Bridge for walking at 1.75 Hz in the case of simulated response using (a) ISO 10137, (b) Eurocode 5, (c) British National Annex, and (d) SÉTRA models and (e) field measurements

Results from the Daigneault Creek Bridge

As described earlier, five test subjects walked naturally on the Daigneault Creek Bridge and their normal step frequencies are listed in Table 3.1. Moreover, test subject P5 walked at nine discrete frequencies ranging from 1.67 Hz to 2.33 Hz. 30 trials were conducted at each pacing frequency to ensure statistical significance. The mid-span vertical response of the bridge is simulated using the DLF values proposed by the design guidelines. Due to the near resonant condition with the second harmonic of the walking frequencies at 1.67 and 1.75 Hz, the contributions from the first two harmonics of the load along with the fundamental frequency of the bridge (3.43 Hz) are of interest. The amplitudes corresponding to these frequencies are estimated from the measured and simulated acceleration data using the TLS-Prony method.

Figure 3.10 compares the measured and simulated amplitudes corresponding to the frequencies of interest, i.e., the first two harmonics of the walking frequency and fundamental frequency, for the five test subjects walking at their normal walking frequency. The estimated amplitudes for the simulated and measured responses are normalized with the respective weight of the test subjects. It can be observed that the design models overestimate the measured response corresponding to the first two harmonics with relatively large deviations for subjects P1 and P2 for the second harmonic of walking frequency (Figure 3.10(b)), which produced near-resonant conditions from the second harmonic. Furthermore, the models significantly underestimate the contribution to the response from the natural frequency of the structure (Figure 3.10 (c)) and this trend has higher deviation for the non-resonant compared to the near-resonant cases.

Figure 3.11 shows the results of intra-subject variability for test subject P5 at different walking frequencies (1.67 Hz to 2.33 Hz), creating near-resonant conditions with the second harmonic of 1.67-1.75 Hz. Comparison of the amplitudes shows that the design models significantly overestimate the measured response contributions (Figures 3.11 (a) and (b)) from the first and second harmonics. The deviation corresponding to the second resonating harmonic (1.67-1.75 Hz) is larger, which was observed as well previously. However, both models are unable to capture the contribution from transients for the non-resonating walking frequencies (1.8-2.4 Hz) to the response (Figure 3.11 (c)). In these cases, there is significant natural frequency contribution to the overall response, which is not captured by the load models. So, an important observation is that the models, while conservative for the resonant region (in this case where the second harmonic matches the first flexural mode), tend to be unconservative in the non-resonant range.

In comparing the simulated amplitudes by all the design models, it is certain that all of the provisions are inconsistent with each other due to different values of DLF with those

by Eurocode 5 being overly conservative.

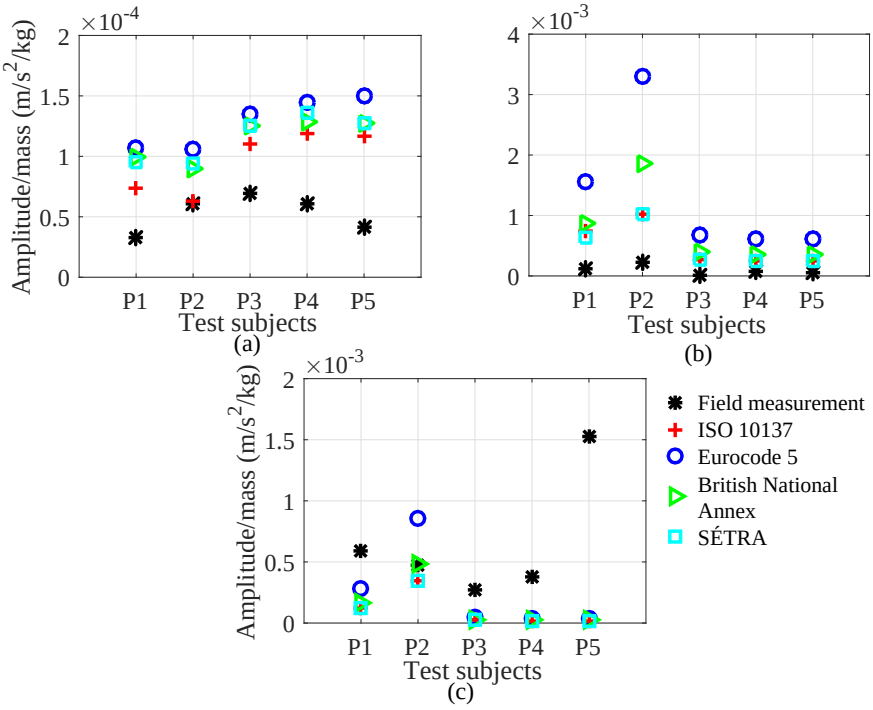

Figure 3.10: Comparison of simulated and measured amplitudes corresponding to: (a) the first harmonic, (b) the second harmonic, and (c) the fundamental frequency, in the case of Daigneault Creek Bridge

Results from the 12.2 m bridge specimen

For the 12.2 m bridge specimen, both inter- and intra-subject variabilities were considered using several trials with six test subjects (Table 3.2) at five sets of frequencies, 30 times each. A total of 900 records were processed considering both inter- and intra-subject variabilities. In this case, there is a possibility of near resonant condition with the fifth and sixth harmonics at 2.33 Hz and 2.0 Hz walking frequencies. Hence, the contributions to the total response from the first, fifth, and sixth harmonics of the excitation frequencies together with the fundamental frequency of the bridge (11.81 Hz) are considered. By applying the TLS-prony method on the simulated and measured acceleration data, the amplitudes corresponding to these frequencies of interest are extracted from the total

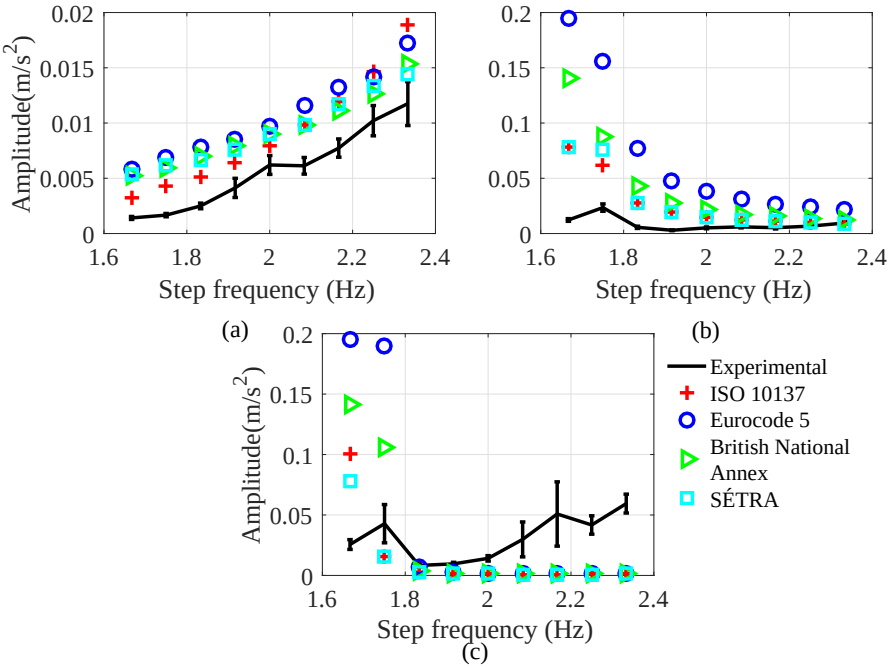

Figure 3.11: Statistical results for simulated and measured amplitudes corresponding to P5 for: (a) the first harmonic, (b) the second harmonic, and (c) the natural frequencies for the Daigneault Creek Bridge

response data series. The extracted amplitudes are normalized by the weight of each test subject and compared in Figure 3.12. Error bars from several trials are also plotted to represent both inter- and intra-subject variabilities.

Similar to the observations from the Daigneault Creek Bridge, all the design load models lead to a response that is dominated by the forcing frequency, with little contribution from the transients. Below 2 Hz, the model predictions and experimental results for the first harmonic follow closely because the DLFs used in the load models were developed for rigid surfaces, which in this case closely resemble a rigid structure with little or no pedestrian-structure interaction. However, for excitation frequencies where there is near-resonance in the higher harmonics (f_s between 2.0 and 2.33 Hz), the models significantly underestimate the acceleration response levels (Figure 3.12 (a)). It is noteworthy that only ISO 10137 includes five harmonics. Thus, other guidelines except ISO 10137 fail to estimate the response contributions from the fifth harmonic, which is near resonance at 2.33 Hz (Figure 3.12 (b)). Also none of the guidelines consider the contributions from the sixth

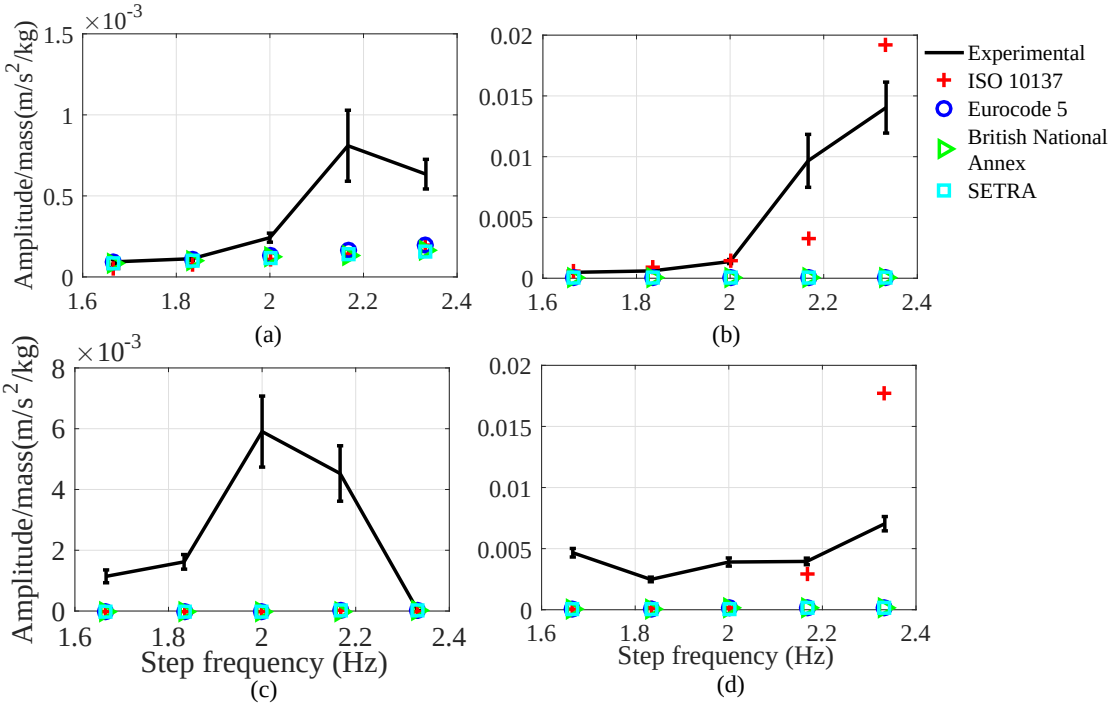

Figure 3.12: Comparison of contributions for simulated and measured amplitudes from the: (a) first harmonic (b) fifth harmonic, (c) sixth harmonic, and (d) natural frequency in the case of the 12.2 m bridge specimen

harmonic, which is near resonant with 2 Hz resulting in a significant contribution in the measured response (Figure 3.12 (b)). Moreover, the natural frequency contributions are significant in the measurements (Figure 3.12(d)) while all the design models lead to very little or negligible contributions at the natural frequency for non-resonating frequencies (1.6-2.0 Hz). It is also seen from Figure 3.12 (b) that there is significant natural frequency contributions in the design model for ISO 10137 for f_s between 2.1-2.33 Hz due to the near resonance condition with the fifth harmonic of walking.

Results from the 22.9 m bridge specimen

For the 22.9 m bridge specimen, eleven test subjects participated in the walking tests (Table 3.3). All of the test subjects were asked to walk at five sets of frequencies, 10-30 times each, as mentioned in the previous section. A total of 975 data series were recorded during this experimental study to cover inter- and intra-subject variabilities. As

the second harmonic for 2.17 Hz and 2.33 Hz walking frequencies are near the natural frequency of the structure (4.58 Hz), the amplitudes corresponding to the first and second harmonics of walking along with the fundamental frequency of the bridge are estimated from the measured and simulated acceleration data series through the TLS-Prony method. Moreover, the third harmonic contribution is also shown as an example of a case where the structure is not in resonance with the walking frequency or its harmonics.

As before, all the extracted measured and simulated amplitudes are normalized with respect to the weight of test subjects. Error bar plots of the measured amplitudes are compared with the simulated results in Figure 3.13. The structure is in a near resonant condition with the second harmonic of the faster walking rates. On the other hand, the structure behaves rigidly with respect to the pedestrian excitation for slower walking frequencies and hence the model predictions are near experimental observations. As the speed of walking increases, the walking harmonic becomes close to the structural frequency and thus, the structure exhibits pedestrian-structure interaction leading to a lower estimation of response contributions from the first two harmonics. This behaviour is also evident in the third harmonic using the British National Annex and ISO 10137, which include upto three harmonics in their predictions. On the other hand, Eurocode 5 overestimates contributions from the second harmonic as the corresponding DLF is almost twice compared to other guidelines. Similar to other cases, the simulated response shows very little contribution from the natural frequency component for the non-resonant condition.

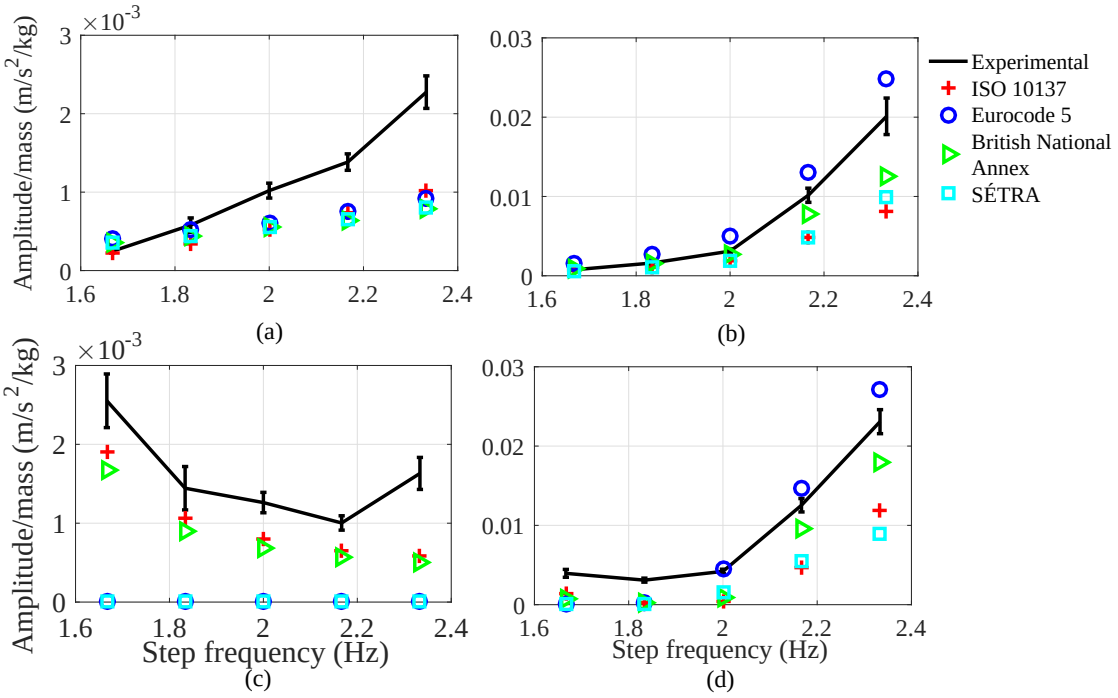

Figure 3.13: Simulated and measured amplitude contributions corresponding to the: (a) first harmonic, (b) second harmonic, (c) third harmonic, and (d) natural frequencies for the 22.9 m bridge specimen

Summary of key findings from single pedestrian studies

Three are three broad findings from a comparison study involving predicted and measured responses under single pedestrian walking:

1. The periodic load models adopted by the guidelines and standards fail to estimate the transient contributions (i.e. at the natural frequency of the structure) for non-resonating cases, while they significantly over-estimate the forced response for the resonant cases.

2. For the case of resonance with a higher harmonic, the contribution from the corresponding non-resonating harmonics are underestimated by the models, which may be due to pedestrian-structure interaction.

3. For a fully non-resonant case (i.e. none of the harmonics are in resonance with the excitation), the models estimate the observations relatively well.

These issues become very important for lightweight structures such as aluminum bridges, which tend to exhibit natural frequencies outside what is typically considered as design frequency ranges, however tend to be lively due to their low inherent damping and light weight. Hence, more sophisticated models that address these shortcomings are needed to better estimate serviceability in such cases.

3.2.2 Serviceability assessment under groups of pedestrians

Response estimation under a crowd is obtained by first estimating the response due to a single pedestrian and then multiplying it with a factor specified by the guidelines. Assuming that the bridges can be modelled as a simply supported beam where only one mode of vibration dominates, the maximum i^{th} mode resonant acceleration under a single pedestrian load can be estimated using the following equation:

$$a_{s,i} = \frac{P_i}{M_i} \frac{1}{2\zeta_i} \tag{3.4}$$

where, P_i, M_i and ζ_i are the generalized (modal) load, mass, and damping ratio of the structure. For an uniformly distributed load $p(x)$, the generalized load is given by $\frac{2}{\pi}p(x)L$ for the first mode of vibration and half of this value for the second mode of vibration. Similarly, the generalized load for a moving load P_{mov} for any mode is $\frac{2}{\pi}P_{mov}$. By replacing the modal load, the maximum acceleration under N pedestrians can be estimated from Equations 3.1 and 3.4 (removing the subscript i):

$$a_N = \frac{S_N G_n \alpha_{mn}}{\pi M_n \zeta_n} \tag{3.5}$$

where, n represents the characteristic value of the parameter suggested by the guidelines. The serviceability of the bridge is assessed through satisfying the following equation:

$$a_{ln} \geq a_N \tag{3.6}$$

None of the guidelines listed in Table 2.3 suggest performing a dynamic analysis for the 12.2 m bridge specimen in the vertical direction, with a frequency of 11.81 Hz, while its lateral frequency (2.30 Hz) falls within the critical range proposed by Eurocode 5 and SÉTRA, and thus a dynamic analysis is required. Similarly, all the guidelines recommend a dynamic analysis in the vertical (4.58 Hz) and the lateral (1.29 Hz) directions for the 22.9 m bridge. The maximum accelerations are estimated from either the formulae available in

the guidelines, or through Equation 3.5 if a suitable formulae is not available, followed by a serviceability assessment using Equation 3.6.

Figures 3.14 (a) to (c) show results from measurements for the 12.2 m bridge in the vertical direction for a density of 1.0 P/m^2. It is evident from Figures 3.14 (b) to (c) that there is a local concentration of vibration energy in the spectrogram around the 12 Hz range. This observation points towards near-resonant conditions prevailing with a higher harmonic of the walking frequency approaching the structural frequency in the 11.5-13.0 Hz range. A similar energy concentration is found in the measurements under other crowd densities (not shown here), while the spectral region containing the peak magnitudes become more concentrated with a decrease in the crowd density. Figures 3.14 (d)-(f) show the measurement results for the same bridge in the lateral direction. Unlike the vertical direction, lateral measurements show a more broad-band response with comparable response contributions from harmonics of the excitation frequency as well as the structural frequency, which is clearly a non-resonant case. As shown in the Figures 3.14 (e) and (f), 0.83 Hz and 2.67 Hz are respectively the first and third harmonics of the walking frequencies in the lateral direction, while 2.3 Hz is the structural frequency. Resonance conditions are difficult to achieve as it requires walking speeds that are unrealistic, especially in pedestrian groups. It is interesting to observe that the design provisions assume this bridge to be in resonance with the second harmonic of lateral walking frequency, which will result in overly conservative estimates of the design accelerations.

Similar to the 12.2 m bridge specimen, Figures 3.15 (a) and (f) are plotted for the 22.9 m bridge specimen for a density of 0.7 P/m^2. The spectrogram and the Fourier spectrum respectively in Figures 3.15 (b) and (c) show that the response of the bridge is non-resonant in the vertical direction. Resonance conditions are unlikely to occur as it requires walking frequency of the group to be near 2.3 Hz, which is difficult to achieve for this pedestrian density (Butz et al., 2008). Lateral synchronization around 1 Hz is also observed in Figures 3.15 (d)-(f). Groups of pedestrians drive the structural frequency (1.29 Hz) down to 1 Hz, which leads to a near resonance condition with the walking frequency.

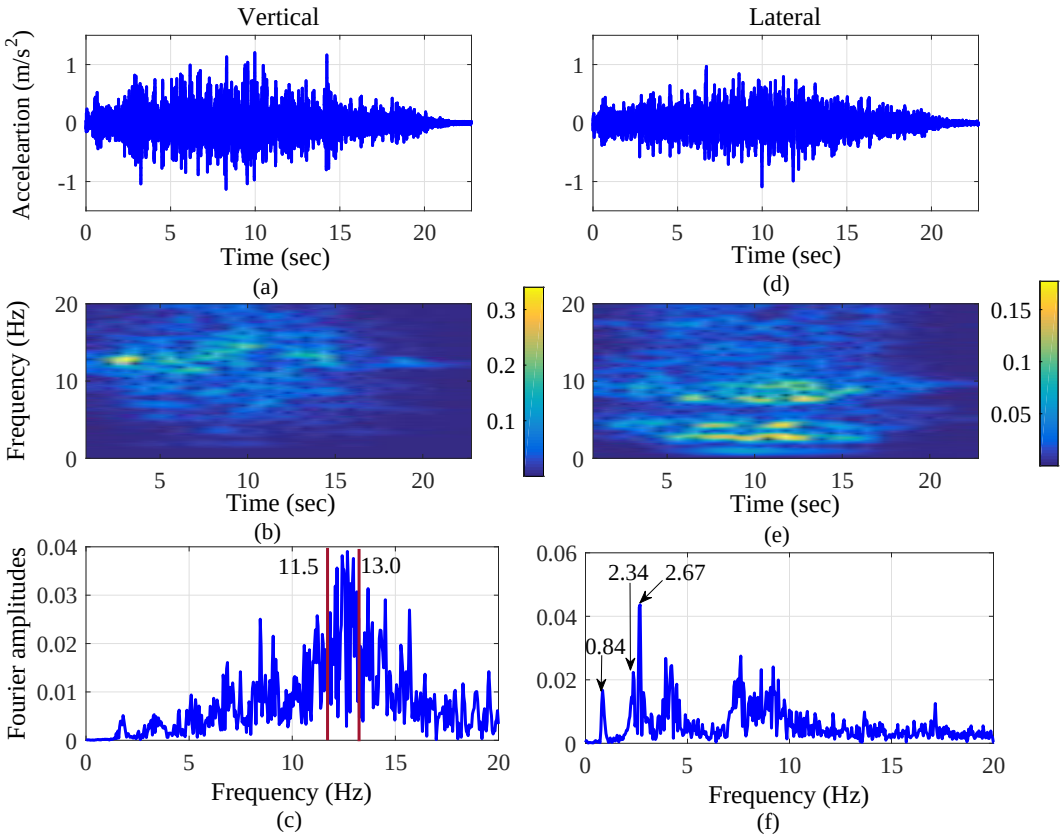

Figure 3.14: Results from the 12.2 m bridge specimen under 1.0 P/m^2 crowd density: (a) acceleration time history in the vertical direction at the center, (b) spectrogram, (c) Fourier spectrum, (d) acceleration time history for the lateral direction at the center and its corresponding (e) spectrogram, (f) Fourier spectrum.

The mean values for the measured peak accelerations and the corresponding standard deviations are listed in Table 3.10. Figures 3.16 and 3.17 show the serviceability results for the 12.2 m and 22.9 m bridge specimens in the vertical and lateral directions, respectively. The measured and simulated peak accelerations by the existing guidelines are plotted in these figures along with the critical acceleration limits as suggested in Table 2.4. The performance of each of the guidelines is discussed in detail in the following section.

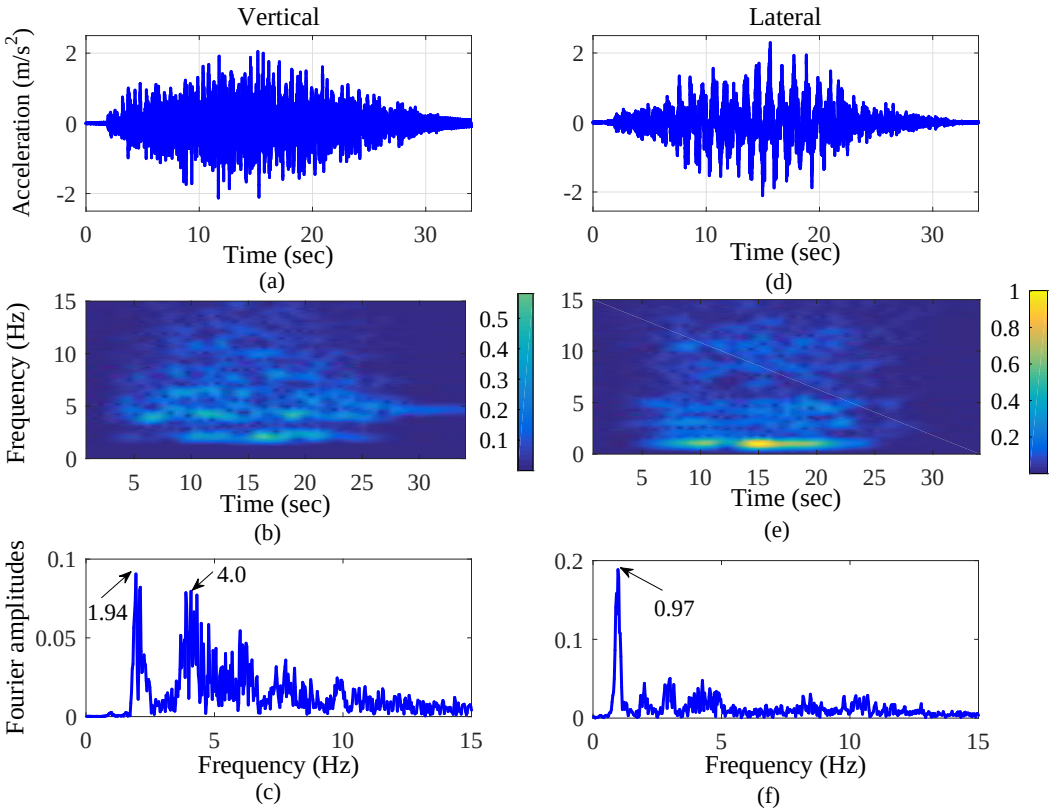

Figure 3.15: Results from the 22.9 m bridge specimen under 0.7 P/m^2 crowd density: (a) acceleration time history in the vertical direction at the center, (b) spectrogram, (c) Fourier spectrum, (d) acceleration time history for the lateral direction at the center and its corresponding (e) spectrogram, (f) Fourier spectrum.

Table 3.10: Mean and standard deviation for the experimental peak accelerations on the 12.2. and 22.9 m bridge specimens

Bridge Length	Walking Tests	Peak Acceleration in m/s^2			
		Vertical Direction		Lateral Direction	
		Mean	Standard Deviation	Mean	Standard Deviation
12.2 m	2 Pedestrians (Synchronous)	1.170	0.250	0.233	0.033
	2 Pedestrians (Asynchronous)	1.132	0.183	0.232	0.029
	0.2 Pedestrians/m^2	0.798	0.199	0.476	0.108
	0.5 Pedestrians/m^2	0.936	0.146	0.622	0.097
	1.0 Pedestrians/m^2	0.951	0.168	0.800	0.159
22.9 m	2 Pedestrians (Synchronous)	1.750	0.451	2.100	0.308
	2 Pedestrians (Asynchronous)	1.486	0.239	1.853	0.564
	4 Pedestrians	1.584	0.547	1.640	0.286
	0.2 Pedestrians/m^2	1.092	0.170	1.503	0.324
	0.3 Pedestrians/m^2	1.285	0.232	1.015	0.301
	0.5 Pedestrians/m^2	1.285	0.285	0.675	0.248
	0.7 Pedestrians/m^2	1.442	0.178	0.679	0.250

ISO 10137

ISO 10137 does not specify critical frequency limits directly and a dynamic response analysis is needed using the harmonic load model in Equation 2.6. However, it implicitly suggests dynamic analysis for the vertical and lateral frequencies up to 12 Hz and 1.2 Hz, respectively. Hence these values can be taken as the limits for frequency evaluation of the structures. In the vertical direction, both the structures are subjected to dynamic analysis as their frequencies are below 12 Hz, while no analysis is required in the lateral direction. Furthermore, this guideline uses root mean square (RMS) values for serviceability checks (Figure 2.8) instead of peak values, which are provided as a function of frequency. For comparison purposes with other guidelines, the current study adopts peak acceleration as the evaluation parameter in lieu of RMS acceleration. The RMS values for the limit acceleration in Figure 2.8 are converted to peak values by multiplying with a $\sqrt{2}$ factor (Živanović et al., 2005), while the peak values for the predicted and experimental accelerations are estimated directly without scaling.

Dynamic load factor coefficients are provided in Table 2.5 for the five harmonics in the vertical direction. As discussed before, either a full dynamic analysis including all the

harmonics or the resonant SDOF approach can be employed here for response estimation. Including all the harmonics in the calculations results in higher estimates for the response as compared to the resonant SDOF approach, which includes only the resonating harmonic. Results from both of these approaches (Equation 3.5 and the procedure described in Section 3.2.1) revealed that the difference between the two approaches is small, with deviations in the range of 4% to 12% under all crowd sizes. Hence, due to its simplicity, the resonant SDOF approach is adopted for further analysis.

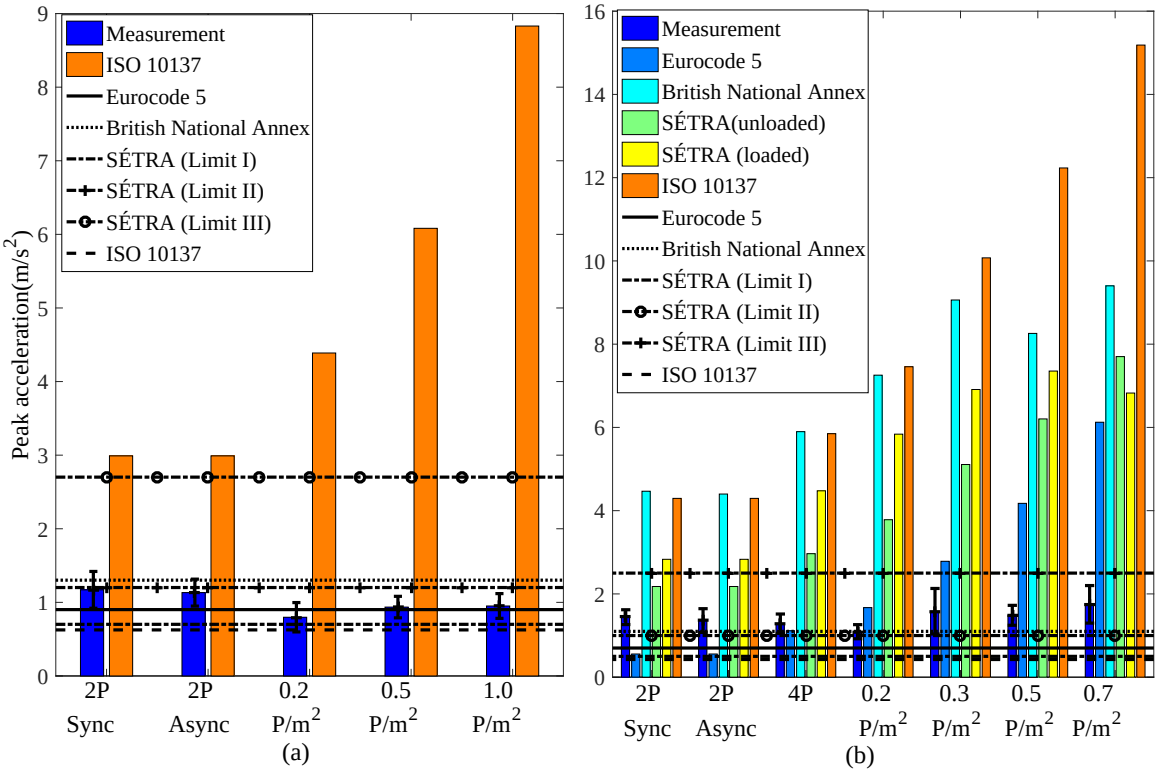

Figure 3.16: Comparison of measured and predicted peak accelerations along with the comfort limits as proposed by guidelines in the vertical direction for the (a) 12.2 m and (b) 22.9 m bridge (P stands for pedestrians; Limit I, Limit II and Limit III by SÉTRA guideline are defined in Table 2.4)

The specified acceleration limit in the vertical direction is 0.63 m/s^2 for the 12.2 m bridge specimen after converting the RMS acceleration to peak from Figure 2.8. As shown in Figure 3.16(a), both the measured and predicted maximum accelerations do not satisfy the specified limit for this bridge. Since no guidance is provided regarding the reduction of

walking speed as a function of the pedestrian density in this guideline, the fifth harmonic of pedestrian walking at 2.3 Hz is assumed to be in resonance with the first vertical frequency of the unloaded bridge (11.81 Hz). This leads to an overestimation of the predicted responses and the deviation increases with an increase in the crowd density (+156 % to +829 %). This increase in the deviation can be explained by a reduction in the effective walking frequency of the group of pedestrians with increasing density and a simultaneous reduction in the natural frequency due to the pedestrian added mass. Furthermore, the larger magnitude of the load factors α_m compared to the values provided in the recent literature (Brownjohn et al., 2004b) also contribute to this overestimation.

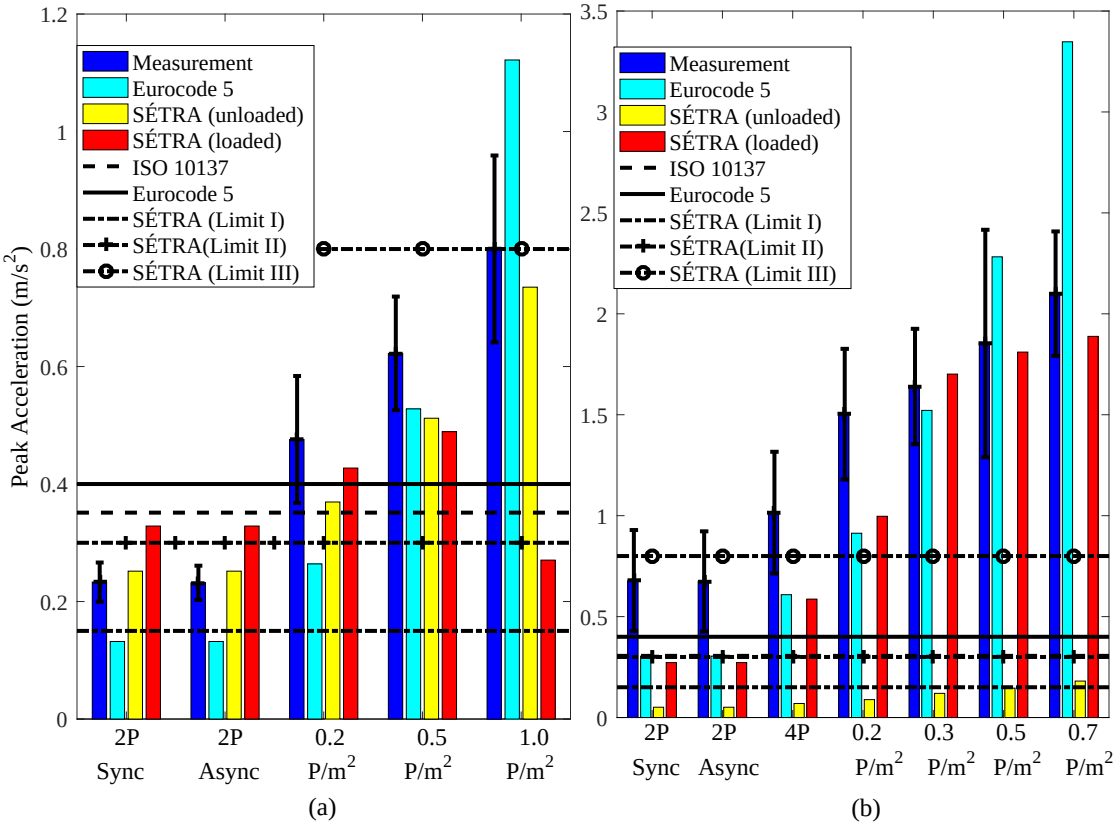

Figure 3.17: Comparison of measured and predicted peak accelerations along with the comfort limits as proposed by guidelines in the lateral direction for the (a) 12.2 m and (b) 22.9 m bridge (P stands for pedestrians; Limit I, Limit II and Limit III by SÉTRA guideline are defined in Table 2.4)

Similar characteristics are observed for the vertical mode of the 22.9 m bridge at 4.58 Hz, (Figure 3.16(b)). The vertical acceleration limit for this bridge is 0.42 m/s^2. This bridge does not satisfy the serviceability criterion, both as measured and as predicted. Furthermore, the guideline assumes a second harmonic of fast walking frequency resonating with the structural frequency. As with the 12.2 m bridge, the discrepancy between the measured and predicted peak accelerations increases with an increase in the crowd density (+198 % to +768 %). While near resonant condition with the second harmonic is observed for sparse density (two pedestrian cases) in the measured data, this does not occur as the density increases (at or beyond 0.7 P/m^2).

The lateral frequencies for both the 12.2 m and the 22.9 bridge specimens (2.3 Hz and 1.29 Hz, respectively) are outside the range of the first harmonic of walking (only the load factor for the first harmonic is provided for the lateral direction). As a result, this bridge cannot be assessed for serviceability according to ISO 10137. However, measurements exceed the vibration limit specified by ISO 10137 under all traffic conditions for both bridges, except for the two pedestrians walking cases (Figure 3.17(a)) for the 12.2 m bridge specimen.

Eurocode 5

The vertical frequency of the 12.2 m bridge specimen (11.81 Hz) falls outside the critical range of 5 Hz (Table 2.3). The limit acceleration prescribed by this guidelines is 0.7 m^2/s and although not explicitly stated, this limit is assumed to apply to frequencies $\leq$ 5 Hz. Hence, this limit is not applicable for the 12.2 m bridge. Hence, this vibration limit is extended beyond 5 Hz by applying the slope of the ISO 10137 curve (Figure 2.8(a)) beyond 8 Hz. This extended vibration limit is then compared with the measured values and shown in Figure 3.16(a). The results show that the serviceability limit falls within the measurement range for all cases. However, they are very close to being considered unserviceable.

As the vertical frequency of the 22.9 m bridge specimen (4.58 Hz) falls below 5 Hz (Table 2.3), a dynamic analysis is required to asses its serviceability. In Figure 3.16(b), both the measurements as well as the predictions show that this bridge does not pass the serviceability check. Starting with under-estimating the peak response for two pedestrians (with deviations around −50 %), the discrepancy between measured and predicted values increases with increasing density (+8 % to +337 %) (good agreement for the case of four pedestrians). Along similar lines to ISO 10137, resonance with the second harmonic (walking frequency around 2.3 Hz) is considered for the prediction, which does not occur as the density increases (at or beyond 0.7 P/m^2). The walking speed decreases as the density

increases and hence near resonance with the third harmonic of slow walking frequency is most probable rather the second harmonic. Furthermore, the deviations between measured and predicted values for Eurocode 5 are lower compared to ISO 10137. Even though both ISO 10137 and Eurocode 5 follow the same approach of multiplying the response obtained from a single moving pedestrian load with a factor, this discrepancy arises because of the multiplication factors in Equations 2.7 ($C(N)$ or $\sqrt{N}$) and 2.8 ($0.23k_{vert}N$). The factor in Eurocode 5 is smaller in magnitude compared to ISO 10137 for this specimen under all the traffic cases considered here. Furthermore, the use of a moving load model representing the behaviour of light traffic does not adequately capture dense crowds and hence results in large deviations with respect to the measurements for such cases.

As the lateral frequency (2.3 Hz) for the 12.2 m bridge falls below the critical frequency of 2.5 Hz, it requires a serviceability assessment for the 12.2 m bridge. Except for the 0.2 P/m^2 crowd density, the serviceability predictions are in good agreement with the observations (Figure 3.17(a)). However, the peak responses are underestimated in most cases except for the 1.0 P/m^2 case. These deviations range from -43 % to $+40$ % with increasing crowd size, with the minimum error for the 0.5 P/m^2 case. The multiplication factor in Equation 2.10 ($0.18k_{hor}N$) is the he main contributing factor for these deviations. This factor results in unconservative estimates in the lateral direction, unlike the vertical direction with mostly conservative predictions. Furthermore, Eurocode 5 uses a single equation for the lateral direction for all frequencies below 2.5 Hz (Equation 2.11) and thus a single dynamic load factor coefficient is used for both first and second harmonics. However, literature (Ricciardelli and Pizzimenti, 2007) has shown that the DLF corresponding to the second harmonic should be lower. The predictions also do not account for the reduced natural frequency from the mass of the pedestrians for higher density cases.

Similar conclusions from the 12.2 m bridge can be drawn for the 22.9 m bridge (lateral frequency of 1.29 Hz), except for the case of two pedestrians where the standard fails to predict a serviceability issue (Figure 3.17(b)). In terms of peak response predictions, the deviations in the predicted responses from measurements range from -55 % to $+59$ % with increasing density, and the predictions are in good agreement with the measurements for 0.3 to 0.5 P/m^2 crowd densities. Except for the case of high density, the responses are generally unconservative in nature.

British National Annex to the Eurocode 1

The vertical frequency of the 12.2 m bridge specimen (11.81 Hz) falls beyond the frequency limit of 8 Hz (Table 2.3). Assuming k_1 to be 1.0 for major urban cities, k_2 to be 1.0 for primary route and k_3 to be 1.1 for a bridge with height $<$ 4 m, the limit acceleration is

estimated to be 1.1 m /s^2 from Equation 2.5. Similar to the Eurocode 5, this limit is applicable below the critical frequency of 8 Hz. Hence the extended limit is estimated as 1.3 m/s^2 by accounting for the frequency dependency beyond 8 Hz based on the ISO 10137 curve in Figure 2.8(a). Comparing this limit with the measured peak response in Figure 3.16(a), it is observed that the measurements fall just below the limit in most cases, which means that the bridge is serviceable according to this standard. As the limit proposed by this standard depends on various qualitative factors, the extended limit could vary and perhaps exceed the vibration limit.

The vertical frequency of the 22.9 m bridge specimen (4.58 Hz) falls below the critical frequency of 8 Hz and thus dynamic analysis is performed in accordance to the proposed moving concentrated (Equation 2.12) or uniformly distributed (Equation 2.13) load models in the vertical direction. A crowd density of 0.7 P/m^2 nearly occupied the entire bridge deck area uniformly and hence Equation 2.13 is used to estimate the response. On the other hand, the moving load model in Equation 2.12 is applied to lower densities when the pedestrians crossed the bridge together in a group. Both the models estimate similar levels of response under 0.7 P/m^2. As shown in Figure 3.16(b), both the measured and predicted responses cross the limit acceleration and thus this bridge does not meet the serviceability limit. Similar to other guidelines, the peak responses are significantly over-estimated, with deviations in the range of 10 % to 65 %. Furthermore, the predicted design response is nearly the same as ISO 10137 for low densities ($\leq$ 0.2 P/m^2) and the discrepancy between the two provisions increases with an increase in the group size beyond 0.2 P/m^2 crowd density. While both the British National Annex and the ISO 10137 adopt the same basic load model (Equation 2.12 and Equation 2.6) and nearly equal magnitudes for the DLFs, the differences arise mainly in the effective number of pedestrians or the multiplication factors (S_N) in Table 3.8. ISO 10137 adopts $\sqrt{N}$ as the effective number of pedestrians, while Equation 2.12 recommends $\sqrt{1+\gamma(N-1)}$. Figure 2.10(b) shows that the factor γ tends to be 1.0 as the number of pedestrians N decreases. This explains the similarity in their predictions for low densities. However, as the group size increases, γ reduces leading to the observed differences.

This guideline suggests serviceability assessment of bridges through a stability criterion. The 2.3 Hz lateral frequency of the 12.2 m bridge satisfies the stability requirement in the lateral direction, which is not the case for the 22.9 m bridge (1.29 Hz). Hence, the stability of this bridge is ascertained though the mass damping parameter D in Equation 2.14, which considers the instability of structure under lateral lock-in phenomenon. Along the same lines of the critical number of pedestrians defined by Dallard et al. (2001), the mass damping factor D specifies the triggering boundary for lateral lock-in through the stability curve in Figure 2.10(c). Lateral instability is assumed to occur when the mass damping factor

cancels the inherent structural damping leading to large amplitude responses. Comparing D with the stability boundary in Figure 2.10(c), the structure is expected to be unstable in all traffic conditions, starting from the two pedestrians case. However, during the experimental study, lateral lock-in was not observed for lower crowd sizes. Very large amplitude responses were observed for higher densities, especially for the 0.7 P/m^2 case (average peak acceleration of 1.75 m/s^2 for the 22.9 m bridge).

SÉTRA

The vertical frequency of the 12.2 m bridge (11.81 Hz) falls outside the critical range between 1.0 Hz to 5.0 Hz according to the SÉTRA guideline. Hence, this bridge need not be analyzed for serviceability. Unlike other guidelines, SÉTRA proposes four comfort levels (maximum, mean, minimum, and unacceptable) as defined in Table 2.4. Although not mentioned explicitly, these limits are applicable within the critical frequency ranges. Hence, the slope obtained from the ISO 10137 curve in Figure 2.8(a) is used to extrapolate the limit acceleration for the 12.2 m bridge. In doing so, the measured peak acceleration in Figure 3.16(a) falls in the minimum or mean comfort class while SÉTRA assumes that this bridge is serviceable at a maximum comfort level.

The vertical frequency of the 22.9 m bridge (4.58 Hz) falls within the critical range (1.0 Hz to 5.0 Hz) and with reference to Table 2.6, it belongs to Range 3 (i.e., very low chance of resonance). Table 2.7 suggests that Load Case 3 (i.e., crowd complement to the second harmonic) is applicable for loads $\geq$ 0.8 P/m^2, while dynamic analysis is not required below 0.5 P/m^2. The experimental studies were performed to a maximum crowd density of 0.7 P/m^2, which according to this guideline satisfies the criteria for not requiring dynamic analysis. However, comparing the measurements with the limits in Figure 3.16(b) it is clear that this bridge falls below the minimum comfort class, which means the bridge is essentially un-serviceable. For dynamic analysis, the design methodology is assumed to be independent of the traffic classes mentioned in Table 2.7 and only dependent on the frequency range in Table 2.6. As the structural frequencies corresponding to the loaded (with added mass from pedestrians) and unloaded (without pedestrian mass) configurations fall under Range 3, Case 3 (second harmonic effect) is applicable. As shown in Figure 3.16(b), the predicted bounds of peak responses (unloaded and loaded) overestimate the measurements, with deviations ranging from 51 % to 340 % for the unloaded case and 96 % to 290 % for the loaded case. Furthermore, the predicted bounds for the peak response are lower than the ISO 10137 and British National Annex, but higher than Eurocode 5. Although this guideline assumes a uniformly distributed pulsating load rather than a moving load, both these models theoretically produce similar magnitudes of response for

the first mode of vibration through Equation 3.5. Moreover, all the guidelines follow the same basic harmonic load model with comparable dynamic load factors. The discrepancy between these guidelines primarily arise due to the effective number of pedestrians used in the calculations. The variation in the predicted magnitude of response for the loaded versus unloaded configurations range from +54 % to −11 %. This variation in trends between the loaded and unloaded cases arises due to the response reduction factor ψ_v (Figure 2.11(a)), which is a function of the natural frequency modified by the contribution of the pedestrians to the overall modal mass.

The first lateral mode of the 12.2 bridge (2.3 Hz) is below 2.5 Hz and corresponds to Range 3 for the frequency in both loaded and unloaded configurations. Although Table 2.7 does not require a dynamic analysis for densities $\leq$ 0.5 P/m^2, Figure 3.17(a) shows significant vibrations leading to a loss of serviceability. Applying Case 3 for analysis, the serviceability predictions are very close to measurements under all traffic classes except for very dense crowd (1.0 P/m^2) as shown in Figure 3.17(a). However, the predicted peak response is underestimated for all crowd densities in the range of 0.2-1.0 P/m^2. The deviations range from +8 % to −8 % without considering the added mass of pedestrians, while they are higher with the added mass, in the range of +41 % to −66 %. The discrepancy between the two bounds is mainly due to the magnitude of ψ_l and the mass contribution from the pedestrians. Comparing the predicted response with Eurocode 5 for the unloaded case, the estimates from SÉTRA tend to be un-conservative for higher densities while estimates from Eurocode 5 tend to be conservative for dense crowds, as shown in Figure 3.17(a). The multiplication factors, $\psi_l n_{eq}$ in Equation 2.16 for the SÉTRA guideline and $0.18 k_{hor} N$ in Equation 2.13 for Eurocode 5 are the main contributing factors for this trend.

The lateral frequency for the unloaded 22.9 m bridge (1.29 Hz) belongs to Range 2 and thus no analysis is required by this guideline for density $\leq$ 0.5 P/m^2. As before, predictions are made for these crowd densities irrespective of the traffic class. The added mass of the pedestrians drives the structural frequency from Range 2 to Range 1 for densities $\geq$ 0.5 P/m^2. Figure 3.17(b) shows that the serviceability predictions are valid for crowd density $\geq$ 0.2 P/m^2 in the loaded case. However, this is not true for the unloaded case. Furthermore, the measurements are underestimated in both the unloaded and loaded cases. While the deviations are very high for the unloaded case (−94 % error), they range from −60% to −10% for the loaded case with an increase in the density. Similar conclusions from the 12.2 m bridge regarding the effect of ψ_l and the added mass from the pedestrians can also be drawn regarding the discrepancies observed for the 22.9 m bridge. Moreover, the predictions from the unloaded case is lower than Eurocode 5. As with the 12.2 m bridge, the multiplication factors are the main source for these discrepancies.

Summary of key observations from crowd loading studies

The key observation from a comparison study of measured and predicted results using four guidelines under groups of pedestrians are as follows:

1. In general, the predicted vertical responses by the guidelines are conservative, while the this is not the case for the lateral direction.
2. All of the standards employ a basic load model with different multiplication factors, which is the primary reason for their different serviceability outcomes by the guidelines.
3. The DLFs used by a majority of these guidelines need to be re-visited, either using more recent studies or through a recalibration procedure.
4. A sufficient number of harmonics should be incorporated, especially for high frequency bridges.
5. The DLFs used are not uniform across the guidelines even though the basic modelling approach and assumptions are largely aligned.
6. The guidelines do not consider traffic dependent average walking speed in a group, and as a result there is ambiguity in selecting the appropriate harmonic for resonance.

Based on these observations, it is clear that the guidelines should be improved so that they are reconciled amongst each other and also with the measurements. An attempt is made in **Chapter 5** to improve the serviceability assessment of the guidelines based on these observations.

Chapter 4

Reliability-based evaluation of design provisions

In this chapter, the design guidelines considered in the current study are evaluated in a reliability-based framework. First, a brief overview on the sources of uncertainties in the design methodologies from different sources are presented. Then, a reliability analysis is conducted incorporating these uncertainties in the serviceability limit state function, followed by investigating them in terms of achieving sufficiency and uniformity. A sensitivity study is also performed to investigate the impact of assumed uncertainty models of key design variables on the overall reliability embodied in the design guidelines.

4.1 Sources of uncertainty

All of the design guidelines covered in the current study consider a deterministic model to predict the resonant response of a bridge for a given design traffic density. As discussed in Section 2.1.3, a probabilistic treatment of pedestrian excitation has already been undertaken by incorporating uncertainties in the parameters corresponding to pedestrian excitation. For example, the multiplication factors in the deterministic models by SÉTRA or the British National Annex to Eurocode 1 are derived by taking into account the uncertainties in the pedestrian arrival time, pacing frequency, step length, and weight. However, they do not account for the uncertainties in the structural properties or the human perception to structural motion. Moreover, none of the existing guidelines have been evaluated for their ability to achieve sufficient and uniform reliability levels across designs and traffic

conditions. Hence, the current study investigates the performance of serviceability-based limit state design provisions by the four guidelines considered here in a reliability framework by incorporating all of the sources of uncertainties in Equation 3.6, which can be rewritten by introducing the expression for a_N from Equation 3.5:

$$a_{ln} \geq \frac{S_N G_n \alpha_{mn}}{\pi M_n \zeta_n} \tag{4.1}$$

In Equation 4.1, the potential sources of uncertainty arise from the pedestrians and the structure itself. The pedestrians constitute both the source of excitation through the imposed walking loads (G and α_m) and the receiver whose comfort levels are the determining factor for the limit acceleration (a_l) (to represent the random variables, subscript 'n' is removed). The random variables associated with the serviceability design equation (4.1) are discussed further in the following sections.

4.1.1 Uncertainties in the pedestrian load

As discussed in Section 2.1.3, the randomness in the pedestrian load is mainly due to the variability in the step frequency (f_s) and the magnitude of the dynamic force as a portion of pedestrian's weight (G), which is calculated by multiplying G with the DLF, α_m. As the design for serviceability is performed assuming resonance, the step frequency becomes deterministic for the appropriate resonating harmonic.

All the guidelines considered here assume a characteristic magnitude of 700 N for the pedestrian's weight (G_n), based on the average weight of the population. As mentioned in the literature (Portier et al., 2007), this magnitude varies with age, geographical location, and gender. Hence, it is reasonable to consider variability in this parameter. The uncertainty model for a mean weight of 700 N is adopted from the literature, assuming a log-normal distribution with a coefficient of variation (COV) 0.17 from the study on distribution of weight based on different regions and groups by Portier et al. (2007). The probability density function of G is shown in Figure 4.1 (a).

None of the guidelines in Table 3.9 specify whether the prescribed characteristic values (α_{mn}) are means or percentiles. Based on footfall force measurements on 40 test subjects, Kerr (1998) proposed mean DLFs for the first harmonic with confidence intervals as a function of the step frequency. For a mean step frequency of 2.0 Hz, the mean DLF is 0.40, which is close to the values adopted by Eurocode 5, the British National Annex, and SÉTRA. The first harmonic in ISO 10137 bears close resemblance to the mean DLF value proposed by Willford et al. (2006). Hence the DLF values in Table 3.9 are assumed to be

the mean DLF values. Moreover, both of these studies have observed significant scatter in the DLF values. Based on Kerr's data, the first DLF harmonic is normally distributed with a COV of 0.16, while Willford et al. (2006) reported a value of 0.17. Both observed large scatter in the DLF values corresponding to higher harmonics, with a COV of 0.40. Based on these studies, the current study adopts a COV of 0.17 for the first harmonic and 0.40 for the higher harmonics, with a normally distributed probability density function. The PDFs for DLFs corresponding to first two harmonics are shown in Figure 4.1 (b). Galbraith and Barton (1970) showed an interdependence between G and α_m, however, they could not quantify this dependency and assumed the two variables to be independent. Similarly, the current study considers G and α_m as independent variables.

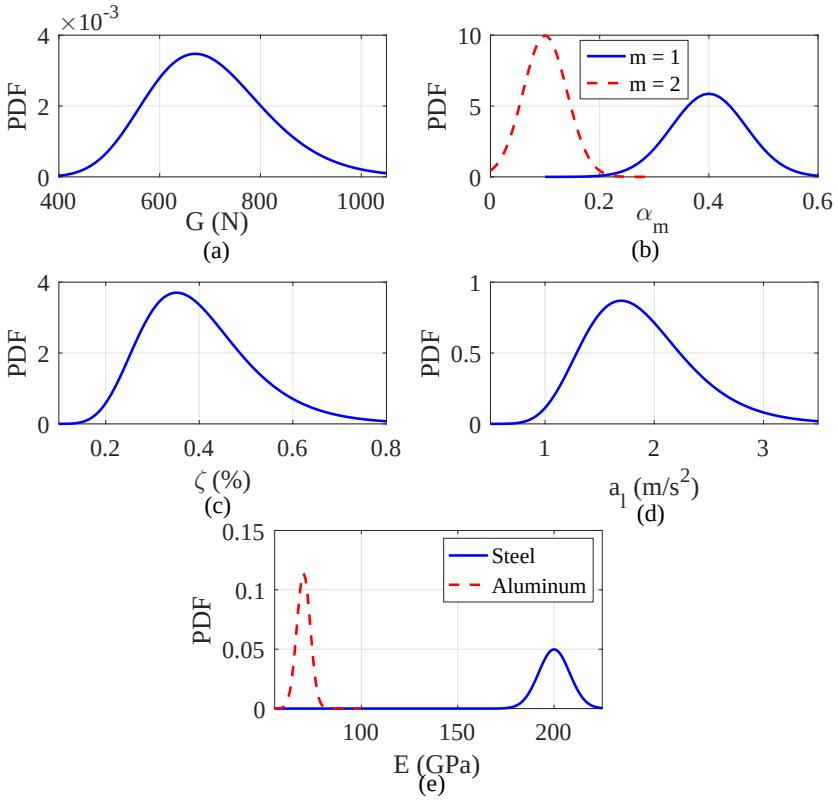

Figure 4.1: Probability density function (PDF) of: (a) pedestrian's weight (G); (b) DLF (α_m); (c) damping ratio (ζ); (d) limit acceleration (a_l), and (e) elastic modulus (E)

4.1.2 Uncertainties in the limit acceleration

The reaction of a human to vibration is a very complex phenomenon. There is no consensus on what these limits should be and this is reflected in the large degree of variability in the values adopted by the guidelines, as evidenced by the characteristic values for the limiting acceleration (a_{ln}) in Table 2.4. Considering the large inter- and intra-subject variabilities, treating the limiting acceleration (a_l) as a random variable is a critical aspect of the serviceability assessment. To the best knowledge of the author, a probabilistic treatment regarding human perception levels, a_l, in PB applications is not available in the literature. However, a number of studies have attempted to quantify the acceptable levels of acceleration under building vibrations using both motion simulators and full-scale studies (Chen and Robertson, 1972; Hansen et al., 1973; Irwin, 1975; Kanda et al., 1988). The limiting acceleration curve for residences in ISO 10137 is similar to the 90$^{\text{th}}$ percentile curve in AIJES-V001, which represents a perception threshold, not a tolerance limit. In comparing the maximum vertical limiting acceleration of 0.6 m/s^2 at 2 Hz in ISO 10137 with other guidelines, the limiting accelerations in the Eurocode 5 (0.7 m/s^2) and the lower comfort limits in the British National Annex and SÉTRA (0.5 P/m^2) appear to be similar. Hence the values in Table 2.4 for these guidelines are assumed to be the 90$^{\text{th}}$ percentile values. With an absence of an uncertainty model for a_l, it is assumed to be log-normally distributed with a COV of 0.20 for the current analysis, as adopted by Bashor et al. (2005) for the serviceability assessment of high-rise buildings. Figure 4.1(d) shows the PDF of a_l corresponding to the 90$^{\text{th}}$ percentile or a characteristic value of 2.5 m/s^2 .

4.1.3 Uncertainties in the structural properties

Dynamic properties such as mass (M_n), stiffness (K_n), natural frequency (f_n), and damping (ζ_n) are key to a reliable estimation of the structural response under dynamic excitation. The current practice is to determine mass (M_n), stiffness (K_n), and natural frequency (f_n) through a finite element (FE) model with prescribed boundary conditions. In order to keep the set of variables manageable, the current study is limited to truss types (pony/through), with simply-supported end conditions only. However, it is believed that the main conclusions from this study can be generalized to other PB types as well.

Simply supported truss bridges can be represented as Euler-Bernoulli beams with simply supported end conditions, where the n^{th} natural frequency can be estimated using:

$$f_n = \frac{n^2\pi}{2L^2}\sqrt{\frac{EI}{m}} \tag{4.2}$$

where E is the elastic modulus of material, I is the second moment of area, m is mass per unit length, and L is the span of the bridge. For the first mode of vibration, the modal mass (M_n) is given by $\frac{mL}{2}$.

The geometric properties such as length (L), width (W), height (H), and the cross sectional areas (A) of structural members are assumed to be deterministic, while uncertainties are introduced in the estimation of I and m. The current analysis assumes I and m to be normally distributed with a COV of 0.05. Two materials, steel and aluminum, are considered with elastic modulii (E) and properties as listed in Table 4.1. The PDF of E for these two materials are plotted in Figure 4.1 (e). The yield strength (f_y) of steel and aluminum are assumed to be 300 MPa and 240 MPa, respectively. The mass densities of these materials are assumed to be 7600 kg/m^3 and 2700 kg/m^3, respectively.

Table 4.1: Statistical properties of elastic modulus for different structural material

Structural material	*Distribution type*	*Mean* (E_m)	*COV* (E_v)	*Reference*
Steel	normal	200 GPA	0.04	Vrouwenvelder and Siemes (1987)
Aluminum	normal	70 GPA	0.05	assumed

Besides stiffness and mass, another important dynamic parameter in vibration evaluation is the damping ratio (ζ), which quantifies the energy dissipation capacity in a structure while undergoing motion. The average damping ratios adopted by the guidelines are listed in Table 4.2 for PBs constructed out of steel or aluminum. Due to its dependency on the connection type and the amplitude of vibration, damping is very difficult to quantify accurately. Hence the code prescribed characteristic values of damping (ζ_n) often do not represent the actual damping of a structure, and it is logical to consider it as an random variable. There are very few studies (Cunha et al., 2005; Reynders et al., 2016) on estimation of damping for PBs, which show large scatter (COV in the range of 0.10-0.50) in the damping estimation. Since damping has not been studied extensively in the context of PBs, the damping ratio is assumed to be log-normally distributed with a COV of 0.30, based on studies performed on building structures (Bashor et al., 2005). A parametric study is then performed in order to investigate the sensitivity of the adopted COV and distribution type on the estimates of reliability index.

Table 4.2: Average damping ratios for steel/aluminum

Design Codes	*Damping (%)*
ISO 10137	0.5
Eurocode 5	—
British National Annex	0.5
SÉTRA	0.4

4.2 Range of design variables

4.2.1 Structural configurations

In order to quantify the level of reliability embodied in the existing guidelines, ranges of design parameters in terms of structural configurations and traffic scenarios are considered to reflect the design space of variables. For this purpose, the design configurations of PBs are established based on descriptions of the geometric properties of PBs around the world (Adeli, 2016). Four length to width ratio combinations are considered: $L/W = [10, 15, 20, 25]$, along with six widths: $W = [1.0, 1.5, 2.0, 2.5, 3.0,$ and 4.0 m$]$. Two length to height ratios (L/H) are considered, depending on the length of the bridge. If $L \leq 20$, L/H is $(0.602L - 0.724)$ and $(0.394L - 0.417)$. For $20 < L \leq 40$, L/H is 10 and 12. For $L > 40$, L/H is 12 and 18. The cross sectional areas (A) for the top and bottom chords are assumed to be the same, with 16 configurations ranging from 0.001 to 0.04 m^2. The cross sectional areas of the diagonals are assumed to be equal to that of the chords. Two configurations for deck thickness are assumed: 0.018 and 0.035 m. The second moments of area (I_n) in the vertical and lateral directions are estimated as $\frac{4AH^2}{4}$ and $\frac{2AW^2}{4}$, respectively.

4.2.2 Design traffic

The design traffic corresponding to serviceability design is the normal traffic on a bridge, i.e., frequently occurring traffic scenarios such as daily commuters. Serviceability limit state (SLS) design does not consider the extreme or rare design events, unlike ULS design. As discussed in Section 2.2, most of the guidelines except Eurocde 5 account for normal traffic sizes, which vary based on the routes and usage of the PBs. In general, the normal traffic size may range from sparse (around 0.2 P/m^2) to very dense or heavy traffic (around 1.0 P/m^2) depending on the usage and route. The probable traffic levels to be considered for designing different PB classes by the guidelines have already been reviewed in Section 2.2, which are summarized again here in Table 4.3. ISO 10137 does not provide any specific

design traffic size but points to the situations to be considered for the design. Eurocode 5 suggests a 0.6 P/m^2 density or 13 distinct pedestrians in a group. The British National Annex and SÉTRA specify four traffic classes depending on usage, ranging from seldom used (negligible crowd density) to frequently used (heavy traffic).

Table 4.3: Traffic classes in various guidelines

Codes	*Traffic class*
ISO 10137	
Case I (8 to 15 P)	average pedestrian flow
Case II (>15 P)	streams of pedestrians
Case II	occasional festive or choreographic events
Eurocode 5	13 (group) or 0.6 P/m^2 (crowd)
British National	
Annex to Eurocode 1	
Class A (2 P or 0 P/m^2):	rural locations seldom used
Class B (4 P or 0.4 P/m^2):	suburban location with occasional variations in pedestrian loading intensity
Class C (8 P or 0.8 P/m^2):	urban routes subject to significant variation in daily usage
Class D (16 P or 1.5 P/m^2):	primary access to major public assembly
SÉTRA (2006)	
Class I (1.0 P/m^2):	urban PB subjected to very heavy traffic frequently
Class II (0.8 P/m^2):	urban PB with occasionally loaded throughout bearing area
Class III (0.5 P/m^2):	PB for standard use, that will never be loaded throughout its bearing area
Class IV:	seldomly used PB (no dynamic assessment)

Besides frequently occurring traffic, a PB can be subjected to rare or in-frequent traffic. This may occur once in the lifetime of the bridge, e.g., during inauguration, sometimes with densities around 1.5 P/m^2 (Very heavy traffic), or periodically due to re-occurring events. Even though rare traffic is typically not considered in SLS design, it can still result in significant economic losses (e.g., the LMB incident in 2001). On the other hand, designing solely based on such rare events may not be economical. To overcome such issues, comfort classes or limiting accelerations (a_{ln}) based on the expected occurrence of the design traffic have been proposed (Heinemeyer et al., 2009). The choice of comfort class is flexible and depends on the owner. However, this idea has not yet been adopted by most

standards. ISO 10137 and Eurocode 5 use a single limiting acceleration (a_{ln}), while the British National Annex proposes a_{ln} based on site usage, route redundancy and the height of structure, which implicitly takes care of the traffic size based on PB class. SÉTRA adopts four different comfort classes (Table 2.4), but does not consider traffic dependent comfort criteria. In the current study, the mean comfort classes for pedestrians, $a_{ln} = 1.0$ m/s^2 (vertical) and $a_{ln} = 0.3$ m/s^2 (lateral) in Table 2.4, are assumed for the reliability analysis based on SÉTRA.

As reported in Table 4.3, there is a large variation in the traffic classes based on the usage recommended by various standards. The British National Annex and SÉTRA provide four PB classes. However, the specified design densities corresponding to these classes are not consistent and furthermore, these standards neglect design densities less than 0.4 P/m^2 (British National Annex) and 0.5 P/m^2 (SÉTRA). The current study adopts SÉTRA crowd densities of 0.5-1.0 P/m^2. Additionally, a new class corresponding to 0.2 P/m^2 is introduced in the current study. All of the structures are designed for the specified design density corresponding to the class and the reliability results in each class are generated including results for other crowd densities expected during the lifetime of the structure, such as rare events with a density of 1.5 P/m^2. The calculation of reliability indices and corresponding results are presented and discussed in the following sections.

Table 4.4: PB classes and corresponding traffic sizes for the reliability analysis

PB class	*Traffic situations*	*Crowd density (P/m^2)*
Class I	PB for seldom use	0.2
Class II	PB for standard use in suburban area	0.5
Class III	urban PBs with occasionally loaded throughout the bearing area	0.8
Class IV	urban PBs linking the major public assembly	1.0

4.3 Calculation of reliability index

Reliability analysis starts with formulating the limit state function encompassing the design random variable space. For the SLS design of PBs under excessive vibration through Equation 3.6, the limit state function $g(\mathbf{X})$ by the existing design guidelines can be written as:

$$g(\mathbf{X}) = a_l - \frac{2S_N(E, I, m, \zeta)G\alpha_m}{\pi L m \zeta} = 0 \tag{4.3}$$

where, the multiplication factor (S_N) (refer to Table 3.8) is a function of E, I, m, and ζ for the British National Annex and SÉTRA. For Eurocode 5, it depends on E, I, and m, while for ISO 10137, it is a constant. $\mathbf{X}$ is the vector of random variables consisting of $[a_l,\ G,\ \alpha_m,\ \zeta,\ E,\ I,\ m]$ for all of the guidelines except ISO 10137, which only considers $[a_l,\ G,\ \alpha_m,\ \zeta,\ m]$. The limit state function $g(\mathbf{X})$ defines the boundary dividing the failure and safe domains, given by:

$$\begin{aligned} \Pi_f &= \mathbf{x}|g(\mathbf{x}) \leq 0 \\ \Pi_s &= \mathbf{x}|g(\mathbf{x}) > 0 \end{aligned} \tag{4.4}$$

where Π_f and Π_s are, respectively, the failure and safe domains. The failure probability is evaluated using:

$$P_f = P[g(\mathbf{x}) \leq 0] = \int_{\Pi_f} f_{\mathbf{x}}(\mathbf{x}) d\mathbf{x} \tag{4.5}$$

The failure probability is related to the reliability index (β) by the following expression (Cornell, 1969):

$$P_f = \Phi(-\beta) \tag{4.6}$$

A total of 1536 geometric configurations are analyzed and only those configurations passing the ultimate limit state design check for bending, as well as the serviceability checks, were retained for the ensuing reliability analysis. The steps of the analysis are as follows:

1. **Static design check:** Given the material properties and section geometry, a quick check for the ultimate bending stress is performed to exclude any failing combinations from the 1536 geometric configurations for each material. The bending stress is calculated under the factored dead (self-weight) and pedestrian induced live load (CAN/CSA S6, 2011) and subsequently compared with the factored critical limit stress ($0.9 f_y$) for the material.

2. **Serviceability design check:** For those designs retained in Step 1, the fundamental frequency is estimated through Equation 4.2 and compared with the critical ranges in Table 2.3. Serviceability design checks (Equation 3.5) are performed for those falling within these critical limits under design loading conditions for the assumed PB classes. To better understand the level of economy reached, a design factor is defined here as follows:

$$\phi_s = \frac{a_l}{\frac{2 S_N G_n \alpha_{mn}}{\pi L m_n \zeta_n}} \geq 1.0 \tag{4.7}$$

For optimally designed structures through Equation 3.5, this factor should be close to 1.0 and an increase in this factor means higher reliability. The current study focuses only on the optimally designed configurations, hence ϕ_s is restricted between 1.0 to 1.1 during the deterministic design check.

3. **Reliability evaluation:** The optimally designed configurations are retained for the reliability analysis. Three standard techniques are employed for the calculation of β: Monte Carlo simulation (MCS), the advanced first-order second-moment (AFOSM) and the second-order reliability method (SORM). The MCS calculation is considered as the benchmark and the indices obtained using the more computationally efficient AFOSM and SORM are compared with the results obtained using MCS.

The reliability index (β) calculated using AFOSM is also known as the modified Hasofer and Lind reliability index (Hasofer and Lind, 1974; Rackwitz and Flessler, 1978). A detailed review of the steps to estimate β using this method are well documented in texts, e.g., in Nowak and Collins (2012). At its core, this method involves converting all non-normal distributions of random variables to equivalent normal distributions through the Rackwitz-Fiessler procedure (Rackwitz and Flessler, 1978), followed by a transformation of the random variables to the standard normal space using:

$$z_i = \frac{x_i - \mu_{x_i}}{\sigma_{x_i}} \tag{4.8}$$

where the search for the most probable point or the design point is performed (z_i^*). In this equation, x_i is the random variable with mean and standard deviation as μ_{x_i} and σ_{x_i}. β is estimated through iterative procedure, which requires solving the following $(2n+1)$ simultaneous equations with (2n+1) unknowns, $\beta, \alpha_1, \alpha_2, ..., \alpha_n, z_1^*, z_2^*, ..., z_n^*$:

$$\alpha_i = \frac{-\frac{\partial g}{\partial z_i}|_{z_i^*}}{\sqrt{\sum_{i=1}^{n}(\frac{\partial g}{\partial z_i}|_{z_i^*})^2}} \tag{4.9}$$

$$z_i^* = \beta\alpha_i \tag{4.10}$$

$$g(\mathbf{X}) = 0 \tag{4.11}$$

with, $i = 1, 2, ..., n$. The derivatives of the limit function with respect to each basic variable in the reduced space are evaluated at the design points (z_i^*) to estimate the sensitivity coefficients (α_i), which represents the weightage of each random variable in the limit function.

The current study follows the matrix procedure presented in Nowak and Collins (2012) to estimate β.

AFOSM is generally acknowledged to be the simplest reliability analysis method, however it approximates the curvature of the nonlinear limit state function by using only a first-order approximation at the minimum distance point. Hence the accuracy of this method depends on the degree of nonlinearity of the limit state in the vicinity of the minimum distance point. Through including the second-order terms, SORM improves the reliability calculations compared to AFOSM. In the current study, the closed-form solution for estimating the second order reliability index using the theory of asymptotic approximations is adopted (Breitung, 1984), which is given by:

$$\beta_{SORM} = -\Phi^{-1}[\Phi(-\beta_{AFOSM}) \prod_{i=1}^{n-1}(1 + \beta_{AFOSM} K_i)^{-1/2}] \tag{4.12}$$

where, K_i denotes the principal curvatures of the the limit state function at the minimum distance point and is estimated as the eigen values of matrix A, whose elements a_{ij} are defined by:

$$a_{ij} = \frac{(RDR^t)_{ij}}{|G|}, \quad \text{where,} \quad i, j = 1, 2, ..n-1 \tag{4.13}$$

Here, D is the $n \times n$ second-derivative matrix of the limit state function estimated in the standard normal space evaluated at design points, R is the rotation matrix, and $|G|$ is the length of the gradient vector (first order differentiation of the limit state function with respect to the random variables) in the standard normal space.

Both AFOSM and SORM require that the limit function in Equation 4.3 to be smooth and differentiable admitting up to and including second order derivatives. The factors k_{vert}, k_{hor}, $k(f_v)$ and ψ (ψ_v or ψ_l) in Figures 2.9, 2.10 and 2.11 are not smooth functions with respect to the structural frequency, f_n, which is again a function of E, I, and m (Equation 4.2). This issue is addressed by performing the reliability analysis region-wise, on the frequency scale. First, the appropriate resonant harmonic is selected for evaluation based on the mean frequency of the structure and the appropriate mean values of α_m are selected. $k(f_v)$ in Figure 2.10(a) is smooth and continuous function of structural frequency within the frequency ranges corresponding to a particular harmonic (e.g., $f_n \leq 2.8$ for first

harmonic) and can be approximated using smooth polynomials as follows:

$$k(f_v) = \begin{cases} -0.07128f_n^7 + 0.6776f_n^6 - 2.202f_n^5 + 2.464f_n^4 & \\ +0.4139f_n^3 - 1.779f_n^2 + 0.8538f_n - 0.1049 & \text{if } f_n \leq 2.8 \\ -0.03033f_n^5 + 0.6949f_n^4 - 6.116f_n^3 + 25.7f_n^2 & \\ -51.31f_n + 39.67 & \text{if } 2.8 < f_n \leq 5.6 \\ 0.05376f_n^3 - 1.128f_n^2 + 7.48f_n - 14.95 & \text{if } f_n > 5.6 \end{cases} \tag{4.14}$$

k_{vert}, k_{hor}, and ψ are not smooth for the entire range of frequencies corresponding to a particular harmonic. Rather, they are piece-wise linear functions for different ranges within a particular harmonic region. For example, ψ_v in Figure 2.11 (a) is not smooth and continuous in the range $1.0 \leq f_n \leq 2.6$ of first harmonic, but piece-wise linear function of f_n in the ranges $1.0 \leq f_n \leq 1.7, 1.7 \leq f_n \leq 21$ and $2.1 \leq f_n \leq 2.6$. Hence, reliability analysis is conducted within the linear zones corresponding to these variables. Furthermore, these factors approach zero, e.g., ψ_v in Figure 2.11 (a) at $1.0, 2.6$, or $5.0\ Hz$. In order to avoid numerical issues resulting from the regions close to zero, their values are assumed to be very small instead of exactly zero.

Unlike other guidelines, SÉTRA estimates the response of a PB with and without the added mass of pedestrians. Hence two values of responses (a_N in equation (3.4)) are calculated using this guideline and the maximum of the two responses is used for serviceability design check. Similarly, the reliability index β is also estimated with and without considering the added mass of pedestrians, β_1 and β_2 respectively and the minimum of these two β values is retained for analysis, i.e.,

$$\beta = min(\beta_1, \beta_2) \tag{4.15}$$

4.4 Reliability analysis

4.4.1 Reliability-based design criteria

In reliability-based design, codes and standards are generally evaluated based on two criteria: *sufficiency and uniformity* over the range of designs covered by the respective codes and standards. The sufficiency criterion requires designing to an acceptable level of safety, usually represented by the target reliability index, β_t, while the uniformity criterion ensures uniform reliability of β_t across all the designed applications. The issue of determining target SLS reliability levels for PBs has not been studied in the literature. Generally applicable

target reliability indices for SLS failures are available, e.g., EN 1990 (2001) recommends a β_t of 2.9 (for a 1 year reference period) and 1.5 (for a 50 year reference period) for medium consequence of irreversible serviceability failures. ISO 2394 (1998) recommends two values of β_t: 1.5 for irreversible and 0 for reversible events, independent of the expected frequency of occurrence of the design load for serviceability analysis. Irreversible SLS means that there are some permanent consequences expected when the actions are removed (e.g., permanent local damage or deformation), while this is not true for the reversible case (e.g., temporary deformation, excessive vibration). Based on these definitions, β_t should be assumed zero in the current context according to ISO 2394. Clearly, even reversible incidents such as the LMB accident have shown that serviceability failures of bridges result in economic losses, either due to lost revenue, bad publicity, or retrofit. For example the retrofit cost was around $8.9 million for the LMB compared to its construction cost of $32 million (Cornell University, 2005) and $3.12 million for the New York Squibb Park bridge, which was only $1 million less than its initial construction cost (Curbed New York, 2016). The reliability results of the PB configurations for SLS design are evaluated and presented in the following sections.

4.4.2 Results from reliability analysis

Figure 4.2 shows the mean of the reliability index evaluated using the guidelines for the ϕ_s range $1.0 - 1.1$ in each bridge class. For comparison purposes, β is calculated using all three procedures: AFOSM, SORM, and MCS. Comparisons of reliability indices obtained by AFOSM and SORM with the MCS results in Figure 4.2 show that all three methods result in similar mean values of β in most cases, except using Eurocode 5 and SÉTRA. The reliability index estimated for all of the acceptable designs in Class II (design traffic of 0.5 P/m^2) is shown in Figure 4.3 as a function of the structure natural frequencies (f_n). Figure 4.3 also shows that all the three methods result in similar β values, with higher discrepancies in a few instances near the discontinuous regions of the response reduction factor curves (Figures 2.9, 2.10 and 2.11). For example, the reliability results around 4.8 Hz for Eurocode 5 (Figure 2.9(a)) or 2.6 Hz for SÉTRA (Figure 2.11 (a)) exhibit significant deviations in β calculated using AFOSM and SORM compared to MCS. These instances of frequency lie near the tails of the k_{vert} and ψ_v functions in Figure 2.9(a) and Figure 2.11(a). AFOSM shows better agreement with the MCS results compared to SORM in such instances. However, these instances are relatively few in number. It is also evident from Figures 4.2 and 4.3 that results from both AFOSM and SORM are similar for all the structures and mostly lower than the MCS results. This implies that the estimates from the AFOSM or SORM can be conservatively used. Being the simplest reliability analysis

method and computationally efficient, β results obtained using AFOSM are only reported for further analysis.

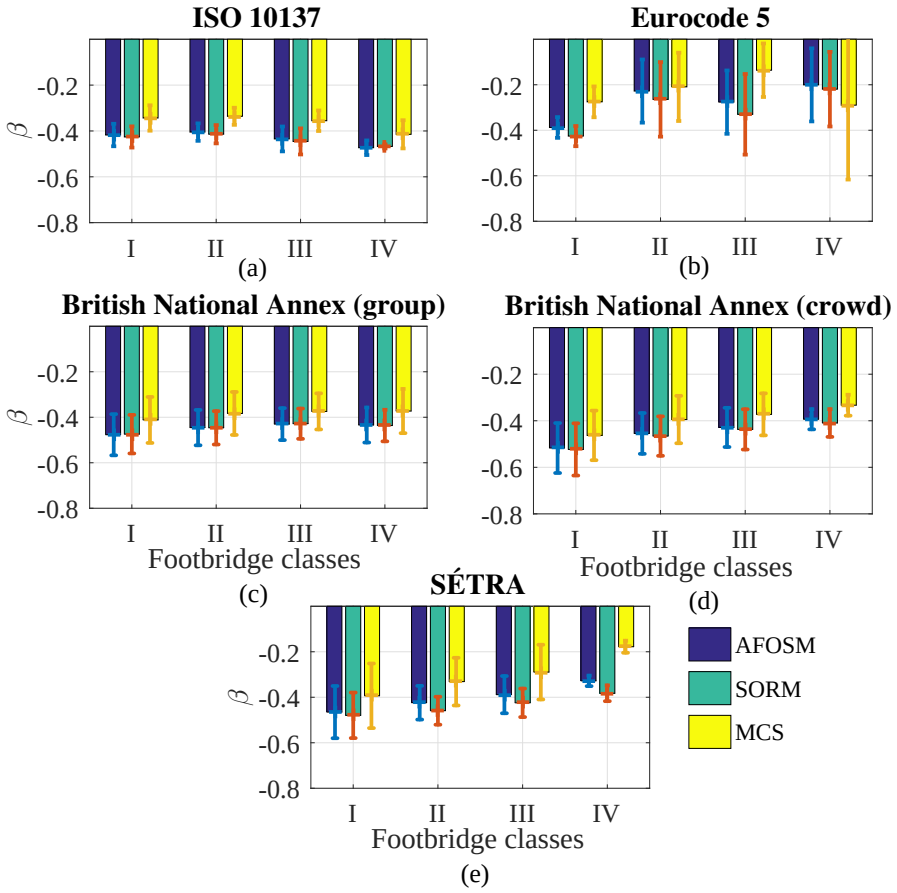

Figure 4.2: Mean of reliability indices estimated for all the designs satisfying $\psi_s = 1.0-1.1$, using three reliability methods for different classes: (a) ISO 10137, (b) Eurocode 5, (c) British National Annex (group), (d) British National Annex (crowd), and (e) SÉTRA

Figure 4.3 also shows that the frequency range and the number of configurations satisfying the SLS design are different amongst the guidelines. This is due to inconsistencies in the design criteria as discussed in the previous sections and hence the designs satisfying the SLS design check according to these standards. For instance, both Eurocode and SÉTRA consider 5 Hz as the upper bound of the critical frequency range (for only the first two harmonics of resonance), while ISO 10137 and British National Annex have upper bounds of 12 Hz (first five harmonics) and 8 Hz (first three harmonics), respectively. Hence, sig-

nificantly more configurations are available for ISO 10137 and the British National Annex compared to others. Furthermore, being conservative compared to SÉTRA, fewer configurations are available for Eurocode 5 (Figures 4.3 (b) and (e)), although they have similar critical frequency ranges. Similarly, ISO 10137 has fewer configurations compared to the British National Annex (Figures 4.3 (a), (c) and (d)). The results in Figure 4.4 for Class IV with higher design traffic density (1.0 P/m^2) underscore the same aforementioned issues.

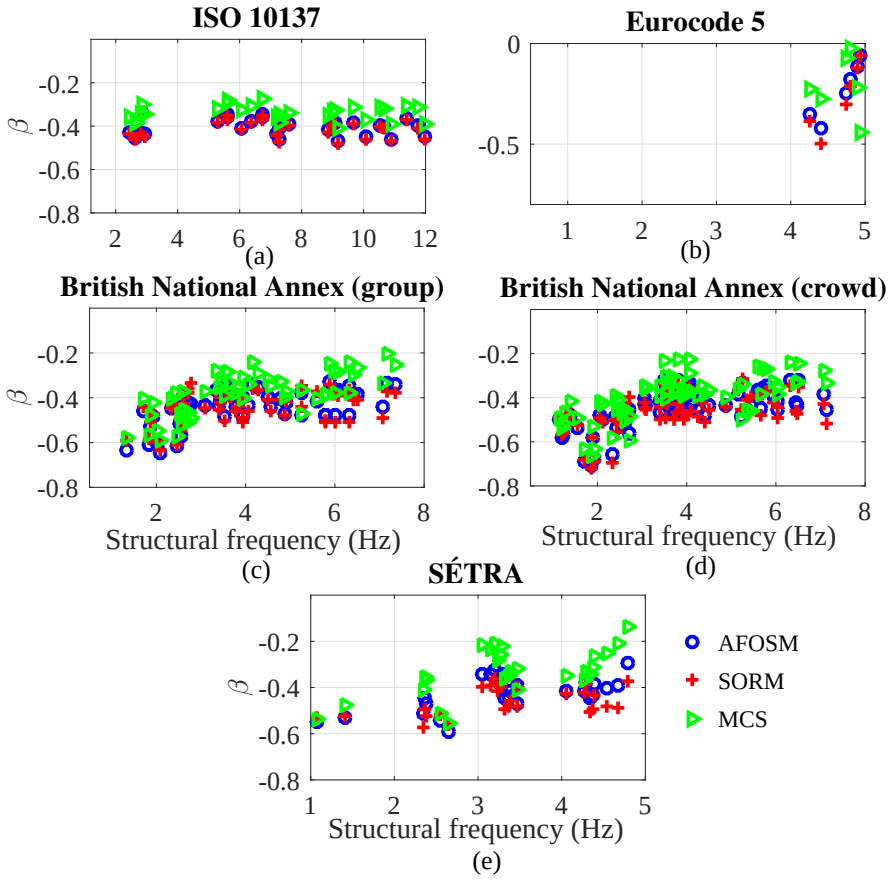

Figure 4.3: Reliability index as a function of structural frequency for Class II bridges under a design traffic of 0.5 P/m^2: (a) ISO 10137, (b) Eurocode 5, (c) British National Annex (group), (d) British National Annex (crowd), and (e) SÉTRA.

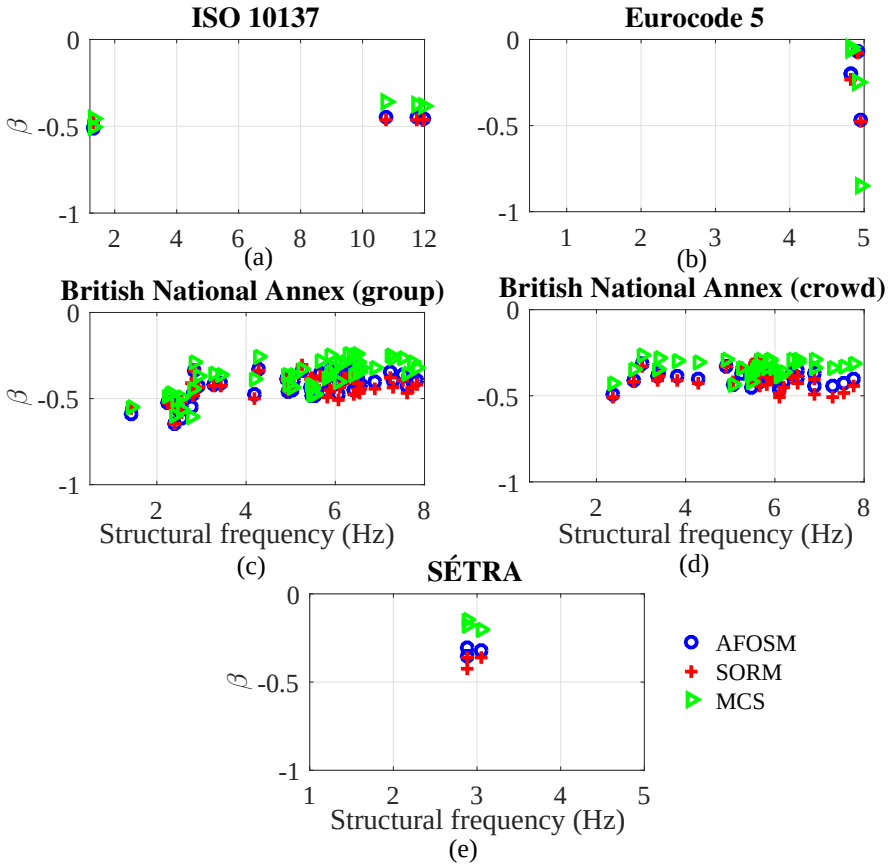

Figure 4.4: Reliability index as a function of structural frequency for Class IV bridges under a design traffic of 1.0 P/m^2: (a) ISO 10137, (b) Eurocode 5, (c) British National Annex (group), (d) British National Annex (crowd), and (e) SÉTRA.

Uniformity criteria

The uniformity criteria are evaluated across all the bridge classes as well as across all the design applications corresponding to each bridge class. The maximum and minimum reliability index (β_{max} and β_{min}) of all the designed applications corresponding to each PB class is shown in Figure 4.5. The results show that the reliability levels embodied in various guidelines are not uniform over the PB classes, except for the British National Annex (group), which results in fairly uniform reliability across the four classes. This non-uniformity in the reliability levels can be explained through Figures 4.3 and 4.4. The primary reason is the different structural configurations passing the optimality condition

for different classes. For example, in SÉTRA, the design traffic proportionally increases with the class, and hence configurations with small values of ψ_v (tails of the curve in Figure 2.11(a)) satisfy the serviceability design checks as shown in Figures 4.3 (e) and 4.4 (e). Aside from the different PB configurations (i.e., span, width, height, mass, etc.), the different numbers of PB configurations passing the deterministic serviceability design is also one of the reasons for the non-uniform reliability levels across the different PB classes. For example, PB Class II has 26 configurations (Figure 4.3 (e)) available for reliability analysis, while Class IV has 3 (Figure 4.4 (e)) in the case of SÉTRA. In order to assess the uniformity in the β values over all of the PB configurations for a specific class, $\beta_{range} = \beta_{max} - \beta_{min}$ can be estimated as reported in Table 4.5. It is observed from this table and Figure 4.5 that β has a significant spread across different PB configurations for some PB classes such as Class I (SÉTRA) or Class II (Eurocode 5). However, β_{range} is very small for ISO 10137, specifically for PB Class IV, which is due to the relatively fewer configurations that are available for analysis (Figure 4.4(a)).

Table 4.5: Ranges of reliability index ($\beta_{range} = \beta_{max} - \beta_{min}$) for different PB classes

Codes	Class I	Class II	Class III	Class IV
ISO 10137	0.273	0.130	0.118	0.065
Eurocode 5	0.158	0.362	0.197	0.393
British National Annex (group)	0.329	0.319	0.330	0.326
British National Annex (crowd)	0.368	0.391	0.380	0.178
SÉTRA	0.519	0.294	0.294	0.046

Sufficiency criteria

In order to examine the sufficiency achieved across PB classes, the minimum reliability index, β_{min} in Figure 4.5 is compared with the target reliability ($\beta_t = 0$). This comparison shows that all the designs for a specified density do not satisfy the sufficiency criteria, i.e., $\beta_{min} < \beta_t$ with β_{min} in the range of -0.5 to -0.8 across the standards. However, the deviation from the target value is low. The sufficiency criteria is also investigated for other traffic situations expected during its lifetime, including rare events associated with a density of 1.5 P/m^2. The minimum reliability index (β_{min}) obtained using the designed configurations for various classes are shown in Figure 4.6. The results show that all of the PB classes produce lower reliability levels when higher traffic densities occur, which is to be expected. Amongst all of the standards, the British National Annex (crowd) and SÉTRA result in the lowest reliability index, between -3.5 to -4.75 (close to a probability of failure,

$P_f = 1$) under rare events (1.5 P/m^2) for Class I. In the case of SÉTRA, Classes II and III results in $\beta_{min} = -4.75$ as well. In general, Classes I and III are shown to perform poorly for all the guidelines under such unexpected events. Hence, designs belonging to these classes (I to III) are deemed insufficient. For Class IV, (with a design traffic of 1.0 P/m^2) most of the designs result in β close to -1.0 under rare events (corresponding to 1.5 P/m^2).

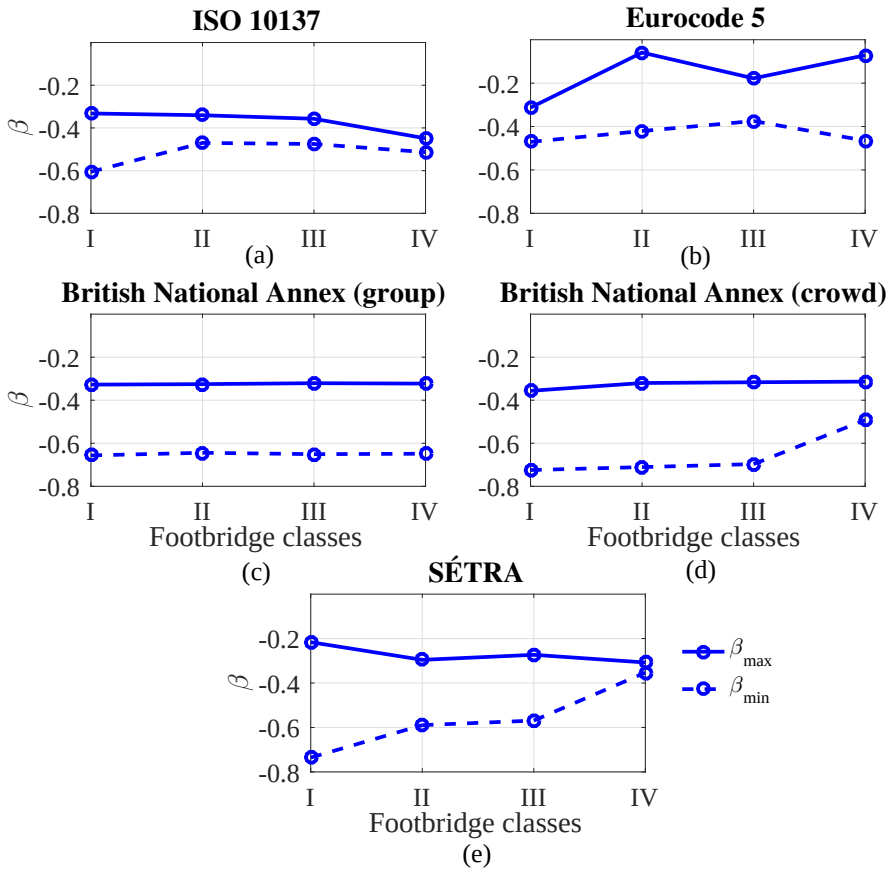

Figure 4.5: Maximum and minimum reliability levels for designs satisfying $\psi_s = 1.0 - 1.1$ for different classes: (a) ISO 10137, (b) Eurocode 5, (c) British National Annex (group), (d) British National Annex (crowd), and (e) SÉTRA

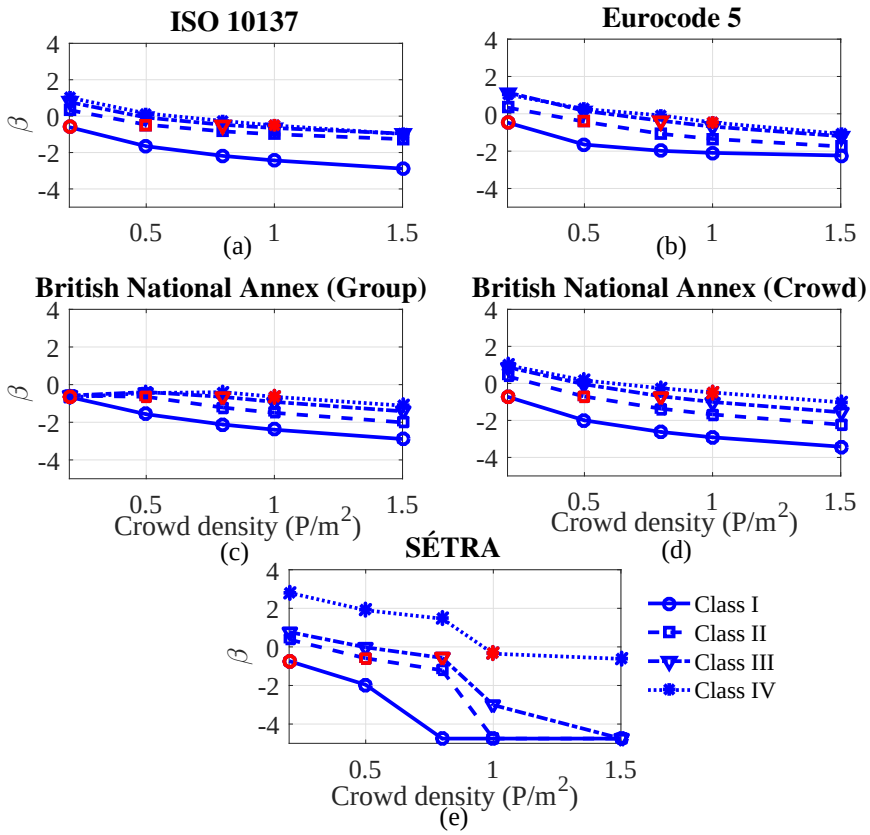

Figure 4.6: Minimum reliability levels (β_{min} calculated for the PBs ($\phi_s = 1.0 - 1.1$) under different design cases: (a) ISO 10137, (b) Eurocode 5, (c) British National Annex (group), (d) British National Annex (crowd), and (e) SÉTRA (red markers correspond to the design traffic of the particular PB class)

Comparison of reliability results by the guidelines

The reliability indices obtained using all of the standards are summarized in Table 4.6. This Table shows the minimum and maximum values for the reliability index obtained for all the optimally designed ($\phi_s = 1.0 - 1.1$) configurations for different classes under all possible traffic situations in their design life as well as the reliability levels achieved by these PBs under design traffic conditions (in parenthesis). Clearly, such bounds are a subset that only encompasses the PB configurations considered in the current study. However, it is believed that these configurations cover a broad range of design applications in terms of

PB class and structural frequency. In comparing the ranges i.e., β_{max} and β_{min} under all possible traffic scenarios in Table 4.6, the various code provisions show disagreement in the β ranges for all classes. Among all of the guidelines, SÉTRA results in the most unconservative estimates for β_{min}, with β_{min} as low as -4.75 for Class I to Class III PBs, which implies a probability of failure of approximately 1.0. While the design traffic for these classes is 0.2 to 0.8 P/m^2, the β_{min} corresponds to 1.5 P/m^2 (rare traffic). However, SÉTRA has a different functional form for the equivalent number of pedestrians n_{eq} under design and rare traffic. For the design traffic case, n_{eq} is $10.8\sqrt{\zeta_n N}$. It is $1.85\sqrt{N}$ for rare traffic. This results in very low β estimates compared to other guidelines, which have a uniform functional form for all traffic densities for design or rare events.

Table 4.6: Summary of reliability results for different PB classes

Codes	Class I		Class II		Class III		Class IV	
	β_{max}	β_{min}	β_{max}	β_{min}	β_{max}	β_{min}	β_{max}	β_{min}
ISO 10137	-0.33	-2.88	0.48	-1.26	0.91	-0.96	1.37	-0.98
	(-0.33)	(-0.61)	(-0.34)	(-0.47)	(-0.36)	(-0.47)	(-0.45)	(-0.51)
Eurocode 5	-0.31	-2.24	1.26	-1.75	1.92	-1.20	2.66	-1.07
	(-0.31)	(-0.47)	(-0.06)	(-0.42)	(-0.18)	(-0.38)	(-0.07)	(-0.47)
British National	-0.27	-2.89	0.47	-2.01	0.95	-1.42	1.19	-1.12
Annex (group)	(-0.33)	(-0.66)	(-0.33)	(-0.64)	(-0.32)	(-0.65)	(-0.32)	(-0.65)
British National	-0.36	-3.42	0.85	-2.23	1.45	-1.56	1.70	-1.02
Annex (crowd)	(-0.36)	(-0.72)	(-0.32)	(-0.71)	(-0.32)	(-0.70)	(-0.31)	(-0.49)
SÉTRA	-0.22	-4.75	5.17	-4.75	2.06	-4.75	3.21	-0.62
	(-0.22)	(-0.74)	(-0.30)	(-0.59)	(-0.27)	(-0.57)	(-0.31)	(-0.35)

Note: Numbers in parenthesis are the minimum and maximum values of reliability indices, estimated for the PB classes under the specified design traffic

Under design traffic (values in parenthesis in Table 4.6), ISO 10137 and Eurocode 5 show significant agreement in terms of β_{min}. This is likely due to the fact that the multiplication factors for both the codes are independent of ζ. Similarly, the SÉTRA estimates for Classes I to III are close to the British national Annex (crowd), which has a functional form of the multiplication factor similar to SÉTRA. In terms of β_{max}, Eurocode 5 results in the most conservative estimates and shows significant disagreement with other guidelines for Classes II to IV. This disagreement is largely due to inconsistencies in the design methodologies and hence the designed configurations available for reliability assessment.

4.4.3 Parametric study

Individual contributions from various random variables on the overall reliability level will help decide the most sensitive variables for future code calibration efforts. Moreover, appropriate information about the uncertainty in the design parameters is needed for code calibration. While uncertainty models for the pedestrian excitation parameters, G and α_m, are established in the literature, those for the structural variables and pedestrian's comfort limit under pedestrian bridge vibration are not explored. For example, uncertainty models for I and m are not available and hence assumed here. The uncertainty models for ζ and a_l are adopted from the literature on occupant's comfort in high rise buildings developed in the wind engineering literature. Hence, a parametric study should be performed in order to investigate the sensitivity of the reliability estimation to these adopted uncertainty models.

Sensitivity to limit acceleration

Due to inter- and intra-subject variabilities, the limit acceleration a_l is associated with significant randomness. For the current study, a_l is assumed to be log-normally distributed with a COV of 0.20, based on the literature on occupant's comfort under wind-induced vibration of high-rise building (Bashor et al., 2005). The sensitivity with respect to a_l is investigated and the results are shown in Figures 4.7 and 4.8. As shown in Figure 4.7, an increase in the COV of a_l decreases the reliability levels for all of the guidelines and the change in β with respect to COV is significant. Comparing the estimates of β for different distribution types of a_l, such as normal, log-normal and extreme value distributions in Figure 4.8, the lowest mean β values result from the use of the extreme value distribution and the highest from a normal distribution. However, the sensitivity of β to the distribution type of a_l is negligibly small. The difference in the estimates obtained using an extreme value distribution versus those obtained using a log-normal distribution is in the range of 6% to 7%. On the other hand, difference in the estimates between normal and log-normal distributions are in the range of 8% to 9%. As β is not sensitive to the distribution type of a_l, for simplicity, a normal distribution is assumed for future calibration.

Sensitivity to structural variables

E, I, m, and ζ are the basic design variables corresponding to structure in Equation 4.3. E, I, and m, which are related to the geometric and material properties of the structure, are associated with low COVs. For the reliability analysis in the current study, a value of 0.05 is assumed for I and m, while the uncertainty model for E is chosen from literature

for steel and assumed for aluminum. The reliability results including uncertainties in these parameters are compared with the ones where E, I, and m are assumed deterministic. Figure 4.9 shows the mean reliability levels estimated for all the classes of PB. It is seen that in most of the cases, uncertainties in these variables do not affect the reliability estimation significantly, mainly due to very low COVs of these parameters. The reliability estimation is sensitive to the uncertainty in E in some instances for Eurocode 5 and SÉTRA. For Class II in Figure 4.10, it is evident that the impact of these variables on the reliability estimates is negligible for ISO 10137, since the multiplication factor is independent of these parameters and the limit state function depends only on m. In other cases, the contribution of these parameters depends on the region in the response reduction factor curve in Figures 2.9 to 2.11. In the tail regions, the contribution of E is significant, but uncertainties in E produce higher estimates for β. Based on these results, it is concluded that E, I, and m can conservatively be treated as deterministic parameters for code calibration purposes.

Unlike E, I, and m, there is significant scatter associated with ζ, as reported in the literature (Bashor et al., 2005) for building. However, there is little information available specific to PBs (Cunha et al., 2005; Reynders et al., 2016). For the current study, ζ is assumed to be log-normally distributed with a COV of 0.30, based on the building literature (Bashor et al., 2005). A sensitivity study is conducted in Figures 4.11 and 4.12, in order to determine the impact of the COV and distribution types for ζ on the reliability estimates. Figure 4.11 shows the mean reliability index achieved by all of the designed configurations for a particular class for various assumed COVs of ζ. An increase in the COV for ζ decreases the reliability level in all of the guidelines. However, the rate of change in the mean β values is not significant with an increase in the COV value. The mean β values for different distribution types such as normal, log-normal and Weibull are compared in Figure 4.12, which shows that the log-normal distribution for ζ produces the lowest mean β values.

It is also investigated in Figure 4.13 whether assuming E, I, m and ζ as deterministic quantities has any significant effect on the reliability estimates. This will help in reducing the number variables for future calibration process. It is observed that the uncertainties in these variables do not contribute significantly into the reliability estimates excepts in a few instances for Eurcode 5. Nevertheless, deterministic structural variables leads to lower reliability estimates and thus is assumed for the code calibration purposes. It should be noted that the current study is limited to truss type PBs constructed from steel and aluminum (metals). The sensitivity study should be performed for other types of PBs with a wider range of material properties in order to choose the most sensitive random variables for code calibration.

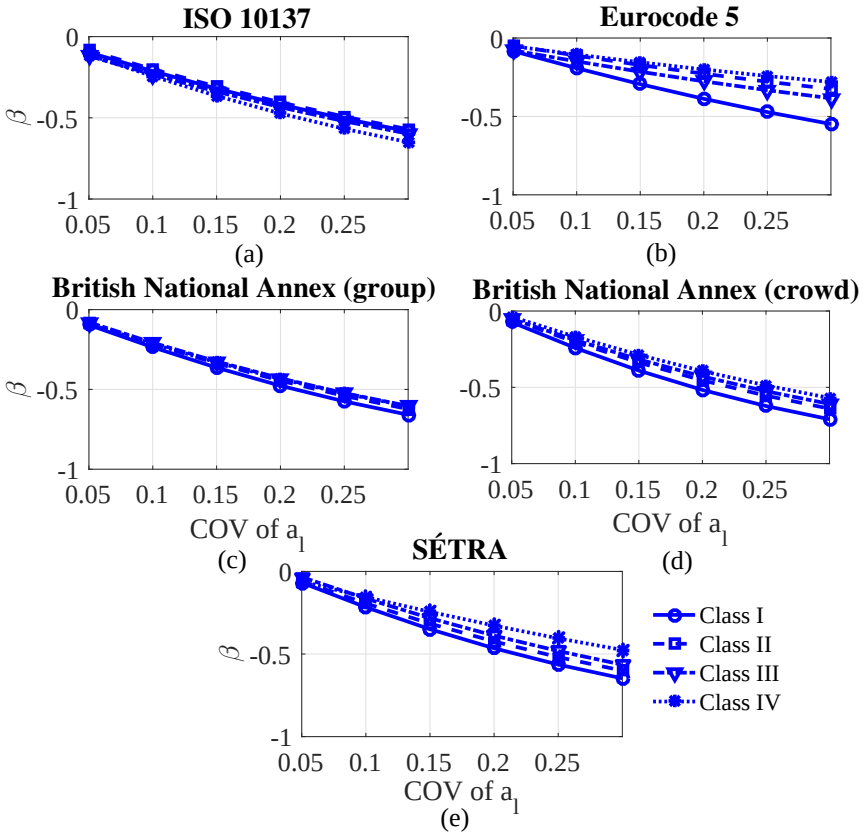

Figure 4.7: Variation of mean reliability index with coefficients of variation for a_l for different PB classes: (a) ISO 10137, (b) Eurocode 5, (c) British National Annex (group), (d) British National Annex (crowd), and (e) SÉTRA

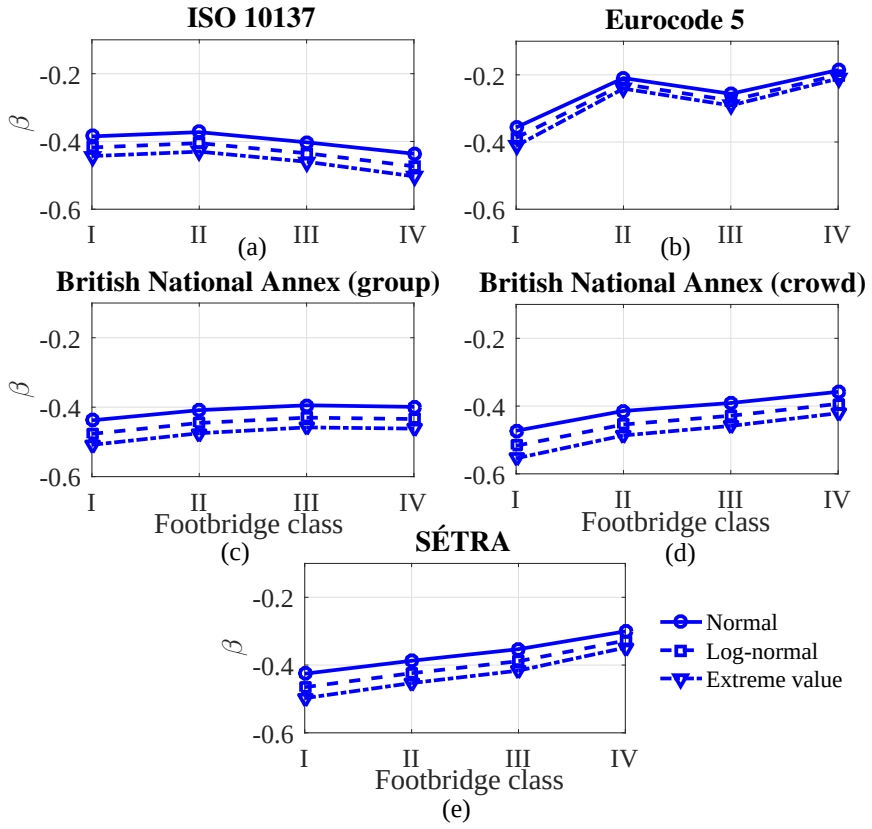

Figure 4.8: Variation of mean reliability index with different distribution of ζ for different PB classes: (a) ISO 10137, (b) Eurocode 5, (c) British National Annex (group), (d) British National Annex (crowd), and (e) SÉTRA

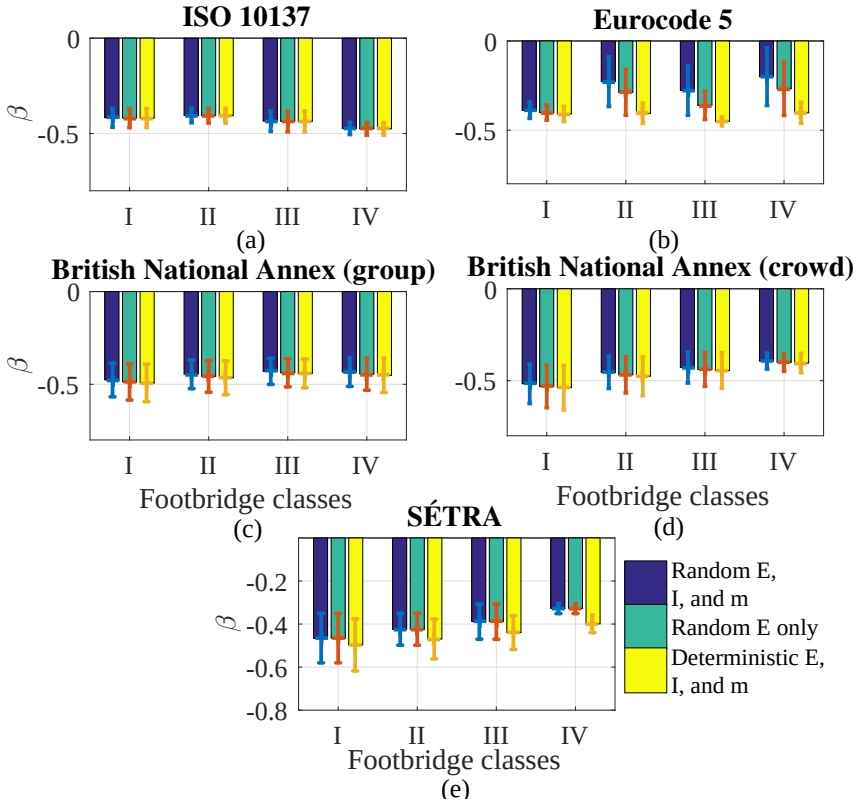

Figure 4.9: Mean of reliability indices estimated for all the optimal designs with and without considering uncertainties in E, I and m for different PB classes: (a) ISO 10137, (b) Eurocode 5, (c) British National Annex (group), (d) British National Annex (crowd), and (e) SÉTRA

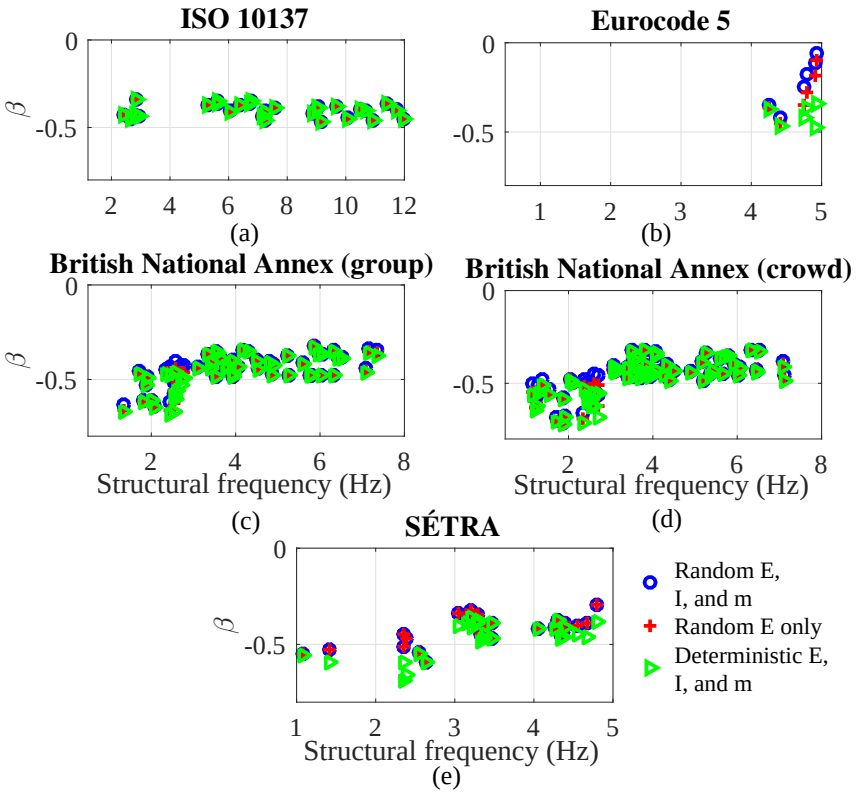

Figure 4.10: Reliability index values estimated with and without considering uncertainties in E, I and m for all the code-designed PBs of class II under design traffic of 0.5 P/m^2: (a) ISO 10137, (b) Eurocode 5, (c) British National Annex (group), (d) British National Annex (crowd), and (e) SÉTRA.

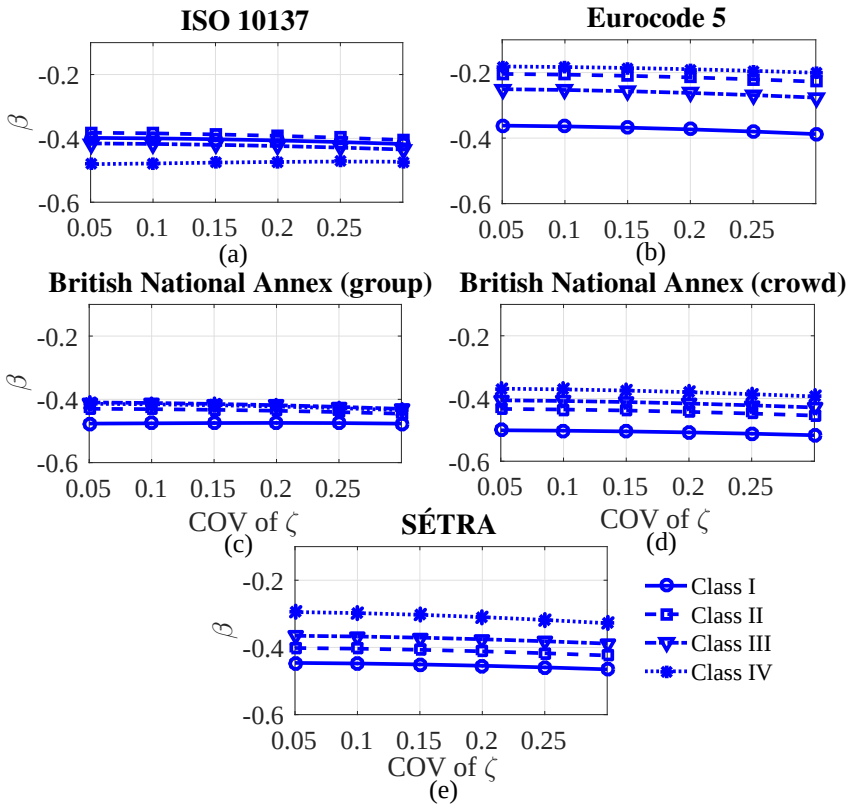

Figure 4.11: Variation of mean reliability index with coefficients of variation of ζ for different PB classes: (a) ISO 10137, (b) Eurocode 5, (c) British National Annex (group), (d) British National Annex (crowd), and (e) SÉTRA

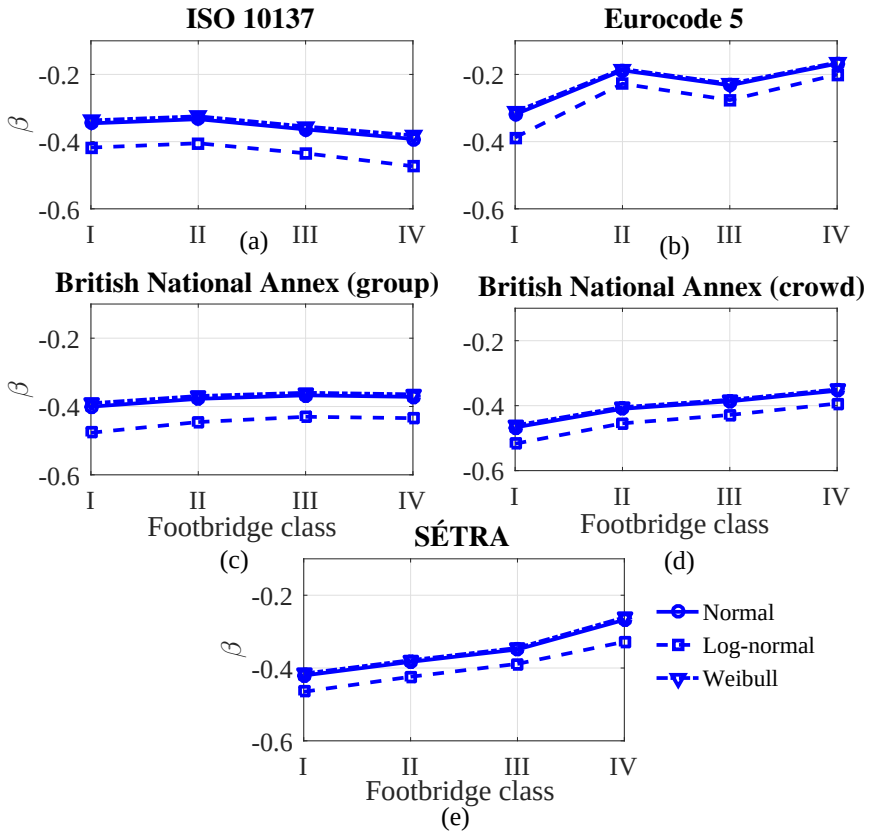

Figure 4.12: Variation of mean reliability index with different distribution of ζ for different PB classes: (a) ISO 10137, (b) Eurocode 5, (c) British National Annex (group), (d) British National Annex (crowd), and (e) SÉTRA

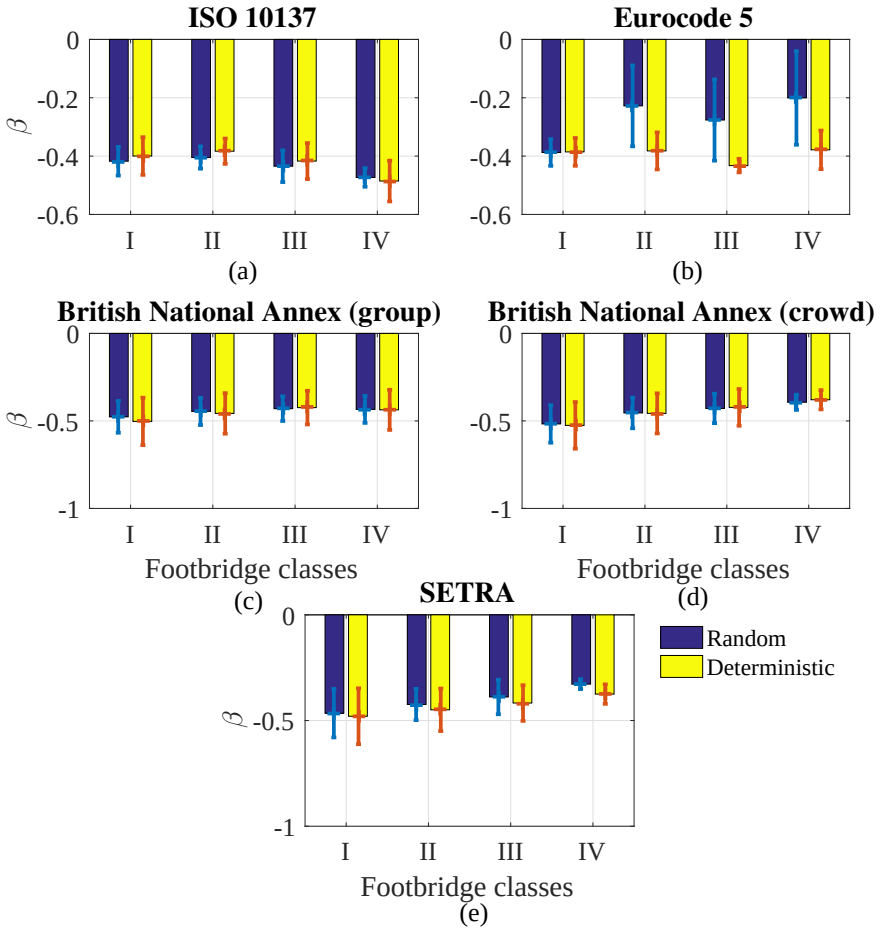

Figure 4.13: Mean of reliability indices estimated for all the optimal designs with and without considering uncertainties in structural variables for different PB classes: (a) ISO 10137, (b) Eurocode 5, (c) British National Annex (group), (d) British National Annex (crowd), and (e) SÉTRA

4.4.4 Summary of key results from the reliability analysis

There are several broad observations resulting from the reliability-based evaluation of the guidelines presented in the previous sections. They are summarized as follows:

1. When a PB is designed for a particular crowd density, it does not satisfy the target reliability index (β_t) value of 0 under the design traffic. However, the deviation from the target value is low.

2. The PBs in Classes I to III fail to satisfy the minimum reliability requirement under very heavy traffic during rare events such as inauguration, while past serviceability failures have shown that such events have to be considered to avoid disproportionate economic losses and damaging negative public perception.

3. Due to inconsistencies in the design provisions, the guidelines result in significant differences in the reliability analysis.

4. A parametric study shows that the structural variables can be assumed deterministic for conservative calibration process.

In the next chapter, these observations are addressed through a code calibration procedure.

Chapter 5

Recommendations to improve existing design provisions and reliability-based code calibration

Thus far, the focus has been on a comprehensive evaluation of the design provisions. This chapter mainly deals with recommendations to improve design provisions so that they better align with experimental observations, both from a deterministic standpoint as well as in a reliability-based framework. First, recommendations are proposed to improve the serviceability design outcomes by the guidelines and to reconcile the observed differences amongst the guidelines and with the measurements. The serviceability outcomes after incorporating the recommendations are then re-evaluated using the previous methodology. Finally, the existing as well as the recommended provisions are calibrated to achieve sufficient reliability under all possible traffic conditions for different PB classes.

5.1 Recommendations for serviceability design

A general observation in **Chapter 3** (Section 3.2.2) from the serviceability assessment results of the full-scale PBs under groups of pedestrians is that the vertical responses are conservative, while this is not the case for the lateral direction. Furthermore, significant inconsistencies are observed in the predictions by the guidelines. The main shortcomings in the existing guidelines as observed in in Section 3.2.2 are summarized below:

- There is little guidance on correctly estimating walking speeds in crowd conditions.

The walking speed in a crowd depends on the traffic size. However, the guidelines do not consider traffic dependency, and hence of the structure with the relevant harmonics of walking frequency.

- The DLFs used are not uniform across the guidelines as shown in Table 3.9 even though the basic modelling approach and assumptions are largely aligned.
- They do not include a sufficient number of higher harmonics, although serviceability issues due to resonance with higher harmonics have been observed.
- The guidelines also adopt different multiplication factors, as described in Table 3.8, which lead to very different serviceability outcomes.
- Except for SÉTRA, the other guidelines do not consider the effect of added mass from pedestrians in the response predictions.

5.1.1 Key design recommendations

An attempt is made in this section to address discrepancies summarized earlier through incorporating the following key design recommendations within the basic design framework in Equation 3.5 adopted by the guidelines:

1. One of the shortcomings in all the guidelines is that they do not account for a reduction of walking speed accompanying an increase in crowd density, which is important in order to choose the proper harmonic of walking frequency for resonance as discussed in Section 3.2.2. In order to address this, the following relationship between the crowd density (d), walking speed (v) and frequency, available in the literature (Butz et al., 2008) can be incorporated:

$$v = 0.126d^2 - 0.819d + 1.779 \tag{5.1}$$

$$f_s = 0.7868v + 0.7886 \tag{5.2}$$

Based on the expected walking frequency f_s and the structural frequency (f_n), the appropriate resonating harmonic (m) of walking frequency can be determined through the nearest integer of $\frac{f_n}{f_s}$. As the even harmonics contain relatively less energy in the lateral direction, they are unlikely to create resonant conditions. Hence, the nearest odd harmonic can be considered in the lateral direction.

2. The DLFs (α'_{mn}) by Brownjohn et al. (2004b) can be considered for response estimation in the vertical direction, because a number of higher harmonics have been quantified in this work. The factors are $0.37f_s - 0.42$, 0.053, 0.042, 0.041, 0.027, and 0.018 for the first six harmonics. The value for the seventh harmonic is currently not available and can be assumed to be 0.010. The recommended values for the first two DLFs for the the lateral direction i.e. 0.05 and 0.01 can be regarded the same as the SÉTRA guideline. The DLFs for the next three higher harmonics are $0.023, 0.0043$, and 0.011 as proposed by (Ricciardelli and Pizzimenti, 2007).

3. The multiplication factor S_N proposed by the British National Annex in Table 3.8 is recommended for the vertical direction, with a response reduction factor $k(f_v) = 1.0$. As the appropriate resonating harmonic is considered through traffic-dependent walking speed, the response reduction factor $k(f_v)$, which takes care of the risk of resonance, can be assumed as 1.0. Hence the recommended multiplication factor (S'_N) is $\sqrt{(1+\gamma(N-1))}$ for concentrated load models under groups of pedestrians and $1.8\sqrt{\frac{\gamma N}{\lambda}}$ for an uniformly distributed crowd model. The multiplication factor proposed by SÉTRA (Table 3.8) with $\psi = 1.0$ i.e., n_{eq} or $10.8\sqrt{(\zeta_n N)}$ for $d < 1.0$ and $1.85\sqrt{N}$ for $d \geq 1.0$, is recommended for the lateral direction. The pulsating moving load model is recommended for transient loading (temporary, where groups cross the bridge together), while the uniformly distributed load model can be used when the pedestrians are on the bridge long enough to create steady state conditions.

4. It is shown in Figures 3.16 and 3.17 for the SÉTRA guideline that the response predictions are sensitive to the added mass from pedestrians, specifically for dense traffic sizes. Hence, the effect of added mass from pedestrians on the response predictions should be considered for other guidelines as well. It can be incorporated as proposed by SÉTRA through estimating the modified structural frequency using Equation 2.17.

These recommendations can be incorporated into the existing guidelines quite easily. For ISO 10137, the numerical coefficients in Table 2.5 can be calibrated with the new dynamic load factors α'_{mn} and extended for higher harmonics in both the directions. The factor $C(N)$ in Equation 2.7 can be replaced with $\frac{S'_N}{N}$. Similarly, simplified equations can be derived for direct calculation of responses as proposed by Eurocode 5. Equations 2.9 and 2.11 can be replaced with $\frac{P_m}{M\zeta}$ for the m^{th} resonating harmonic. P_m is $200, 25, 20, 20, 15, 10$, and 5 respectively, for the first seven harmonics ($m = 1$ to 7) in the vertical direction, while it is $20, 5, 10, 2$, and 5 respectively, for the first five harmonics ($m = 1$ to 5) in the lateral

direction. The multiplication factors in Equations 2.8 ($0.23k_{vert}N$) and 2.10 ($0.18k_{hor}N$) can be replaced by the recommended S'_N in the vertical and lateral directions. For British National Annex, F_0 and $k(f_v)$ in Equations 2.12 and 2.13 can be replaced with $\alpha'_{mn}G_n$ and 1.0, respectively. In all of these guidelines, the response under the loaded structure should also be estimated along with the unloaded case, and the higher of the two cases should be used for design. In Equation 2.16 for SÉTRA, α_{mn}, and ψn_{eq} should be replaced by, respectively, α'_{mn} and S'_N for the first mode of vibration.

5.1.2 Effect of the recommended changes

To understand and quantify the effect of the proposed design recommendations on the experimental results obtained from the two laboratory bridges studied in the current work, the proposed changes are incorporated into the basic design model in Equation 3.1. First the response under a single pedestrian, a_s, is estimated using Equation 3.4. For the first mode of vibration, the load P_i is given by $\frac{2\alpha'_{mn}G_n}{\pi}$ for both the moving concentrated and the uniformly distributed load models. It should be noted however that P_i is $\frac{\alpha'_{mn}G_n}{\pi}$ for the second mode of vibration under uniformly distributed load, while it is the same for all the modes of vibration under concentrated moving load. Equation 3.1 is then applied to estimate the response under crowd loading, with $S_N = S'_N$. The higher of the two responses obtained from loaded (with added mass of pedestrians) and unloaded (without added mass of pedestrians) structural conditions is considered for design.

The results of the recommended methodology are shown in Figures 5.1 (a) and (b) for both the 12.2 m and 22.9 m bridge specimens in the vertical direction. It is observed that the modified results are significantly better than the responses originally predicted and shown in Figure 3.16. For the 12.2 m bridge specimen, the errors between measured and predicted responses under all the traffic classes are bounded between 12% and 113% from their original values of 155% and 828% (ISO 10137). Similarly, for the 22.9 m bridge specimen, these error bounds are 57% and 238% compared to their original values of −61% by the Eurocode 5 and 767% by the ISO 10137. Although the recommendations improve the predictions of peak measurements, the trends are different between the experimental and predicted responses as shown in Figures 5.1 (a) and (b). This is mainly due to the level of synchronization achieved during the tests, which is random, and depends on the crowd size and human-structure interaction. However, this is deterministic and constant for the simulated cases under all crowd sizes. The recommendations are proposed in the deterministic framework similar to the existing guidelines. By taking the random nature of the level of synchronization into account, the predictions in trends observed during the

experiments can be vastly improved. However, this investigation is beyond the scope of the current thesis.

The lateral peak responses are shown in Figure 5.1 (c) and (d) for both the 12.2 m and 22.9 m bridge specimens. As shown in Figure 3.17, the existing guidelines in general underestimate the peak responses under medium to light traffic conditions. The recommended results in Figures 5.1 (c) and (d) are in better agreement with the measurements and yield conservative estimates. In case of the 12.2 m bridge specimen, the errors in recommended predictions range from 164% to 270% while the existing guidelines have errors of −43% (Eurocode 5) to 41% (SÉTRA). Similarly, the errors for the 22.9 m bridge specimen range from 18% to 71% while existing guidelines have errors ranging from −60% by the SÉTRA to 60% by the Eurocode 5.

It should be stressed that these recommendations are proposed to harmonize existing design guidelines through DLFs and crowd multipliers in a relatively simple manner. However, they are drawn based on the experimental observations from only two aluminum pedestrian bridges and hence there is significant scope to expand upon this evidence through further testing on a broader variety of pedestrian bridges.

5.1.3 Reliability analysis after the proposed modifications

Along the same lines as described in the previous chapter (Section 4.2), reliability analysis is performed to investigate the effect of the proposed recommendations on the overall reliability of the PB configurations. For this purpose, a model error term (θ_{en}) is defined in Equation 5.3 to capture these proposed recommendations in the limit state design equation 4.1:

$$\theta_{en} = \frac{a_{rec}}{a_N} \tag{5.3}$$

where, a_{rec} is the response calculated through the procedure described in Section 5.1 and a_N is the predicted response by the existing design provision before the recommended changes are incorporated. After introducing this model error term, the Equation 4.1 is modified to:

$$a_{ln} \geq \theta_{en} \frac{S_N G_n \alpha_{mn}}{\pi M_n \zeta_n} \tag{5.4}$$

Subsequently, the modified SLS function can be wriiten as:

$$g'(\mathbf{X}) = a_l - \theta_e \frac{2 S_N G \alpha_m}{\pi L m \zeta} \tag{5.5}$$

The characteristic value of θ_e (represented as θ_{en} in Equation 5.4) is estimated through Equation 5.3 by estimating a_N and a_{rec}. θ_e is assumed to be normally distributed with a mean equal to the predicted characteristic value from Equation 5.3 and COV of 0.10. This term could potentially be calibrated using experimental observations on various PBs in the future.

The reliability bounds (β_{max} and β_{min}) are estimated for all the guidelines with the assumed uncertainties in the model error term (θ_e). Figure 5.2 shows these reliability bounds along with the bounds calculated using $g(\mathbf{X})$ without θ_e in Equation 4.3. θ_e is seen to have a significant impact on the reliability calculations using ISO 10137 and Eurocode 5, which result in more conservative predictions compared to other guidelines as observed previously. The impact is less for the British National Annex, as the recommended procedure already employs the same multiplication factor (S_N) as the the British National Annex in the vertical direction. These observations are also evident in Figure 5.3, which shows β values for Class IV. The introduction of θ_e in the design equation results in a larger number of configurations passing the deterministic check for ISO 10137, Eurocode 5 and SÉTRA, while the effect of θ_e on the design equation for the British National Annex is less. The sensitivity of the reliability results to the uncertainty in θ_e is also investigated in Figure 5.4. The reliability increases with an increase in the COV of θ_e. The assumption of a deterministic θ_e results in the lowest estimates for reliability indices. Hence, to calibrate the guidelines with the modified design procedures, θ_e can be assumed deterministic.

5.2 Reliability-based calibration

A reliability-based evaluation of PBs showed that PBs designed for a particular crowd density do not satisfy the target reliability level (β_t) of 0 under design traffic conditions. However, the deviation from this target value is low. On the other hand, the evaluation results also show that the PBs with lower design traffic (Class I to III) fail to satisfy the minimum reliability requirement under very dense traffic resulting from rare events such as inauguration, etc. Past serviceability failure experiences have shown that such events may have to be considered to avoid disproportionate economic loss and damaging negative public perception. This issue could be addressed by calibrating the design guidelines that result in an over-design for Class I to III bridges under design crowd densities, so that they perform better during rare loading events.

It should be stressed that the reliability estimates in the previous chapter are based on uniform comfort limits for pedestrians during both design and rare traffic conditions. As calibrating the PB classes to meet sufficiency during rare events could result in very

conservative designs, comfort limits based on the occurrence frequency of traffic are recommended. This will ensure that economical designs can be achieved, while at the same time resulting in acceptable performance during rare loading events. For this purpose, lower comfort limits as compared to the design case can be assigned for rare traffic density. As the reliability estimates are lower for bridge classes with lower design densities (Figure 4.6), reliability required for calibrating the guidelines for sufficiency for the rare event will be higher for such classes. Thus, the reliability required for calibration i.e., at the design level, will not be uniform across the PB classes. This can be resolved through calibrating the design guidelines across all bridge classes with the same reliability as required for Class I as this class results in the lowest reliability under the rare event or requires the largest reliability index for calibration as compared to other classes. However, this leads to an uneconomical design for classes with dense design densities such as III or IV, which can be improved through establishing class-based design comfort limits.

To study this further, several cases are established in Table 5.1 based on different choices of acceleration limits under both design and rare traffic events. A rare traffic density case of 1.5 P/m^2 (Heinemeyer et al., 2009) is adopted for analysis in addition to the design density corresponding to a bridge class (Table 4.4). In Table 5.1, D and R stands for design and rare events, respectively, where the reliability analysis is conducted during the respective events. It should be noted that irrespective of the events D and R, the structures are first optimally designed for the design traffic density corresponding to a bridge class and then the reliability analysis is performed for traffic density corresponding to the design or rare events. Two sets of cases are developed in Table 5.1: D_1 to R_{15} and D_2 to R_{25}. In the first set, the structures are designed in accordance to the code prescribed limit acceleration values (a_{ln}) as in Table 2.4 for maximum comfort of pedestrians. The second set is developed for uniform design performance across all PB classes, at the same time producing economic designs. In this case, mean comfort limits are desired for designing structures corresponding to Class III and IV, while designs of Class I and II retain the code prescribed limit accelerations similar to the first set. The mean comfort limit, $a_{ln} = 1.0$ m/s^2 by SÉTRA is chosen as the characteristic value for Class III and IV in the second set. However, if this design limit (1.0 m/s^2) for the second set is smaller than a_{ln} in Table 2.4, a_{ln} in Table 2.4 are retained resulting in identical design limits for the first and second sets.

For each set ($i = 1, 2$), 6 cases are developed, where only one is related to the design event (D_i), while the other 5 (R_{i1} to R_{i5}) are for the rare event. The reliability analysis for cases D_i and R_{i1} are performed assuming the same comfort limits as adopted for design. Other 4 cases (R_{i2} to R_{i5}) are developed based on different limit accelerations, ranging from 1.0 m/s^2 to 2.5 m/s^2, expected during the rare loading event. These acceleration

Table 5.1: Summary of cases based on comfort limits for pedestrians

Cases	*Acceleration limit (m/s^2)*
D_i	Same as adopted in i^{th} design case
R_{i1}	Same as adopted in i^{th} design case
R_{i2}	Maximum of 1.0 m/s^2 and the limit in i^{th} design case
R_{i3}	Maximum of 1.5 m/s^2 and the limit in i^{th} design case
R_{i4}	Maximum of 2.0 m/s^2 and the limit in i^{th} design case
R_{i5}	Maximum of 2.5 m/s^2 and the limit in i^{th} design case

*D_i: reliability analysis for only design loading event
**R_{ij}: reliability analysis for both design and rare loading events

limits are taken from the mean or minimum comfort limits by SÉTRA. Moreover, if these acceleration limits for the rare event are less than the one used for design i.e, the design limit acceleration, this design limit for the rare traffic density is adopted for the calculation of reliability index.

As observed in Figures 4.3 and 4.4, very few configurations are available in certain instances, for example, for Class IV. As the calibration process is being performed to achieve a higher reliability index, it is to be expected that very few configurations will satisfy the calibrated design equation if the existing design space of configurations presented in the previous chapter is retained. Hence, for the calibration process, the design space is extended (from Section 4.2) by incorporating 11 configurations for cross sectional area ranging from 0.05 m^2 to 0.15 m^2, 2 configurations of thickness (0.050 m and 0.075 m), 1 configuration of width (5.0 m) and 1 length to width ratio (30). This results in an increase in the total number of configurations from 1536 to 7560 for each material. To exclude any failing combinations, the designs are checked for ultimate bending stress. The retained configurations after the static check are employed for serviceability design and subsequently the calibration process is carried out on the designs which pass this check.

5.2.1 Calibration process

Code calibration is a technique used to achieve a specified target reliability level (β_t). Through such a calibration process, the variation in reliability indices across designs is significantly minimized. The results form the parametric study in Section 4.4.3 suggests that uncertainties from the limit acceleration (a_l) and pedestrian load (G and α_m) are sufficient for the calibration process. Hence, the modified SLS function for the design

guidelines can be written as:

$$g(\mathbf{X'}) = a_l - \theta_{en}\frac{2S_N}{\pi L m_n \zeta_n} G\alpha_m \tag{5.6}$$

where, $g(\mathbf{X'})$ represents the general limit state function for the design guidelines both without (existing) and with (improved) the model error term, θ_{en}. $\mathbf{X'}$ is the vector consisting of 3 random variables, $[a_l,\ G,\ \alpha_m]$. The calibration process will result in an estimate for the partial factors corresponding to the random variables. These partial factors are nothing but a scaling factor which allows the designer to convert the characteristic values of the basic variables to the design value needed to achieve the target reliability. After calibration, the design equation in 5.4 can be written in a load resistance factor design (LRFD) format (EN 1990, 2001):

$$\gamma_{a_l} a_{ln} \geq \theta_{en}\frac{2S_N(\gamma_G G_n)(\gamma_{\alpha_m}\alpha_{mn})}{\pi L m_n \zeta_n} \tag{5.7}$$

where, γ_{a_l}, γ_G and γ_{α_m} are the partial factors for the limit acceleration (a_l), pedestrian's weight (G) and the dynamic load factor (α_m). These factors together with the characteristic values of the design variables in Equation 5.7 will ensure an acceptable reliability index of β_t during design. The steps to estimate these factors for a given β_t are discussed in the following section.

Procedure to estimate the partial factors

The procedure to estimate partial factors, γ_{a_l}, γ_G and γ_{α_m}, for a given β_t, starts with formulating the limit state function and the design equation as in equations 5.6 and 5.7. The method allows at most two unknown mean values and the estimated factors become independent of the mean values of those unknown variables. The current study assumes that the mean of a_l is unknown so that the partial factors are independent of the mean limit acceleration. The factors are estimated iteratively as follows (Nowak and Collins, 2012):

1. Estimate the initial mean value of the unknown variable (a_l) from $g(\mathbf{X'}) = 0$ (Equation 5.6) at the mean values of other random variables.

2. Obtain the initial design point x_i^* assuming $(n-1)$ random variables where n is the number of random variables and equals to 3 for the current analysis. Generally, the mean values of the variables are a reasonable choice as the initial design point. Solve the value of the remaining random variables from $g(\mathbf{X'}) = 0$ (Equation 5.6). This ensures that the design point is on the failure boundary.

3. For each design value corresponding to a non-normal distribution, determine the equivalent mean and standard deviation through the Rackwitz-Fiessler procedure (Rackwitz and Flessler, 1978).

4. Determine the partial derivative of the limit state function ($g(\mathbf{X'})$) with respect to the reduced variables (z_i) and estimate the sensitivity coefficients α_i using Equation 4.9.

5. Determine the new design point (${z_i}^*$) for the $n-1$ variables in the reduced coordinates corresponding to a target reliability index β_t using:

$$ {z_i}^* = \alpha_i \beta_t \tag{5.8} $$

6. Covert the estimated design points in the previous step to the original coordinates for the $n-1$ variables using:

$$ {x_i}^* = \mu_{x_i} + {z_i}^* \sigma_{x_i} \tag{5.9} $$

7. Estimate the design value of the remaining random variable by using $g(\mathbf{X'}) = 0$ at the design point, where ${x_i}^*$ must be on the failure surface satisfying the limit state function $g(\mathbf{X'}^*) = 0$.

8. Update the mean value of the unknown variable through using the following expression:

$$ \mu_{x_i} = \frac{{x_i}^*}{1 + \alpha_i \beta_t V_{x_i}} \tag{5.10} $$

   where V_{x_i} is the COV of the unknown variable.

9. Repeat steps 3 to 8 until the sensitivity coefficients α_i converges.

10. Estimate the partial factors for the random variable x_i after achieving convergence using:

$$ \gamma_{x_i} = \frac{{x_i}^*}{{x_i}^n} \tag{5.11} $$

    where ${x_i}^n$ represents the characteristic value of the random variable.

Target reliability

As mentioned earlier code calibration in general, is performed to achieve an acceptable reliability level, known as target reliability, which is based on the consequence of failure, economic loss, etc. Along similar lines, the serviceability design provisions are calibrated here to achieve acceptable performance not only at the design level, but also for rare loading events. For the purpose of calibration, which is conducted at the design level event, the target reliability should be known or established *a priori*. As a cost based analysis to estimate the target reliability (β_t) is not performed here, an index β_d known as the desired reliability at the design event level is introduced. β_d is estimated through iteration so that the mean reliability achieved by all the designs during the design as well as rare traffic is more than 0, which is the proposed target reliability by ISO 2934 for sufficiency. Once β_d is estimated for each case in Table 5.1, then the corresponding partial factors can be assigned to Equation 5.7.

The overall implementation procedure is undertaken in two stages:

- **Estimation of partial factors:** The partial factors, γ_{a_l}, γ_G and γ_{α_m} corresponding to Equation 5.7 are estimated for assumed β_t levels ranging from 0.25 to 4.5 with an increment of 0.25 though the steps discussed in the previous section.
- **Estimation of desired reliability:** The desired reliability (β_d) is estimated iteratively for each case in Table 5.1 as follows:
    1. For an initial estimate of β_d, a reliability analysis is first conducted for a traffic density corresponding to the case under consideration (Table 5.1) for Class I, designed according to Equation 5.4 for design density of 0.2 P/m^2. The closest β_t level (listed in the previous step) to the estimated reliability index is chosen as the desired reliability for the first iteration.
    2. The structural configurations satisfying the static checks and the frequency limits are designed for Class I in accordance to the serviceability design equation in 5.7 with partial factors corresponding to the assumed β_d from the previous step, and those satisfying this equation are retained for reliability analysis.
    3. Reliability analysis is performed on the limit state function in Equation 5.6 following AFOSM method for all the optimally designed configurations. In case of D_1 or D_2, the mean reliability index from all the designs is estimated only for the design density (0.2 P/m^2) and retained for the next step, epresented by β_{et}. In the case of R_{i1} to R_{i1}, both the design (0.2 P/m^2) and rare (1.5 P/m^2)

traffic densities are considered and two mean values of β corresponding to the design (β_D) and rare (β_R) traffic events are estimated. The minimum of these reliability indices is retained for the next step as:

$$\beta_{et} = min[\beta_D, \beta_R] \tag{5.12}$$

4. If β_{et} is less than 0, then steps 2 and 3 are repeated using β_d as the next β_t until β_{et} is greater than 0 and the corresponding β_t is the desired reliability for the particular case. On the other hand, if β_{et} is greater than 0 at the first iteration, then steps 2 and 3 are repeated using β_t from the previous step until β_{et} is less than 0. Then, the final value of the desired reliability is $\beta_t + 0.25$.
5. The partial factors corresponding to the estimated β_d are the design partial factors for the particular case in Table 5.1.

5.2.2 Results of calibration

Partial factors

The partial factors, γ_{a_l}, γ_G and γ_{α_m} are first estimated for different target reliability indices ranging from 0.25 to 4.5 and reported in Table 5.2. It should be noted that while increments of β_t are limited to 0.25, smaller increments can be employed using the same methodology for a more accurate estimation of the desired reliability.

Table 5.2 reports only one set of factors corresponding to a target reliability level as the calibration process leads to identical factors for all the guidelines. Furthermore, the factors are independent of the PB classes. It has been already discussed in the previous chapter that the main inconsistency amongst the guidelines lies in the multiplication factor, S_N (Table 3.8) and limit acceleration, a_{ln} (Table 2.4), although they are based on the same basic framework. However, the calibration process assumes S_N as deterministic. On the other hand, as the procedure of calibration only requires known mean values from 2 variables which are G and α_m for the current analysis. Thus, despite different values of limit accelerations employed by the guidelines, estimation of the partial factors are independent of the different values of limit acceleration. Furthermore, the distribution type and COV for all the variables are identical in the guidelines. Due to these reasons, the factors across all the design provisions and all the PB classes are identical. Moreover, as the model error term is assumed deterministic, incorporation of this error term will not affect the partial factors. It is also seen in Table 5.2 that the factors for the first harmonic is different from the higher harmonics. This is due to the significantly higher COV (=0.40) for higher

Table 5.2: Partial factors corresponding to different target reliability index

β_t	m=1			m>1		
	γ_{a_l}	γ_G	γ_{α_m}	γ_{a_l}	γ_G	γ_{α_m}
0.250	0.770	1.008	1.023	0.778	1.001	1.081
0.500	0.742	1.031	1.044	0.758	1.018	1.158
0.750	0.713	1.053	1.063	0.735	1.037	1.229
1.000	0.683	1.075	1.082	0.711	1.056	1.296
1.250	0.651	1.096	1.098	0.683	1.075	1.358
1.500	0.617	1.116	1.113	0.654	1.094	1.414
1.750	0.581	1.134	1.126	0.622	1.113	1.466
2.000	0.544	1.150	1.138	0.588	1.131	1.511
2.250	0.504	1.163	1.146	0.551	1.147	1.550
2.500	0.463	1.173	1.153	0.511	1.161	1.581
2.750	0.419	1.177	1.156	0.468	1.172	1.604
3.000	0.373	1.177	1.156	0.422	1.177	1.616
3.250	0.326	1.171	1.152	0.372	1.177	1.616
3.500	0.277	1.159	1.143	0.319	1.170	1.600
3.750	0.228	1.140	1.131	0.264	1.154	1.566
4.000	0.179	1.116	1.113	0.206	1.130	1.509
4.250	0.131	1.087	1.091	0.149	1.099	1.427
4.500	0.085	1.055	1.065	0.094	1.062	1.317

harmonics of DLF values ($m > 1$) as compared to the first harmonic (COV=0.17). It should be stressed that these factors will depend on the uncertainty models used for the random variables. Moreover, if the uncertainties from structural properties are incorporated, the factors will not be consistent across the guidelines.

Desired reliability

After obtaining the partial factors with respect to a particular target reliability level in Table 5.2, β_d is estimated through iteration for all the cases listed in Table 5.1. Figure 5.5 shows β_d estimated for cases D_1 to R_{15}, which are also reported in Table 5.3. As the estimation of β_d is performed based on Class I of PBs and D_2 to R_{25} are identical cases with respect to D_1 to R_{15} for this class of PBs, β_d for cases D_2 to R_{25} will remain the same as those for D_1 to R_{15}. Hence, only the results corresponding to D_1 to R_{15} are reported here.

It is observed in Figure 5.5 that β_d is uniform across all the guidelines for D_1, as the sufficiency criteria is based on the design traffic density and the reliability embodied in the guidelines for design density is nearly uniform across different classes of PBs and guidelines (in the range of -0.46 to -0.37). Hence, $\beta_d = 0.25$ is sufficient for all the guidelines to achieve an acceptable performance under design traffic. It should be stressed that β_d can be different across the guidelines if an accurate estimation of β_d is performed with lower increment of β_t than the current one (i.e. 0.25). However, such values of β_d will lie between 0 to 0.25, exhibiting relatively small deviations. On the other hand, cases R_{11} to R_{15} are developed to satisfy sufficiency for both the design and rare loading events. In such cases, estimates of β_d are not always uniform, which is attributed to inconsistent reliability indices implied in the design guidelines during rare traffic conditions. To enable further comparisons, Figures 5.6 to 5.10 are shown for the mean reliability indices achieved by the guidelines. Sub-plots (a) and (b) for each figure compare the reliability levels achieved by the guidelines before and after the calibration process for the existing design provisions (without model error term, θ_{en}). Subplot (c) is introduced in each figure by showing the mean reliability indices by the calibrated guidelines with θ_{en}. Both of the subplots (b) and (c) are the results after calibrating the design provisions with β_d as listed in Table 5.3. In the next few paragraphs, the results from Figures 5.6 to 5.10 are discussed in detail with respect to each guideline.

Table 5.3: Desired reliability by different guidelines for different cases

Cases	ISO 10137	Eurocode 5	British National Annex		SÉTRA
			Group	Crowd	
D_i	0.25	0.25	0.25	0.25	0.25
R_{i1}	2.50	4.25	1.75	2.75	4.25
R_{i2}	1.00	3.75	1.75	2.75	3.25
R_{i3}	0.25	3.00	1.75	2.50	2.25
R_{i4}	0.25	2.25	1.25	2.00	1.50
R_{i5}	0.25	1.75	0.50	1.50	1.00

ISO 10137 (Figure 5.6): Comparison of subplots (a) and (b) in Figure 5.6 shows how the calibration process helps in meeting sufficiency as well as uniformity criteria across the PB classes. For instance, β_{mean} is -0.382, -0.371, -0.373 and -0.360 respectively for Class I to IV of PBs under the design event D_1. After calibrating all the classes uniformly with $\beta_d = 0.25$, β_{mean} becomes 0.366, 0.362, 0.358, and 0.363 respectively for Class I to IV of PBs. On the other hand, sufficiency for case R_{11} is dominated by the rare traffic density of 1.5 P/m^2 with β_{mean} being -2.12, -1.41, -1.01 and -0.77 for Classe I to IV before the calibration (subplot (a)). As already discussed in the previous sections, all the PB classes are assigned uniform β_d, which are estimated considering Class I, in order to achieve uniformity across bridge classes. After calibrating all the bridge classes with $\beta_d = 2.50$, corresponding β_{mean} becomes 0.140, 1.27, 1.82 and 2.15 as shown in subplot (b) for Class I to IV of PBs. In the case of R_{11}, the desired reliability is large due to the same comfort limits expected during both design and rare loading events. This leads to a very conservative design for Class III and IV. Nevertheless, less comfort, i.e., higher acceleration limits during the rare traffic event will translate to higher reliability as shown in Figure 5.6 (a) for the case of R_{12} to R_{15}. Thus, β_d required decreases as the acceleration limits expected becomes higher during the rare traffic density as shown in Figure 5.5, leading to a more economical design. It is also observed in Figure 5.6 (a) that the reliability implied in the case R_{14} and R_{15} is positive under the rare events and thus the calibration process is dominated by the design traffic with β_d same as D_1 (i.e., 0.25 as in Table 5.3). In order to further make the designs economic, it is also possible to design Classes III and IV with lower comfort as compared to the other classes. Hence, cases D_2 to R_{25} are established, which are the same as D_1 to R_{15}, except with different design acceleration limits for Class III and IV. The reliability results in subplot (b) or (c) also agrees with the fact that comfort limits based on bridge classes indeed is a better choice for economical design. For example, in the case of R_{15} in subplot (b), β_{mean} for Class IV is estimated as 3.45 after calibrating the design codes for $\beta_d = 0.25$, while designing the class with mean comfort of 1.0 m/s^2 results in β_{mean} of 2.11, which is more economical.

Eurocode 5 (Figure 5.7): The results for Eurocode 5 in Figure 5.7 are in agreement with ISO 10137 in that traffic dependent comfort limits lead to lower desired reliability for sufficiency during the rare loading event. At the same time, designing Class III and IV for mean comfort leads to economical designs. Unlike ISO 10137, sufficiency is dominated by the rare traffic density for cases R_{14} and R_{15}, which has β_{mean} values of -2.11 and -1.8, respectively before calibration (subplot (a)). Obviously, β_d is higher than the ISO 10137 for such cases as shown in Table 5.3. For the case of ISO 10137, the design limit acceleration is lower than Eurocode 5 and thus, the difference between the comfort limits during design

and rare traffic densities are higher for ISO 10137. This leads to a lower reliability index implied in Eurocode 5 as compared to ISO 10137 at the rare loading event.

British National Annex to Eurocode 1 (Figures 5.8 and 5.9): The mean reliability indices by the British National Annex before and after the calibration process are shown in Figures 5.8 and 5.9 in the case of group and crowd models. Similar to ISO 10137 and Eurocode 5, the results are also in agreement with the fact that adopting comfort limits based on occurrence frequency of the loading events as well as the bridge class leads to acceptable performance during design and rare traffic densities, while at the same time ensuring economic designs. It is also observed that the reliability indices for R_{i1} and R_{i2} are same for some bridge classes. For example, both R_{11} and R_{12} are the same for Class I in Figure 5.8. It can be explained through Equation 2.5 used to estimate the limit acceleration for this guideline, which depends on site, usage, bridge height, exposure etc. Case R_{11} is based on the same acceleration limit as the design one from Equation 2.5, while R_{21} is assigned as the maximum of the design limit and 1.0 m/s^2. The design acceleration limit is more than 1.0 m/s^2 for Class I and thus, the limit acceleration for the rare case R_{12} is the design one instead of 1.0 m/s^2, which in turn is the same as R_{11}. Hence, R_{11} and R_{12} results in the same β_d and the reliability level embodied in the guideline.

SÉTRA (Figure 5.10): The mean reliability indices by the SÉTRA guideline in Figure 5.10 also confirms that calibrating the guidelines for higher reliability along with traffic and bridge class dependent comfort limits results in an economic design. In Table 5.3, it is also observed that SÉTRA requires higher β_d similar to Eurocode 5, as compared to the other guidelines, which is primarily due to the lower design acceleration limits compared to others.

Sensitivity of calibration process to COV of acceleration limit

The partial factors listed in Table 5.2 are limited to a COV for a_l equal to 0.20, which is assumed in the current analysis based on the wind engineering literature. A different COV will result in a different set of partial factors and corresponding reliability levels required to satisfy sufficiency and uniformity across all design applications. A parametric study is conducted in this section to study the sensitivity of the estimated partial factors to different values of the COV for a_l. Figure 5.11 shows the variation of partial factors for a_l, G, and α_m in the case of the first ($m = 1$) and higher harmonics ($m > 1$) of the walking frequency.

It can be seen from Figure 5.11 that the values of the partial factors are very sensitive to the COV of the acceleration limit and thus appropriate uncertainty modelling of the acceleration limit for bridge vibration is necessary to calibrate the design provisions. The results also show that with a decrease in the COV value, there is an increase in the values for all of the partial factors. An increase in γ_{a_l} implies a low impact of a_l on the overall reliability of the PBs, while an increase in γ_G and γ_{α_m} points towards a higher impact of these variables on the overall reliability. This means that as the COV of a_l decreases, the contribution of a_l decreases while there is an increase in the contributions of G and α_m on the reliability estimates. For example, γ_{a_l} becomes close to 1 for a COV of 0.05 as shown in Figures 5.11 (a) and (b), implying a insignificant contribution to the overall reliability. At the same time, the contribution of forcing variables increases as shown in Figures 5.11 (c) to (f) for a COV of 0.05.

It is obvious that β_d for different cases (Table 5.1) can be different based on the combinations of the partial factors corresponding to the COV value of a_l. Figure 5.12 illustrates the variation in β_d for different COV values of a_l for the case of R_{15}, which are also reported in Table 5.4. From these results, different estimates of β_d values are observed based on COV of a_l. For instance, Eurocode 5 has β_d of 2.25, 2.00, 2.00, and 1.75 respectively, for COVs of 0.05, 0.10, 0.15, and 0.20. Although different COVs result in the same β_d for several cases, the calibrated limit state function achieves different reliability values due to different COVs as shown in Table 5.4. For example, in the case of Eurocode 5, a COV of 0.10 and 0.15 requires a β_d of 2.0, which leads to different β_{mean} values of 0.049 and 0.173. In the current study, as β_d is estimated iteratively from a range of β_t values based on an increment of 0.25, a difference in β_d values is not evident in certain cases. However, an accurate estimate of β_d will likely not be the same for different COVs of a_l.

From this discussion, it can be concluded that the values of partial factors and subsequently the desired reliability for calibration are sensitive to the COV of acceleration limit and thus proper information concerning acceleration limit uncertainty is necessary to calibrate the design provisions for vibration serviceability of PBs.

Table 5.4: Desired reliability and reliability implied (in brackets) by different guidelines for Class I of PBs in case of R_{15} for different COVs of a_l

Codes	COV of a_l			
	0.05	0.10	0.15	0.20
ISO 10137	0.250	0.250	0.250	0.250
	(0.394)	(0.384)	(0.371)	(0.366)
Eurocode 5	2.250	2.000	2.000	1.750
	(0.161)	(0.049)	(0.173)	(0.122)
British National	0.750	0.500	0.500	0.500
Annex (group)	(0.205)	(0.009)	(0.042)	(0.075)
British National	2.000	1.750	1.500	1.500
Annex (crowd)	(0.146)	(0.049)	(0.008)	(0.130)
SÉTRA	1.250	1.250	1.250	1.000
	(0.054)	(0.117)	(0.205)	(0.089)

Key conclusions from the calibration exercise

A general observation from the results of the code calibration is that it is possible to achieve sufficient and uniform reliability levels across all of the bridge classes under both design and rare loading events, while at the same time ensuring economical designs through adopting comfort limits for pedestrians depending on the occurrence of traffic events and the bridge class. Although all of the guidelines require the same β_d for the sufficiency during the design loading event, β_d is largely inconsistent across the guidelines for sufficiency requirement considering the rare loading events. The inconsistencies are mainly attributed to the different configurations passing the design equation and different design limit accelerations prescribed by the guidelines. Thus, in spite of the fact that calibration process ensures sufficient and uniform reliability under all possible traffic densities across the PB classes, the calibrated guidelines will remain inconsistent in terms of the reliability level implied in the design provisions at design. In order to reconcile this, the guidelines should simply be calibrated with the β_d, that is the maximum of all β_d's estimated for all of the guidelines in the case of a particular event. Hence, the desired reliability for all of the guidelines will be $[0.25,\ 4.25,\ 3.75,\ 3.0,\ 2.5,\ 2.0]$ for all the cases listed in Table 5.3.

It is also observed that the partial factors and the desired reliability for the calibration process are sensitive to the COV of the acceleration limit. Hence, appropriate uncertainty modelling of acceleration limit is required in order to adopt suitable partial factors for the calibrated design.

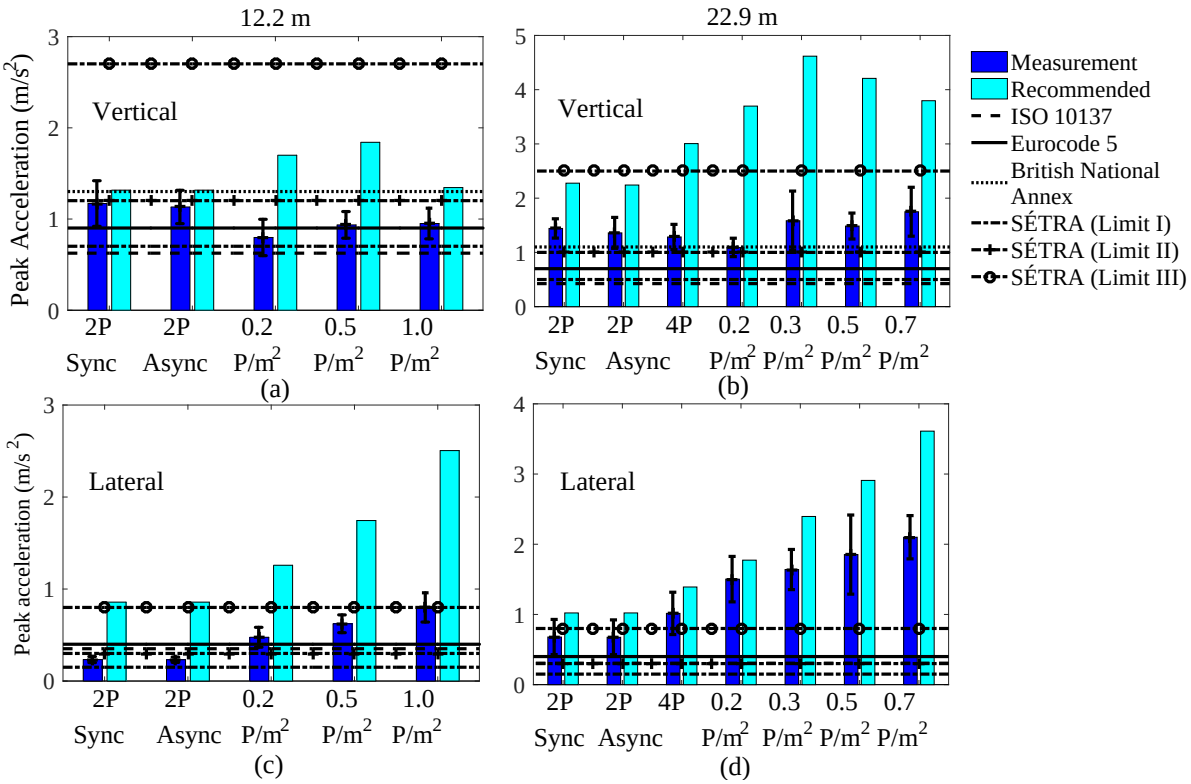

Figure 5.1: Comparison of measurements and peak accelerations predicted by the recommended methodology with comfort limits as proposed by several guidelines in the vertical ((a) and (b)) and the lateral directions ((c) and (d)) for the 12.2 m ((a) and (c)) and 22.9 m ((b) and (d)) bridge specimens (P stands for pedestrians; Limit I, Limit II and Limit III by SÉTRA guideline are defined in Table 2.4)

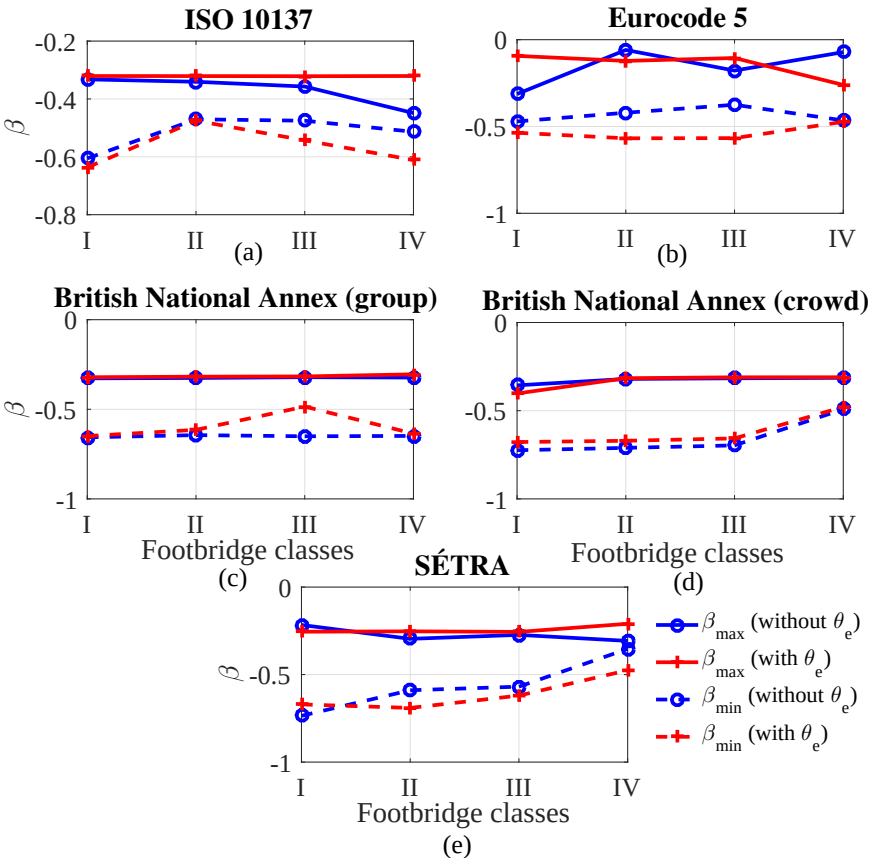

Figure 5.2: Maximum and minimum reliability levels for different footbridge classes designed with and without θ_e: (a) ISO 10137, (b) Eurocode 5, (c) British National Annex (group), (d) British National Annex (crowd), and (e) SÉTRA

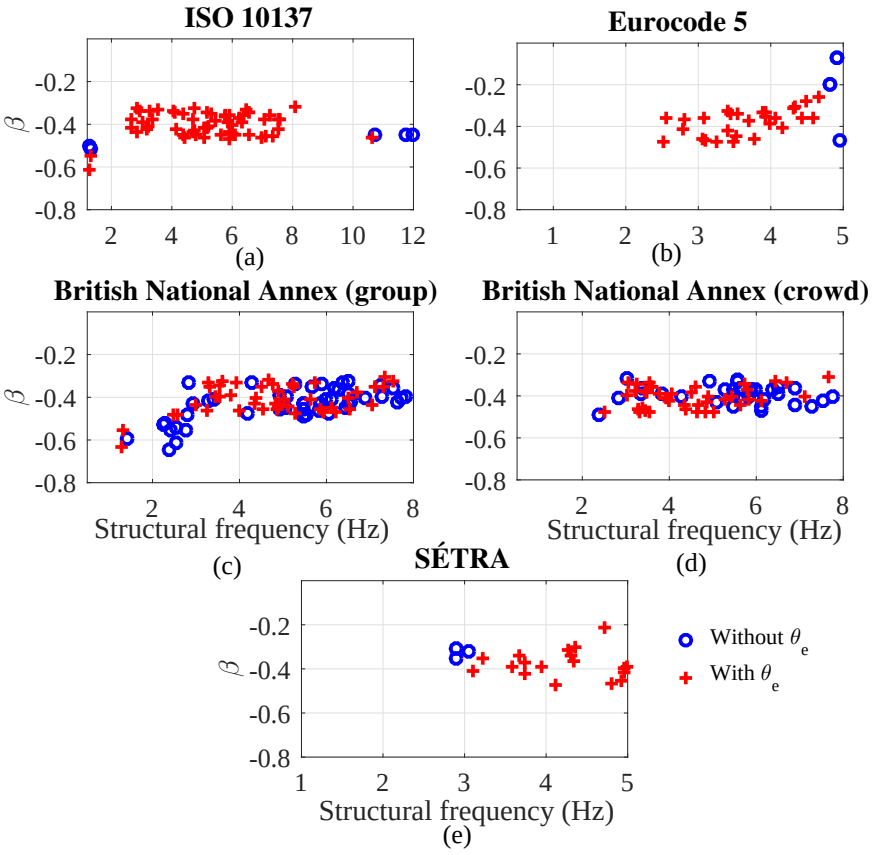

Figure 5.3: Reliability index for the optimally designed PBs of Class IV with and without considering θ_e: (a) ISO 10137, (b) Eurocode 5, (c) British National Annex (group), (d) British National Annex (crowd), and (e) SÉTRA

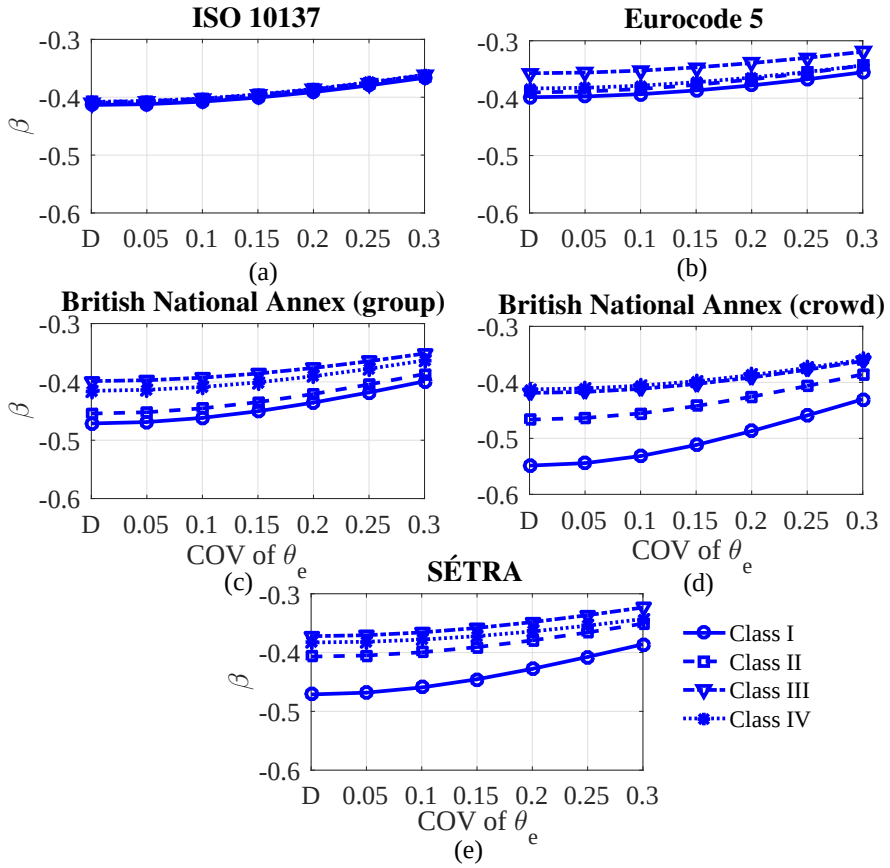

Figure 5.4: Variation in the mean reliability index with different levels of uncertainty (COV) in the model error term (θ_e) for various classes of PBs: (a) ISO 10137, (b) Eurocode 5, (c) British National Annex (group), (d) British National Annex (crowd), and (e) SÉTRA (D stands for deterministic θ_e)

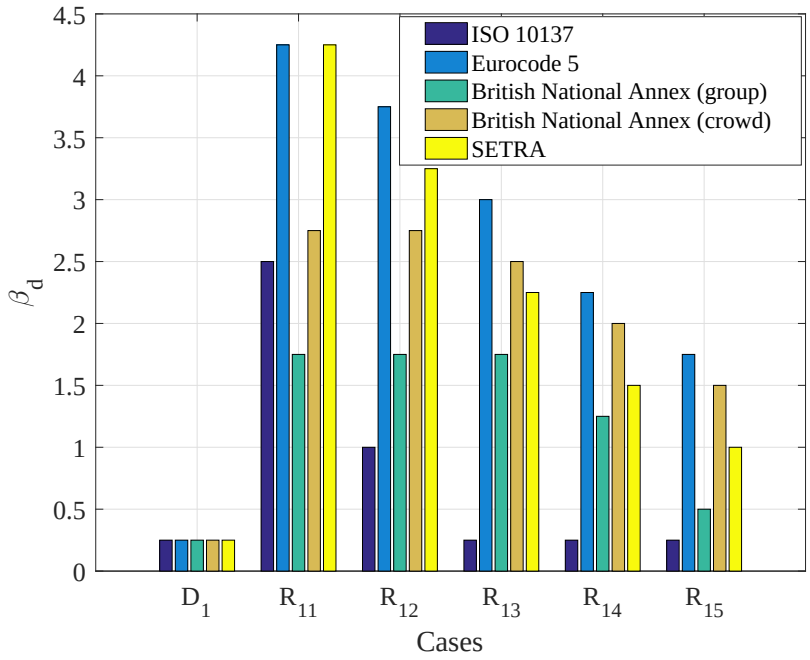

Figure 5.5: Desired reliability by different guidelines for different cases of comfort limits

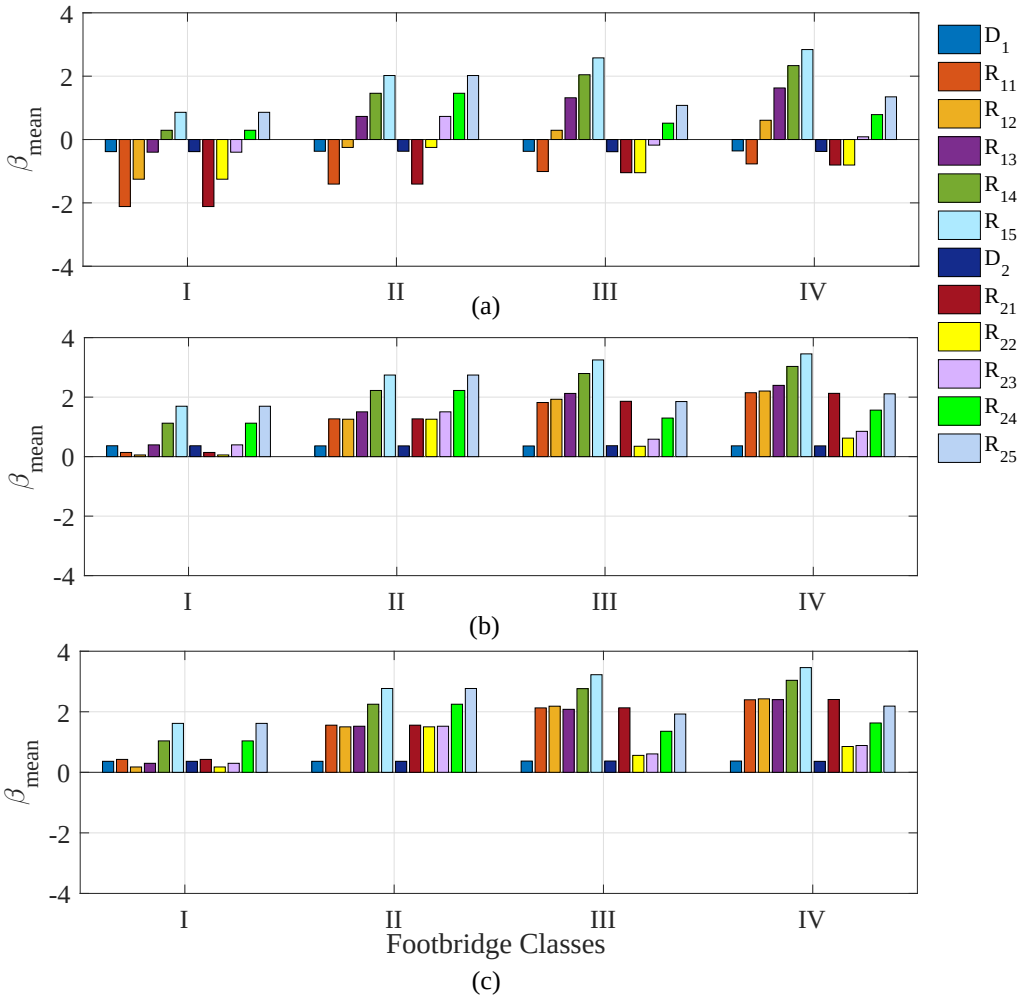

Figure 5.6: Mean reliability levels implied in ISO 10137 for different PB classes: (a) before calibration (without θ_{en}), (b) after calibration (without θ_{en}) and (c) after calibration (with θ_{en})

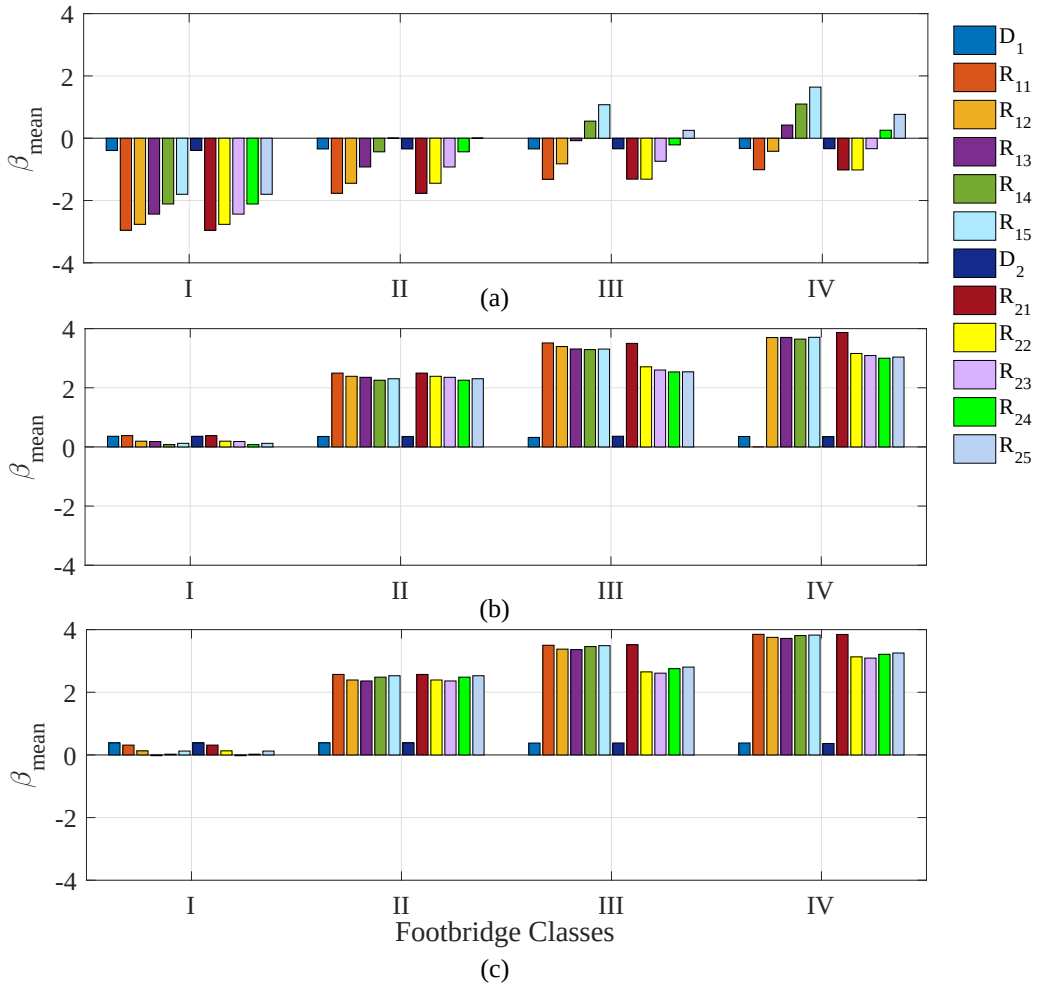

Figure 5.7: Mean reliability levels implied in Eurocode 5 for different PB classes: (a) before calibration (without θ_{en}), (b) after calibration (without θ_{en}) and (c) after calibration (with θ_{en})

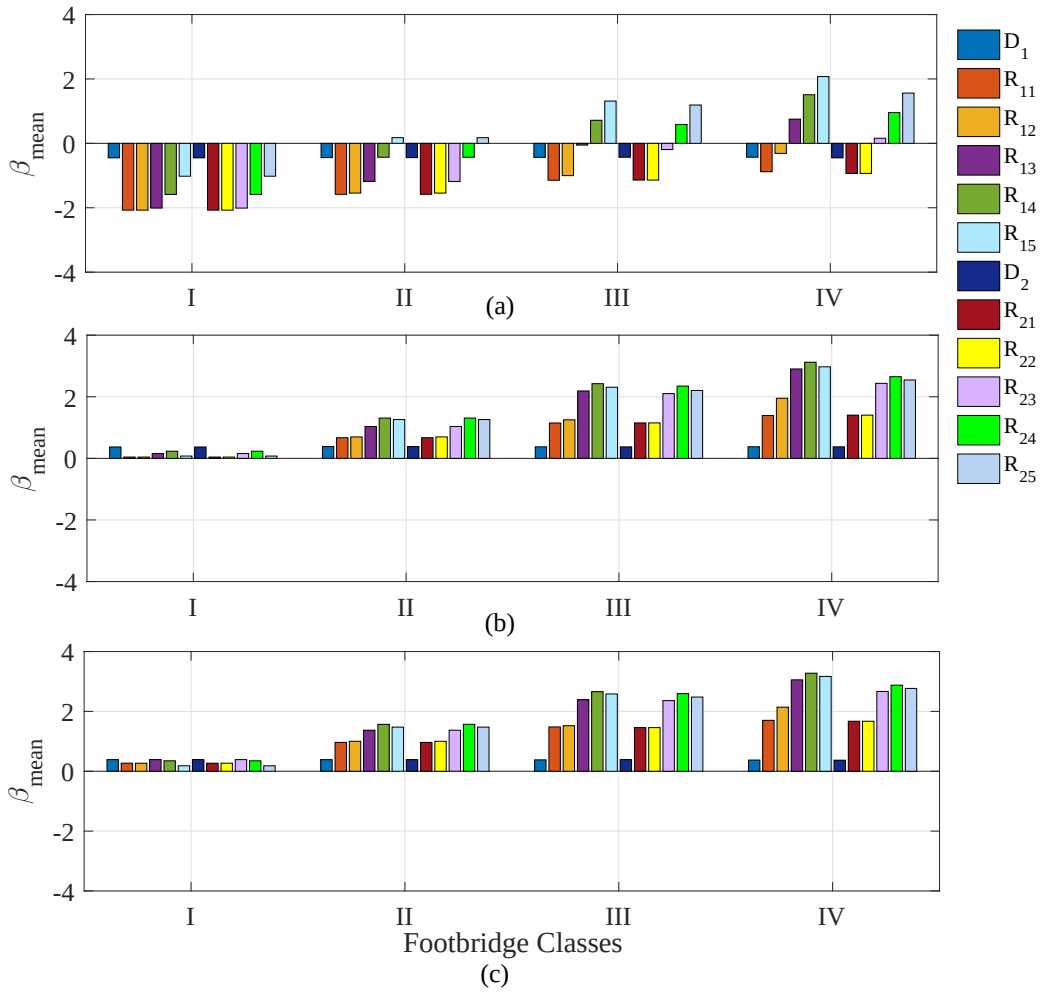

Figure 5.8: Mean reliability levels implied in British National Annex to Eurocode 1 (group) for different PB classes: (a) before calibration (without θ_{en}), (b) after calibration (without θ_{en}) and (c) after calibration (with θ_{en})

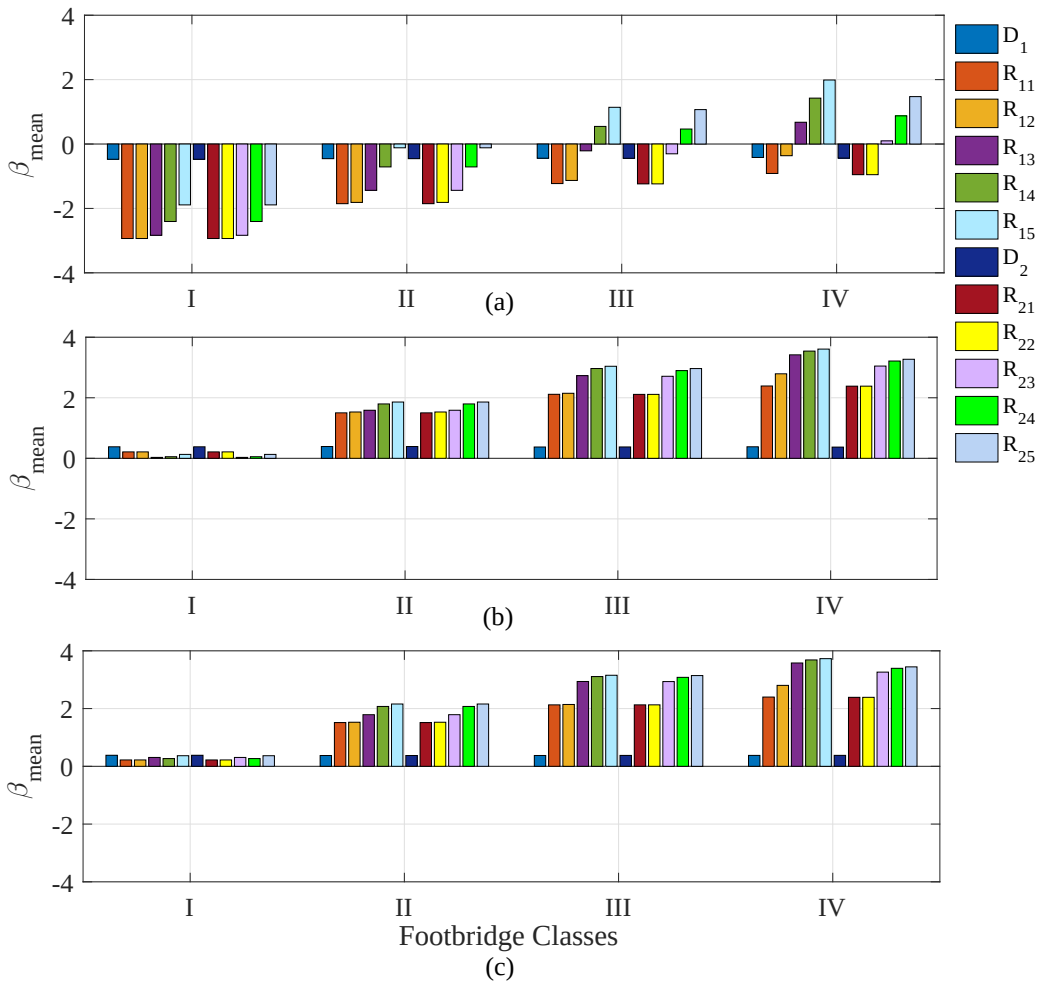

Figure 5.9: Mean reliability levels implied in British National Annex to Eurocode 1 (crowd) for different PB classes: (a) before calibration (without θ_{en}), (b) after calibration (without θ_{en}) and (c) after calibration (with θ_{en})

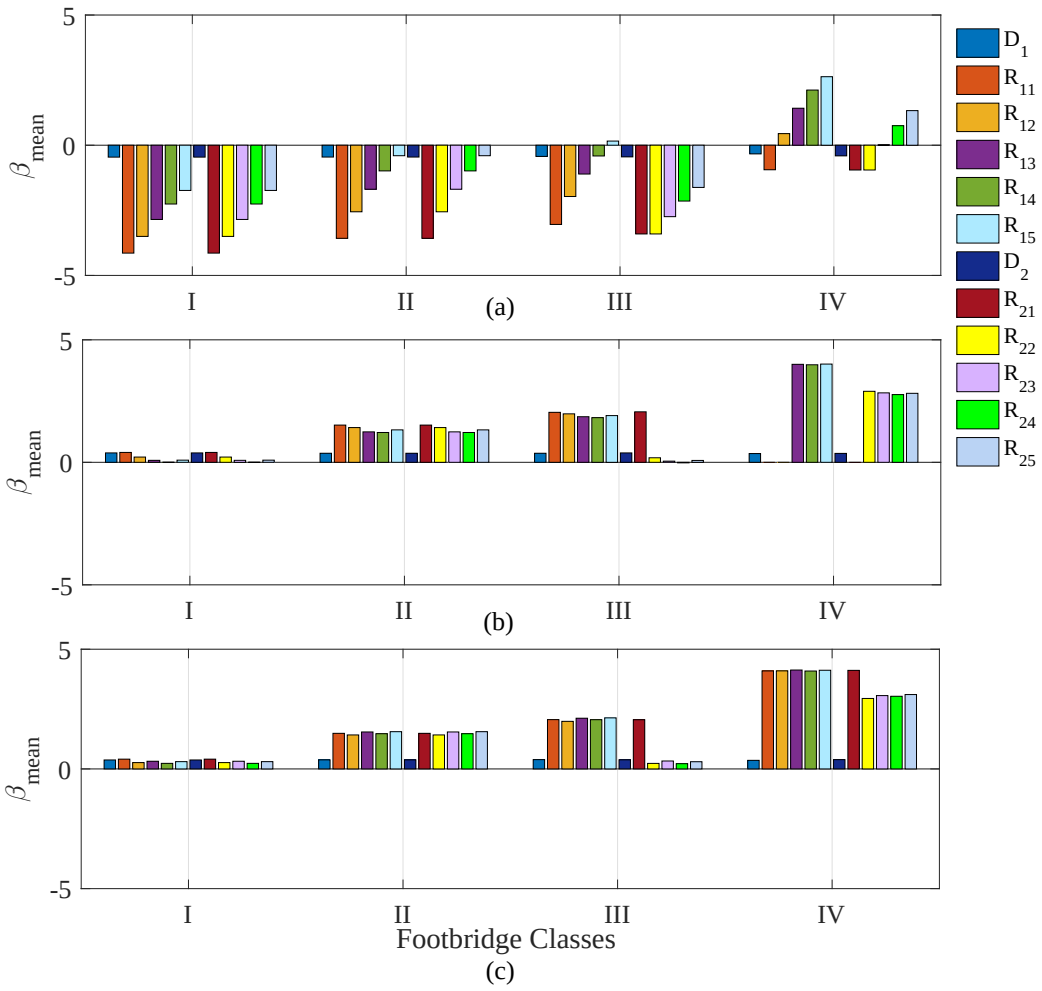

Figure 5.10: Mean reliability levels implied in SÉTRA for different PB classes: (a) before calibration (without θ_{en}), (b) after calibration (without θ_{en}) and (c) after calibration (with θ_{en})

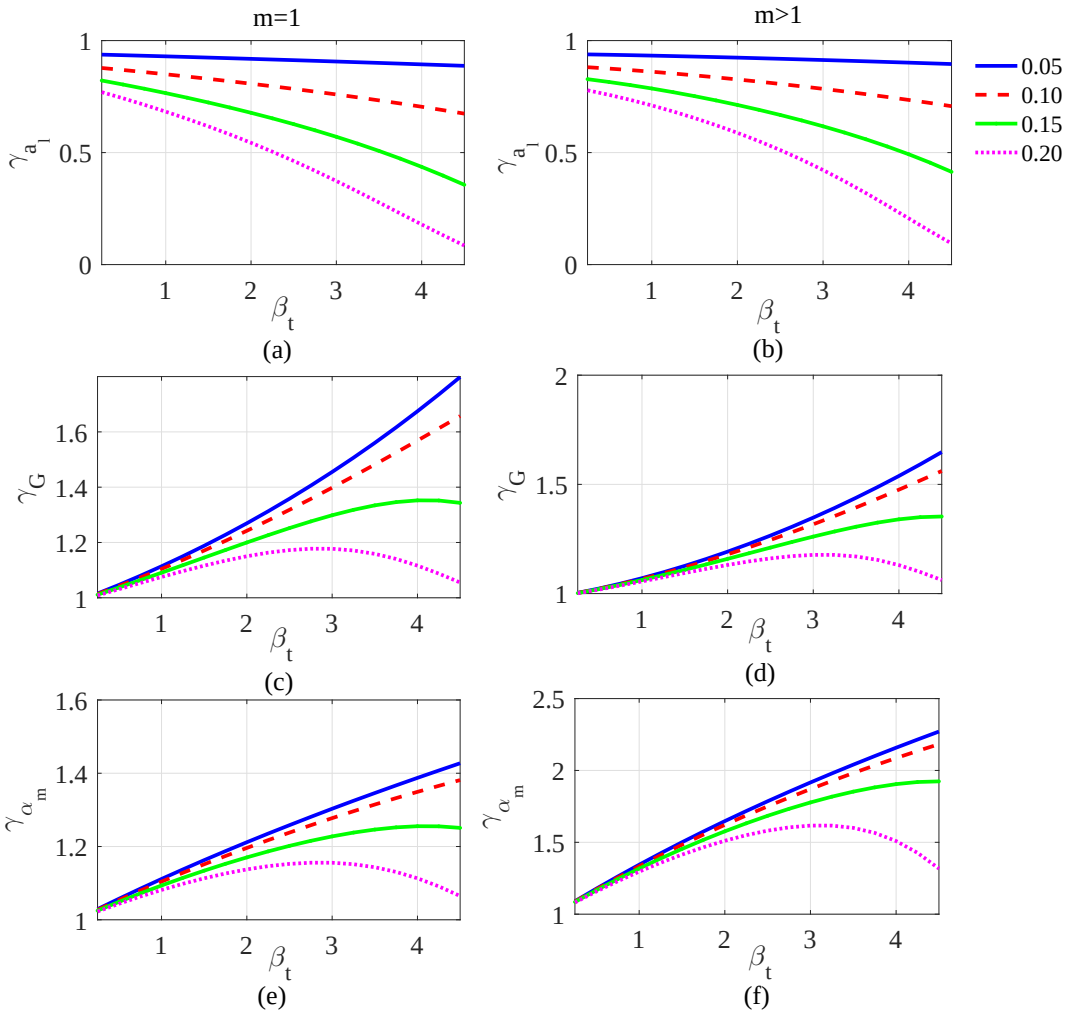

Figure 5.11: Variation in partial factors with COV of limit acceleration for different target reliability levels (β_t) corresponding to (a) a_l (m=1), (b) a_l ($m > 1$), (c) G ($m = 1$), (d) G ($m > 1$), (e) α_m ($m = 1$) and (f) α_m ($m > 1$), where m is the resonating harmonic of walking frequency

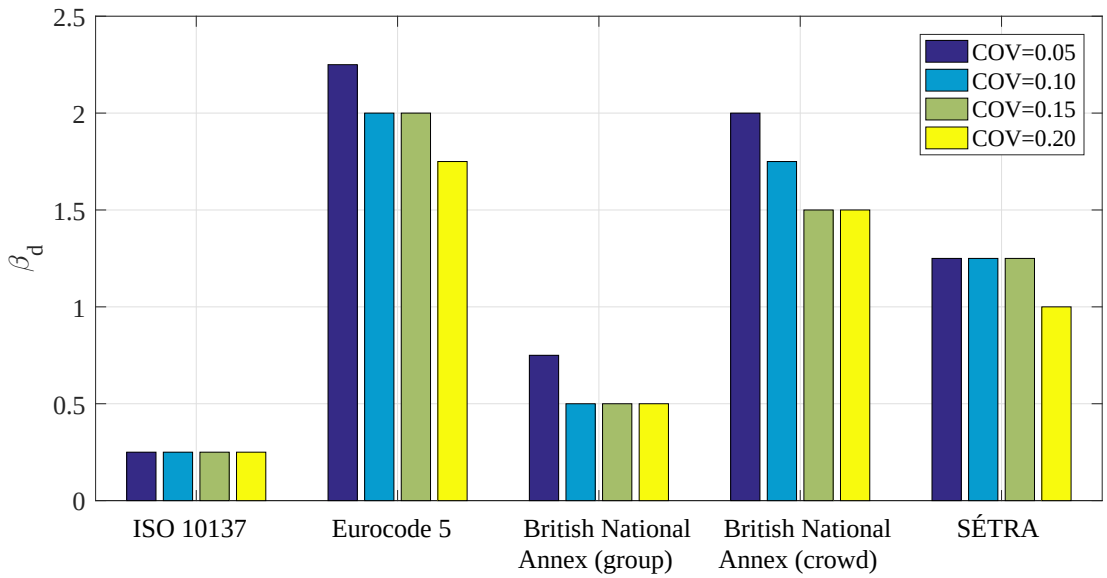

Figure 5.12: Desired reliability by different guidelines for Class I of PBs in case of R_{15} for different COVs of a_l

Chapter 6

Conclusions and recommendations

A comprehensive serviceability assessment of PBs under walking-induced excitations has been undertaken in this dissertation under a controlled set of tests. The performance of the popular serviceability design provisions under single and groups of pedestrians has been evaluated both in deterministic and probabilistic frameworks. This study has resulted in several recommendations to the existing guidelines in order to better align them with experimental observations. This chapter highlights the significant contributions, key conclusions, and recommendations for future work.

6.1 Significant contributions

The present research has led to several key contributions, which are summarized as follows:

1. A comprehensive experimental database of walking trials under different traffic scenarios has been developed on three full-scale PBs with emphasis on bridges that resonate with the higher harmonics of the walking frequency. This database is useful for verification of popular design load models and for effective comparison of their performances, which is especially important in order to improve the vibration serviceability design of PBs. Additionally, as the PBs are lively and the human-structure interaction phenomena was observed, the database will significantly contribute to the investigation of such interaction phenomenon.

2. The capabilities of the design guidelines to reliably assess the serviceability performance of the three bridges considered in the study have been investigated. The large

discrepancies between the computed and measured responses point towards improving the design provisions to produce reliable and economical designs.

3. Based on the study on the three bridges spanning a range of dynamic conditions, key recommendations have been proposed to reconcile the design guidelines through design parameters, which already exist in the literature. The recommendations can be easily incorporated into the existing design framework of the design methodologies and thus could contribute towards the better design of PBs.

4. Although the uncertain nature of pedestrian-induced walking load has been well acknowledged and accounted for in the standards, uncertainties in the acceleration limit and structural properties have not been studied. Hence, a reliability-based evaluation has been conducted for the design guidelines by incorporating uncertainties from all sources including the pedestrian and the structure. The current study is the first study to evaluate these guidelines in a reliability-based framework.

5. The results from the reliability analysis show that the guidelines fail to achieve sufficient reliability under rare traffic events, which could result in significant economic losses. Hence, the guidelines have been calibrated in order to achieve acceptable performance of the designs during rare traffic events, while at the same time producing economical designs. Assessing the guidelines in a reliability-based framework and subsequently calibrating them for improved design is a novel step towards the performance-based design of PBs under the serviceability limit state.

6. Several peer-reviewed journal and conference articles have directly resulted from this work by the author.

6.2 Conclusions

Having highlighted the significant contributions, the key conclusions resulting from this dissertation are summarized as follows:

1. One of the main conclusions of this study is that PBs that resonate with the higher harmonics of walking frequency, and not just the lowest harmonic, may be subjected to excessive vibrations, thus leading to serviceability issues.

2. A comparison study between the measured and simulated responses under single pedestrian walking tests for different scenarios of resonant and non-resonant conditions shows that the design walking load models are unable to capture the contributions from the transients, i.e. at the natural frequency of the structure for non-resonating cases (with respect to any of the harmonics), while they over-estimate for the resonant cases where the natural frequency and the excitation frequency (or one of the harmonics) overlap. For the case of resonance with a higher harmonic, the contribution from the corresponding non-resonating harmonics are underestimated by the models, which may be due to pedestrian-structure interaction. Moreover, for a fully non-resonant case (i.e. none of the harmonics are in resonance with the excitation), the models estimate the observations relatively well. These issues become very important for aluminum PBs, which tend to exhibit natural frequencies outside what is typically considered as the design frequency range, however tend to be lively due to their low inherent damping and light weight. Hence, more sophisticated models, which address these shortcomings are needed to better estimate the serviceability performance of such PBs.

3. The serviceability assessment under different crowd loads in accordance with the existing design guidelines shows that the response in general is overestimated in the vertical direction and underestimated in the lateral direction. Key recommendations are proposed in order to better align predictions through incorporating DLFs from more recent studies with higher number of harmonics, traffic-dependent walking speed, appropriate harmonics for resonance, added mass from pedestrians, and appropriate multiplication factors. It is observed from the comparison study that the existing design methodologies can be improved substantially by adopting the recommendations proposed here.

4. The design provisions are also evaluated in terms of *sufficiency* and *uniformity* by considering all possible traffic situations expected during the design life of the structure including design and rare traffic events. The reliability bounds, i.e., maximum and minimum reliability indices, reveal significant scatter over the range of designed configurations and classes of PBs. In terms of sufficiency, when a structure is designed for a specific crowd density (class), it does not satisfy the target value of 0 (according to ISO 2934 for reversible failures) under the design traffic. However, the minimum reliability levels for all of the designs are close to 0. Classes I to III PBs, with low to dense design traffic levels, achieve very low reliability levels under heavy traffic corresponding to rare loading events. Hence, it is suggested that the guidelines should be calibrated for higher reliability at the design event in order to achieve suf-

ficient reliability during rare events. However, always designing for very dense traffic may not be sound economically. Thus, it is recommended that comfort limits based on the frequency of occurrence of traffic be adopted to achieve economical designs for Class I to III bridges, while at the same time ensuring acceptable performance during rare loading events. Furthermore, design comfort limits should be established based on bridge class to yield economic designs along with uniform reliability across the classes.

5. A parametric study is performed to investigate the sensitivity of the reliability estimates to the uncertainties associated with a number of the key model variables. The study shows that the uncertainties in the bridge moment of area and mass per unit length have virtually no impact on the reliability estimates. On the other hand, the uncertainty in the elastic modulus has a significant contribution in the case of all of the design provisions except those in ISO 10137 for very low values of the response reduction factors. On the other hand, the reliability results are not very sensitive to the COV of damping. In general, all the variables corresponding to the structure can conservatively be treated as deterministic for code calibration purposes. The study also suggests that assuming a normal distribution for the limiting acceleration instead of log-normal or an extreme value distribution will not have a significant impact on the reliability estimates of the bridges.

6. A model error term is introduced in order to incorporate the recommendations in the existing framework of the design provisions. Reliability analysis is carried out by introducing uncertainty in the model error term, which shows a positive impact on the reliability estimates, and hence this term can be assumed deterministic for calibration purposes.

7. An attempt to calibrate the guidelines is made in the current thesis. The guidelines achieve acceptable performance during the design as well as rare loading events after calibrating for a higher reliability at the design level. Moreover, adopting comfort limits based on occurrence frequency of traffic and bridge class ensures economic designs through the calibrated design provisions. Similar to target reliability, a new term called the desired reliability is introduced in the current study, which is required for the calibration process. The desired reliability and corresponding partial factors are estimated for all the guidelines. Although the partial factors are identical in all the guidelines for a given reliability index, the desired reliability is inconsistent across the guidelines and subsequently the resulting partial factors for the calibrated design. It is also observed that estimates of the desired reliability and partial factors are sensitive to the choice of COV for the acceleration limit. Hence, an appropriate

uncertainty model for acceleration limit is required in order to adopt the suitable partial factors for the calibrated design procedures.

6.3 Limitations of the current study

After summarizing the key conclusions resulting from this dissertation, the limitations of the current study are outlined below:

- The current study adopts truss type metal PBs with simply supported boundary conditions, idealized as a simply supported beam. Moreover, the structural response has been estimated in the modal domain with one dominating mode of vibration. Despite these assumptions, it is expected that the key observations will remain the same in terms of the performance of the design load models in deterministic as well as reliability-based frameworks, while the partial factors estimated in Chapter **5** are limited to only metal PBs, for which the structural variables can be assumed deterministic. A sensitivity study should be performed with the uncertainty models of the structural variables for different material characteristics and the assumption whether the structural variables can be assumed deterministic needs to be re-investigated for such cases.
- The key recommendations proposed in Chapter **5** to improve the design guidelines for serviceability assessment of PBs under crowd loads are based on observations from only a limited number of PBs. While most of the recommendations are expected to be applicable to other bridges, the accuracy of the recommended multiplication and dynamic load factors should be investigated based on more experiments on different types of bridges.

6.4 Recommendations for future study

There are several possible extensions to the present work to improve the serviceability design of PBs under walking-induced excitations, which are beyond the current scope of study. These include:

1. The comprehensive database of walking tests developed in the current study can serve as a good test-bed for investigating human-structure interaction phenomena observed in many failures.

2. The current study is only limited to the performance of time-domain periodic load models, which are adopted by the design guidelines. Recently, there is a trend towards biomechanical models. A performance verification for such load models could be carried out using this current database.

3. During the course of this experimental study, forces at the supports of the laboratory bridge specimens were also measured using load cells. The walking-induced force models can be calibrated thorough these measured forces in the future, which can substantially contribute towards further improving the design guidelines.

4. The measured acceleration responses can be useful in order to estimate walking-induced forces through inverse analysis, which can substantially contribute towards investigating the effect of human-structure interaction on the induced walking force.

5. The key recommendations proposed in the current study to improve the vibration serviceability assessment of PBs under crowd loads are primarily based on experimental observations from two aluminum PBs. Additional bridge types and tests could add to the value and accuracy of the main conclusions from this work.

6. Based on the key recommendations proposed in the current study, a model error term has been introduced to the existing design provisions. This term can be calibrated using experimental observations on various PBs in the future.

7. The reliability analysis and corresponding code calibration is limited to the vertical direction. The analysis can be easily extended to the lateral direction by adopting different configurations of PBs, which are more sensitive to the lateral vibrations and are within the lateral critical frequency ranges as suggested by the guidelines in Table 2.3.

8. In the absence of a target reliability for calibration, the current study has iteratively estimated the reliability level required for achieving sufficient reliability without conducting any cost-based analysis. In the future, a target reliability index can be determined using other measures such as consequence of failure.

References

AASHTHO LRFD. Guide specifications for the design of pedestrain bridges. *AASHTHO LRFD Bridge Design*, 2007.

M. Abu-Hilal and M. Mohsen. Vibration of beams with general boundary conditions due to a moving harmonic load. *Journal of Sound and Vibration*, 232(4):703–717, 2000.

H. Adeli. *Historic bridges: Evaluation, preservation, and management*. CRC Press, 2016.

AIJES-V001. Guidelines for the evaluation of habitability to building vibration. Standard, Architectural Institute of Japan Recommendations, Tokyo, Japan, 2004.

D. E. Allen and T. M. Murray. Design criterion for vibrations due to walking. *AISC Journal*, 30(4):117–129, 1993.

P. Archbold, P. J. Fanning, and A. Pavić. Interactive horizontal load model for pedestrians crossing footbridges. *Bridge Structures*, 1(3):169–176, 2005.

AS 5100. Bridge design, part 2: Design loads. *Australian Standard*, 2004.

H. Bachmann and W. Ammann. *Vibrations in structures: induced by man and machines*, volume 3. Iabse, 1987.

H. Bachmann, A. J. Pretlove, and H. Rainer. *Dynamic forces from rhythmical human body motions. In: Vibration problems in structures: practical guidelines*. Basel: Birkhauser, 1995.

R. Bashor, T. Kijewski-Correa, and A. Kareem. On the wind-induced response of tall buildings: the effect of uncertainties in dynamic properties and human comfort thresholds. In *Proceedings of Americas Conference on Wind Engineering, Baton Rouge, LA*, volume 31, 2005.

J. Blanchard, B. L. Davies, and J. W. Smith. Design criteria and analysis for dynamic loading of footbridges. In *Proceeding of a Symposium on Dynamic Behaviour of Bridges at the Transport and Road Research Laboratory, Crowthorne, Berkshire, England, May 19, 1977*, 1977.

M. Bocian, J. H. G. Macdonald, and J. F. Burn. Biomechanically inspired modelling of pedestrian-induced forces on laterally oscillating structures. *Journal of Sound and Vibration*, 331(16):3914–3929, 2012.

M. Bocian, J. H. G. Macdonald, and J. F. Burn. Biomechanically inspired modeling of pedestrian-induced vertical self-excited forces. *Journal of Bridge Engineering*, 18(12): 1336–1346, 2013.

K. Breitung. Asymptotic approximations for multinormal integrals. *Journal of Engineering Mechanics*, 110(3):357–366, 1984.

J. M. W. Brownjohn, P. Fok, and P. Roche, M.and Moyo. Long span steel pedestrian bridge at singapore changi airport-part 1: Prediction of vibration serviceability problems. *Structural Engineer*, 82(16), 2004a.

J. M. W. Brownjohn, A. Pavić, and P. Omenzetter. A spectral density approach for modelling continuous vertical forces on pedestrian structures due to walking. *Canadian Journal of Civil Engineering*, 31(1):65–77, 2004b.

BS 5400. Steel concrete and composite bridges: Specification for loads; appendix c: Vibration serviceability requirements for foot and cycle track bridges. *UK: British Standards Association, London*, 1978.

C. Butz. Codes of practice for lively footbridges: State-of-the-art and required measures. *Proceedings of footbridge*, 2008.

C. H. Butz, C. H. Heinemeyer, A. Goldack, A. Keil, M. Lukic, E. Caetano, and A. Cunha. *Advanced Load Models for Synchronous Pedestrian Excitation and Optimised Design Guidelines for Steel Footbridges - SYNPEX).* European Commission - Directorate-General for Research; EUR 23318; ISBN 978-92-79-08303-7, ISSN 1018-5593, 2008.

E. Caetano and A. Cunha. Dynamic tests on a lively footbridge. *Proc., and Footbridge 2002*, pages 1–11, 2002.

E. Caetano, Á. Cunha, F. Magalhães, and C. Moutinho. Studies for controlling human-induced vibration of the pedro e inês footbridge, portugal. part 1: Assessment of dynamic behaviour. *Engineering Structures*, 32(4):1069–1081, 2010.

CAN/CSA S6. Canadian highway bridge design code. *Canadian Standards Association, Canada*, 2011.

C. C. Caprani, J. Keogh, P. Archbold, and P. Fanning. Characteristic vertical response of a footbridge due to crowd loading. 2011.

C. C. Caprani, J. Keogh, P. Archbold, and Fanning P. Enhancement factors for the vertical response of footbridges subjected to stochastic crowd loading. *Computers & Structures*, (102):87–96, 2012.

P. W. Chen and L. E. Robertson. Human perception thresholds of horizontal motion. *Journal of the structural division*, 92(8):1681–1695, 1972.

C. A. Cornell. A probability-based structural code. In *Journal Proceedings*, volume 66, pages 974–985, 1969.

Cornell University. Explaining why the millennium bridge wobbled, November 2005. URL https://www.sciencedaily.com/releases/2005/11/051103080801.htm.

A Cunha, E. Caetano, C. Moutinho, and F. Magalhães. Damping identification in a stress-ribbon footbridge. *Proceedings of EURODYN 2005*, 2005.

Curbed New York. Squibb park bridge will cost $3.12m to fix once and for all, October 2016. URL http://ny.curbed.com/2016/10/7/13201020/squibb-park-bridge-brooklyn-construction-cost.

F. T. da Silva, H. M. B. F. Brito, and R. L. Pimentel. Modeling of crowd load in vertical direction using biodynamic model for pedestrians crossing footbridges. *Canadian Journal of Civil Engineering*, 40(12):1196–1204, 2013.

P. Dallard, T. Fitzpatrick, A. Flint, et al. London millennium bridge: pedestrian-induced lateral vibration. *Journal of Bridge Engineering*, 6(6):412–417, 2001.

F. Danbon and G. Grillaud. Dynamic behaviour of a steel footbridge: Characterization and modelling of the dynamic loading induced by a moving crowd on the solferino footbridge in paris. *Proceedings of Footbridge*, 2005.

F. Dierick, M. Penta, D. Renaut, and C. Detrembleur. A force measuring treadmill in clinical gait analysis. *Gait & posture*, 20(3):299–303, 2004.

A. Ebrahimpour, R. L. Sack, W. N. Patten, and A. Hamam. Experimental measurements of dynamic loads imposed by moving crowds. In *Structures Congress XII*, pages 1385–1390, 1994.

A. Ebrahimpour, A. Hamam, R. L. Sack, and W. N. Patten. Measuring and modeling dynamic loads imposed by moving crowds. *Journal of Structural Engineering*, 122(12): 1468–1474, 1996.

H. Elftman. The measurement of the external force in walking. *Science*, 88(2276):152–153, 1938.

B. R. Ellis. The influence of crowd size on floor vibrations induced by walking. *Structural Engineer*, 81(6):20–27, 2003.

EN 1990. Eurocode - basis of structural design. *European Committee of Standardization, Eurocode 0*, 2001.

EN 1995-2. Design of timber structures - part 2: Bridges. *European Committee of Standardization, Eurocode 5*, 2004.

FIB. Guidelines for the design of footbridges. *Bulletin 32, Lausanne*, 2005.

Y. Fujino, B. M. Pacheco, S. Nakamura, and P. Warnitchai. Synchronization of human walking observed during lateral vibration of a congested pedestrian bridge. *Earthquake engineering & structural dynamics*, 22(9):741–758, 1993.

F. W. Galbraith and M. V. Barton. Ground loading from footsteps. *The Journal of the Acoustical Society of America*, 48(5B):1288–1292, 1970.

S. A. Gard, S. C. Miff, and A. D. Kuo. Comparison of kinematic and kinetic methods for computing the vertical motion of the body center of mass during walking. *Human movement science*, 22(6):597–610, 2004.

R. J. Hansen, J. W. Reed, and E. H. Vanmarcke. Human response to wind-induced motion of buildings. *Journal of the structural division*, 99(7):1589–1605, 1973.

F. C. Harper. The mechanics of walking. *Research applied in Industry*, 15(1):23–28, 1962.

A. M. Hasofer and N. C. Lind. Exact and invariant second-moment code format(for reliability analysis in multivariate problems). *American Society of Civil Engineers, Engineering Mechanics Division, Journal*, 100:111–121, 1974.

C. Heinemeyer, C. Butz, A. Keil, M. Schlaich, A. Golbeck, S. Trometor, M. Lukic, B. Chabrolin, A. Lemaire, P. Martin, A. Cunha, and E. Caetano. Design of lightweight footbridges for human induced vibrations. EUR - Scientific and Technical Research Reports JRC53442, 2009. URL http://publications.jrc.ec.europa.eu/repository/handle/JRC53442.

M. A. B. U. Hilal and H. S. Zibdeh. Vibration analysis of beams with general boundary conditions traversed by a moving force. *Journal of Sound and Vibration*, 229(2):377–388, 2000.

F. B. Hildebrand. *Introduction to numerical analysis, section 9.4*. New York: McGraw-Hill, 1956.

HIVOSS. Design of footbridges. *Human induced vibration of steel structures*, 2008.

J. Humar. *Dynamics of Structures*. CRC press,, 2012.

A. W. Irwin. Human reactions to oscillations of buildings-acceptable limits. *Build International*, 8(2):7, 1975.

ISO 10137. Bases for design of structures - serviceability of buildings and walkways against vibrations. *Ethiopian Standards Agency*, 2007.

ISO 2394. General principles on reliability for structures. *Zurich: ISO*, 1998.

J. Kanda, Y. Tamura, and K. Fujii. Probabilistic criteria for human perception of low-frequency horizontal motions. In *Proceedings of symposium/workshop on serviceability of buildings, Ottawa*, pages 260–269, 1988.

M. Kasperski and C. Sahnaci. Serviceability of pedestrian structures. In *Proceedings of the 25th international modal analysis conference, Orlando, Florida*, pages 774–98, 2007.

S. C. Kerr. *Human Induced Loading on Staircases*. PhD Thesis, Mechanical Engineering Department, University College London, UK, 1998.

S. Kim, K. Cho, M. Choi, M. S. Choi, and J. Y. Lim. Development of human body model for the dynamic analysis of footbridges under pedestrian induced excitation. *Journal of Steel Structures*, 8:333–345, 2008.

H. Kramer and H. W. Kebe. Man-induced structural vibrations. *Der Bauingenieur*, 54(5): 195–199, 1980.

J. H. G. Macdonald. Pedestrian-induced vibrations of the clifton suspension bridge, uk. *Proceedings of the ICE-Bridge Engineering*, 161(2):69–77, 2008.

W. Mader and A. Pieper. Schwansbell bridge celebrating 50th birthday. *Structural engineering international*, 16(4):356–359, 2006.

Y. Matsumoto, T. Nishioka, H. Shiojiri, and K. Matsuzaki. Dynamic design of footbridges. In *IABSE proceedings*, volume 2, 1978.

NA to BS EN 1991-2. UK national annex to Eurocode 1. actions on structures-part 2: Traffic loads on bridges. *British Standards Institution*, 2003.

S. Nakamura. Field measurements of lateral vibration on a pedestrian suspension bridge. *Structural Engineer*, 81(22), 2003.

A. S. Nowak and K. R. Collins. *Reliability of structures*. CRC Press, 2012.

A. Pachi and T. Ji. Frequency and velocity of people walking. *Structural Engineer*, 83(3), 2005.

L. Pedersen. Damping effect of humans. In *Topics on the Dynamics of Civil Structures, Volume 1*, pages 1–6. Springer, 2012.

L. Pedersen and C. Frier. Sensitivity of footbridge vibrations to stochastic walking parameters. *Journal of Sound and Vibration*, 329(13):2683–2701, 2010.

G. Pernica. Dynamic load factors for pedestrian movements and rhythmic exercises. *Canadian Acoustics*, 18(2):3, 1990.

J. Perry. Gait analysis. *Normal and pathological function*, 1, 1992.

R. L. Pimentel. *Vibrational performance of pedestrian bridges due to human-induced loads*. PhD thesis, University of Sheffield, 1997.

K. Portier, T. J. Keith, and S. M. Roberts. Body weight distributions for risk assessment. *Risk analysis*, 27(1):11–26, 2007.

J. W. Qin, S. S. Law, Q. S. Yang, and N. Yang. Pedestrian–bridge dynamic interaction, including human participation. *Journal of Sound and Vibration*, 332(4):1107–1124, 2013.

V. Racic and J. M. W. Brownjohn. Stochastic model of near-periodic vertical loads due to humans walking. *Advanced Engineering Informatics*, 25(2):259–275, 2011.

V. Racic, J. M. W. Brownjohn, and A. Pavić. Human walking and running forces: Novel experimental characterization and application in civil engineering dynamics. In *Proceedings IMAC XXVI Conference, Orlando/Florida/USA*, 2008.

R. Rackwitz and B. Flessler. Structural reliability under combined random load sequences. *Computers & Structures*, 9(5):489–494, 1978.

M. D. Rahman and K. Yu. Total least squares approach for frequency estimation using linear prediction. *Acoustics, Speech and Signal Processing, IEEE Transactions on*, 35 (10):1440–1454, 1987.

J. H. Rainer, G. Pernica, and D. E. Allen. Dynamic loading and response of footbridges. *Canadian Journal of Civil Engineering*, 15(1):66–71, 1988.

E. Reynders, K. Maes, G. Lombaert, and G. De Roeck. Uncertainty quantification in operational modal analysis with stochastic subspace identification: Validation and applications. *Mechanical Systems and Signal Processing*, 66:13–30, 2016.

F. Ricciardelli and A. D. Pizzimenti. Lateral walking-induced forces on footbridges. *Journal of bridge engineering*, 12(6):677–688, 2007.

P. O. Riley, G. Paolini, U. Della Croce, K. W. Paylo, and D. C. Kerrigan. A kinematic and kinetic comparison of overground and treadmill walking in healthy subjects. *Gait & posture*, 26(1):17–24, 2007.

I. Roos. Human induced vibrations of footbridges: Application and comparison of pedestrian load model. Master's thesis, Delft University of Technology, Netherlands, 2009.

C. Sahnaci and M. Kasperski. Random loads induced by walking. In *Proceedings of the sixth European conference on structural dynamics*, volume 1, pages 441–6, 2005.

R. Salgado, J. M. Branco, P. J. S. Cruz, and G. Ayala. Serviceability assessment of the góis footbridge using vibration monitoring. *Case Studies in Nondestructive Testing and Evaluation*, 2:71–76, 2014.

W. W. Sanders and R. E. Abendroth. Construction and evaluation of a continuous aluminum girder highway bridge. *American Welding Society(USA)*, pages 107–114, 1995.

H. Schulze. Dynamic effects of the live load on footbridges. *Signal und Schiene*, 24(2): 91–93, 1980.

SÉTRA. Assessment of vibrational behaviour of footbridges under pedestrian loading. *Technical guide SÉTRA, Paris, France*, 2006.

F. T. Silva and R. L. Pimentel. Biodynamic walking model for vibration serviceability of footbridges in vertical direction. In *Proceeding of the 8th International Conference on Structural Dynamics (Eurodyn 2011)*, pages 1090–1096, 2011.

G. G. Simoneau. Kinesiology of walking. *Kinesiology of the musculoskeletal system: foundations for physical rehabilitation*, 1:523, 2002.

T. Siwowski. Aluminium bridges–past, present and future. *Structural engineering international*, 16(4):286–293, 2006.

M. G. Stewart. Optimization of serviceability load combinations for structural steel beam design. *Structural Safety*, 18(2):225–238, 1996.

A. Sychterz. Vibration characterisation of aluminium pedestrian bridges. 2014.

A. Sychterz, A. Sadhu, S. Narasimhan, and S. Walbridge. Results from modal testing of the daigneault creek bridge. In *CSCE 2013 General Conference, Montral, Qubec, May 29 to June 1*, 2013.

T. Tredgold. *Elementary principles of carpentry*. E. & FN Spon, 1890.

K. Van Nimmen, G. Lombaert, G. De Roeck, and P. Van den Broeck. Vibration serviceability of footbridges: Evaluation of the current codes of practice. *Engineering Structures*, 59:448–461, 2014.

A. C. W. M. Vrouwenvelder and A. J. M. Siemes. Probabilistic calibration procedure for the derivation of partial safety factors for the netherlands building codes. *HERON, 32 (4), 1987*, 1987.

J. E. Wheeler. Prediction and control of pedestrian-induced vibration in footbridges. *Journal of the structural division*, 108(ST-9), 1982.

M. W. Whittle. *Gait analysis: an introduction*. 2003.

M. Willford. Dynamic actions and reactions of pedestrians. In *Proceedings of the International Conference on the Design and Dynamic Behaviour of Footbridges, Paris, France, November 20-22*, pages 66–74, 2002.

M. R. Willford, P. Young, and M. CEng. *A design guide for footfall induced vibration of structures*. Concrete Society London, UK, 2006. ISBN 9781904482291.

M. Yamasaki, T. Sasaki, and M. Torii. Sex difference in the pattern of lower limb movement during treadmill walking. *European journal of applied physiology and occupational physiology*, 62(2):99–103, 1991.

P. Young. Improved floor vibration prediction methodologies. In *Proceedings Arup's Seminar on Structural Vibration and Structure-Borne Noise: Current Developments in Assessment and Design, 4 October 2001, ImechE, London*, 2001.

F. Zheng, L. Shao, V. Racic, and J. Brownjohn. Measuring human-induced vibrations of civil engineering structures via vision-based motion tracking. *Measurement*, 83:44–56, 2016.

S. Živanović. *Probability-based estimation of vibration for pedestrian structures due to walking.* PhD thesis, University of Sheffield, 2006.

S. Živanović. Benchmark footbridge for vibration serviceability assessment under the vertical component of pedestrian load. *Journal of Structural Engineering*, 138(10):1193–1202, 2012.

S. Živanović, A. Pavić, and P. Reynolds. Vibration serviceability of footbridges under human-induced excitation: a literature review. *Journal of sound and vibration*, 279(1): 1–74, 2005.

S. Živanović, A. Pavić, and P. Reynolds. Probability-based prediction of multi-mode vibration response to walking excitation. *Engineering Structures*, 29(6):942–954, 2007.

S. Živanović, A. Pavić, and E. T. Ingólfsson. Modeling spatially unrestricted pedestrian traffic on footbridges. *Journal of Structural Engineering*, 136(10):1296–1308, 2010.

APPENDICES

Appendix A

Response simulation

The analytical solution for Equation 2.24 are derived, based on the works by Abu-Hilal and Mohsen (2000) and Hilal and Zibdeh (2000), through employing the principle of superposition of responses from a constant moving load G and the harmonic loading terms. The displacement response X_n under a constant moving load $P(t) = G$ as shown in Figure 2.12 is given by (Hilal and Zibdeh, 2000):

$$X_n = \frac{G\exp(-\zeta_n\omega_n t)(Y_{n1} + \exp(\zeta_n\omega_n t)Y_{n2})L}{\omega_{dn}M_n((\zeta_n\omega_n L)^4 + 2(\zeta_n\omega_n L^2\omega_{dn})^2 + 2(\zeta_n\omega_n L v\pi)^2 + (\omega_{dn}L)^4 - 2(\omega_{dn}Lv\pi)^2 + (v\pi)^4)} \tag{A.1}$$

with,

$$\begin{aligned} Y_{n1} &= (v\pi\zeta_n^2\omega_n^2L^2 + v^3\pi^3 - \omega_{dn}^2L^2v\pi)\sin(\omega_{dn}t) + 2\zeta_n\omega_nL^2\omega_{dn}v\pi\cos(\omega_{dn}t) \\ Y_{n2} &= (-L\omega_{dn}v^2\pi^2 + L^3\omega_{dn}\zeta_n^2\omega_n^2 + L^3\omega_{dn}^3)\sin(\frac{v\pi t}{L}) - 2L^2\omega_{dn}\zeta_n\omega_n v\pi\cos(v\pi t/L) \end{aligned} \tag{A.2}$$

where, $\omega_{dn} = \omega_n\sqrt{1-\zeta_n^2}$ with ω_n and ζ_n being the nth natural frequency and damping constant of the structure.

The displacement response due to the sinusoidal moving force $P(t) = G\alpha_m\sin(m2\pi f_s)$ for m^{th} harmonic can be derived as (Abu-Hilal and Mohsen, 2000):

$$X_{mn} = F_2(t_1 + t_2 + t_3 + t_4 + t_5 + t_6 + t_7 + t_8 + t_9 + t_{10}) \tag{A.3}$$

where, the terms, $t_1 \cdots t_{10},\ F_2$, are given by:

$$
\begin{aligned}
F_2 &= \frac{G\alpha_{mn}}{4M_n\omega_{dn}} \\
t_1 &= -(\frac{q_3}{q_4} + \frac{q_9}{q_{10}})\cos((\frac{v\pi}{L} + \omega_m)t) \\
t_2 &= (\frac{q_5}{q_6} + \frac{q_7}{q_8})\cos((\frac{v\pi}{L} - \omega_m)t) \\
t_3 &= -(\frac{\zeta_n\omega_n}{q_4} - \frac{\zeta_n\omega_n}{q_{10}})\sin((\frac{v\pi}{L} + \omega_m)t) \\
t_4 &= (\frac{\zeta_n\omega_n}{q_6} - \frac{\zeta_n\omega_n}{q_8})\sin((\frac{v\pi}{L} - \omega_m)t) \\
t_5 &= -(\frac{q_1q_3}{q_{13}} - \frac{q_1q_3}{q_{14}})\exp(t\frac{v\pi}{L})\cos(\omega_m t) \\
t_6 &= (\frac{q_2q_4}{q_{15}} - \frac{q_2q_4}{q_{16}})\exp(-t\frac{v\pi}{L})\cos(\omega_m t) \\
t_7 &= (\frac{q_3q_{11}}{q_{13}} + \frac{q_3q_{12}}{q_{14}})\exp(t\frac{v\pi}{L})\sin(\omega_m t) \\
t_8 &= -(\frac{q_4q_{11}}{q_{15}} + \frac{q_4q_{12}}{q_{16}})\exp(-t\frac{v\pi}{L})\sin(\omega_m t) \\
t_9 &= (\frac{q_3}{q_4} - \frac{q_5}{q_6} - \frac{q_7}{q_8} + \frac{q_9}{q_{10}} + \frac{q_1q_3}{q_{13}} - \frac{q_1q_3}{q_{14}} - \frac{q_2q_4}{q_{15}} + \frac{q_2q_4}{q_{16}})\exp(-t\zeta_n\omega_n)\cos(\omega_{dn}t) \\
t_{10} &= (\frac{\zeta_n\omega_n}{q_4} - \frac{\zeta_n\omega_n}{q_6} - \frac{\zeta_n\omega_n}{q_8} + \frac{\zeta_n\omega_n}{q_{10}} - \frac{q_3q_{11}}{q_{13}} + \frac{q_3q_{12}}{q_{14}} + \frac{q_4q_{11}}{q_{15}} - \frac{q_4q_{12}}{q_{16}})\exp(-t\zeta_n\omega_n)\sin(\omega_{dn}t)
\end{aligned}
$$

Here, ω_m equals to $m2\pi f_s$ for the m^{th} harmonic and the terms $q_i, i = 1, 2...16$ are defined

as follows:

$$
\begin{aligned}
q_1 &= \zeta_n\omega_n + \frac{v\pi}{L};\quad q_2 = \zeta_n\omega_n - \frac{v\pi}{L};\quad q_3 = \omega_{dn} - \frac{v\pi}{L} - \omega_m \\
q_4 &= (\zeta_n\omega_n)^2 + (\omega_{dn} - \frac{v\pi}{L} - \omega_m)^2;\quad q_5 = \omega_{dn} - \frac{v\pi}{L} + \omega_m \\
q_6 &= (\zeta_n\omega_n)^2 + (\omega_{dn} - \frac{v\pi}{L} + \omega_m)^2;\quad q_7 = \omega_{dn} + \frac{v\pi}{L} - \omega_m \\
q_8 &= (\zeta_n\omega_n)^2 + (\omega_{dn} + \frac{v\pi}{L} - \omega_m)^2;\quad q_9 = \omega_{dn} + \frac{v\pi}{L} + \omega_m \\
q_{10} &= (\zeta_n\omega_n)^2 + (\omega_{dn} + \frac{v\pi}{L} + \omega_m)^2;\quad q_{11} = \omega_{dn} - \omega_m \\
q_{12} &= \omega_{dn} + \omega_m;\quad q_{13} = (\zeta_n\omega_n + \frac{v\pi}{L})^2 + (\omega_{dn} - \omega_m)^2 \\
q_{14} &= (\zeta_n\omega_n + \frac{v\pi}{L})^2 + (\omega_{dn} + \omega_m)^2;\quad q_{15} = (\zeta_n\omega_n - \frac{v\pi}{L})^2 + (\omega_{dn} - \omega_m)^2 \\
q_{16} &= (\zeta_n\omega_n - \frac{v\pi}{L})^2 + (\omega_{dn} + \omega_m)^2
\end{aligned}
$$

The total displacement response for mode n can be written as the sum of the static and dynamic parts contributed by m harmonics of the excitation force as follows:

$$Y_n = X_n + \sum_{i=1}^{m} X_{mn} \tag{A.4}$$

Appendix B

Mode shapes from finite element models

The first vertical and lateral mode shapes of the three full scale pedestrian bridges from the finite element models are shown in Figures B.1 to B.5.

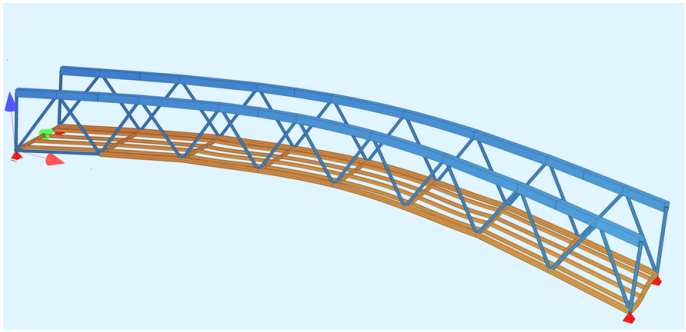

Figure B.1: First lateral mode at 2.3 Hz for the 12.2 m bridge specimen

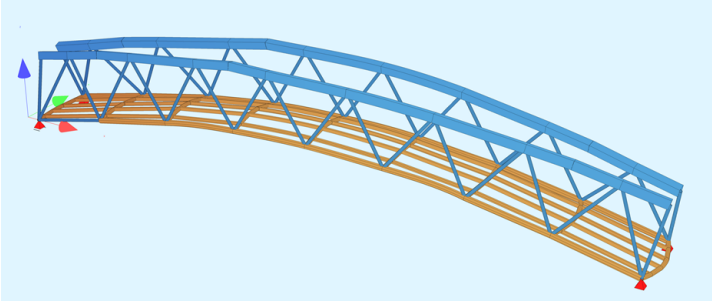

Figure B.2: First vertical mode at 13.0 Hz for the 12.2 m bridge specimen

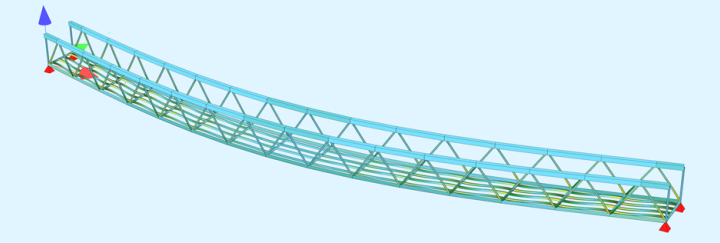

Figure B.3: First lateral mode at 1.0 Hz for the 22.9 m bridge specimen

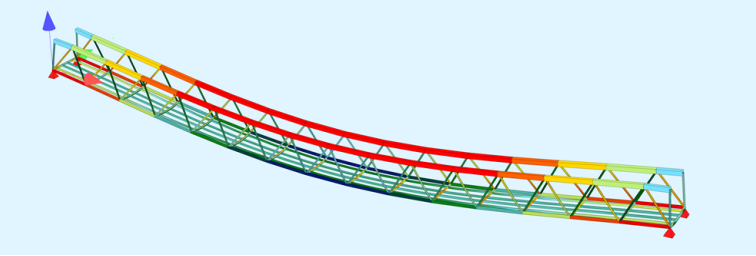

Figure B.4: First vertical mode at 4.4 Hz for the 22.9 m bridge specimen

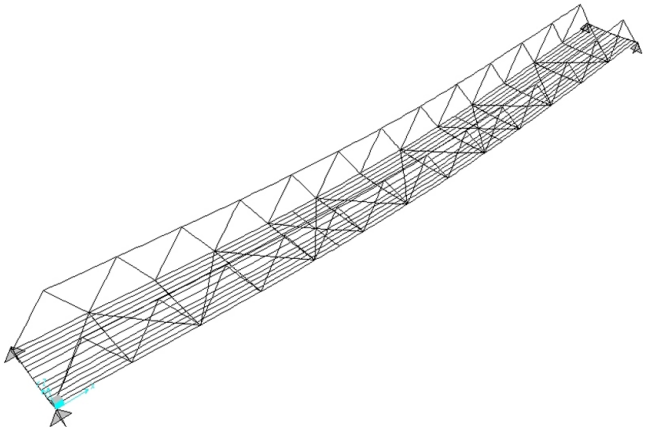

Figure B.5: First vertical mode at 3.40 Hz for the Daigneault Creek bridge specimen (taken from Sychterz et al. (2013))

Appendix C

Modal identification through free vibration tests

The free vibration tests performed in the current study for identification of modal frequency and damping ratios involve measurement of the bridge acceleration after the application of an impulse through hammer (in vertical direction) or imposed displacement (in lateral direction). The modal identification methodologies adopted in this thesis are discussed in the following section:

C.1 Fast Fourier Transform or FFT method

The Fast Fourier Transform or FFT method is the simplest form of modal analysis in order to estimate the modal frequency of a structure. A Fast Fourier Transform is performed on the time-series data collected on the bridge during the modal testing such as impact loading test. Since these tests only apply an impact without any frequency from the excitation on the structure, peaks in the FFT from these free vibration response of the structures correspond to the natural frequencies of the structure. Figure 3.5 show sample vertical acceleration time histories and corresponding FFT plots of the 22.9 m laboratory specimens during hammer tests on the bridge. The first three vertical natural frequencies are shown in the FFT plots through picking the peaks of the FFT amplitudes.

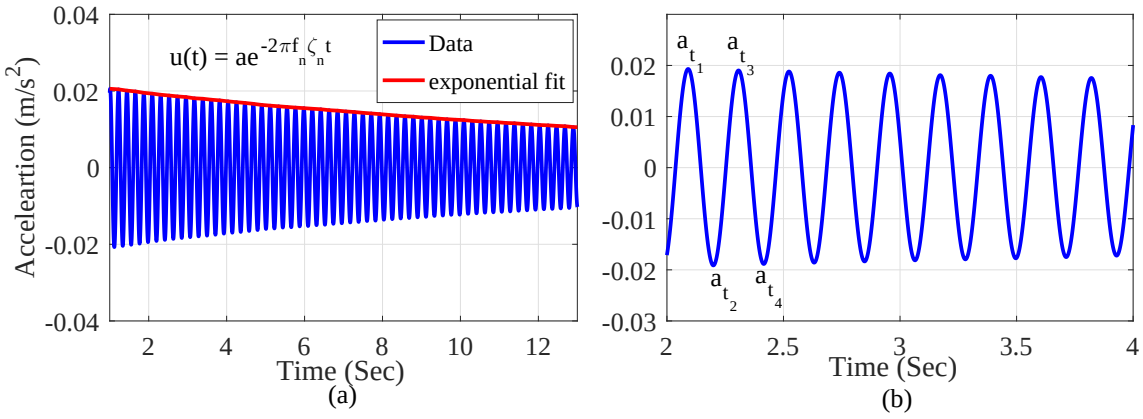

Figure C.1: (a) Exponential envelop fitted to first vertical modal acceleration time history and (b) illustration of decaying time history with successive peaks, measured at the mid span of the 22.9 m bridge specimen during hammer test

C.2 Modal damping estimation

The current study employs the simple free vibration decay method to estimate the damping. As the decays measured after application of the impact force should contain only the contribution of a single mode, the mode of interests are isolated through applying band-pass filters. Figure C.1 (a) shows the acceleration data from the 22.9 m bridge specimen corresponding to the natural frequency of 4.58 Hz. The exponential decay method is applied to the filtered data in order to estimate the damping ratio corresponding to that mode. The most common methods of acquiring damping ratio from free vibration decay data are the exponential envelope and log-decrement methods.

In the exponential envelope method, an exponential curve is fitted to the peaks of the filtered acceleration time history as shown Figure Figure C.1 (a). The fitted curve is in the form of $u(t) = ae^{-2\pi f_n \zeta_n t}$, from which the damping ratio ζ_n can be estimated with known value of structural frequency f_n. On the other hand, in log-decrement method, the successive peaks are obtained from the decaying time-history trace, for example, a_{t_1}, a_{t_2}, a_{t_3} and a_{t_4}, in Figure C.1 (b) at respectively times t_1, t_2, t_3 and t_4. The damping ratio can be determined as (Humar, 2012):

$$\zeta_n = \frac{1}{2\pi} \ln \frac{a_{t_1} - a_{t_2}}{a_{t_3} - a_{t_4}} \tag{C.1}$$

In the current study both the methods of estimating damping ratio is employed. As

negligible deviations were observed between the two methods, only the damping values obtained using logarithmic decrement are reported in Table 3.7.

Appendix D

TLS-Prony's method

The original Prony analysis computes h_k and z_k in three basic steps. First, a linear prediction model is constructed using the observed data set and solved for coefficients c_i $(i = 1, 2, ...M)$. c_i's are the coefficients of the M^{th} order polynomial $\psi(z)$ whose roots are the unknown exponents z_k. The linear predictive model can be written as:

$$y[n] = \sum_{k=1}^{M} c_k y[n-k] \tag{D.1}$$

The N data samples provide the following matrix equation:

$$\begin{pmatrix} y_M & y_{M-1} & \cdots & y_1 \\ y_{M+1} & y_M & \cdots & y_2 \\ \vdots & \vdots & \ddots & \vdots \\ y_{N-1} & y_{N-2} & \cdots & y_{N-M} \end{pmatrix} \begin{pmatrix} c_1 \\ c_2 \\ \vdots \\ c_M \end{pmatrix} = \begin{pmatrix} y_{M+1} \\ y_{M+2} \\ \vdots \\ y_N \end{pmatrix} \tag{D.2}$$

The above Equation can be written as:

$$A\tilde{c} = b \tag{D.3}$$

Rahman and Yu Rahman and Yu (1987) rearranged Equation D.3 into a homogeneous set of Equations (Equation D.4) so that a total least squares criterion can be applied to solve for $\tilde{c}$.

$$(A - b) \begin{pmatrix} \tilde{c} \\ 1 \end{pmatrix} = 0 \tag{D.4}$$

This can be written as:

$$Dd = 0 \tag{D.5}$$

The rank L of matrix D', which minimizes $||D' - D||_F$, is determined. The solution for $\tilde{d}$ can be estimated using:

$$\tilde{d} = \frac{1}{\alpha} \sum_{i=L+1}^{\beta} v^*_{i,M+1} V_i \tag{D.6}$$

where:

$$\beta = \text{rank}(B); \;\; \alpha = \sum_{i=L+1}^{\beta} |v_{i,M+1}|^2 \tag{D.7}$$

In Equation D.6, v_{ij} is the j^{th} element of V_i. σ_i, U_i and V_i are the i^{th} singular values, left and right singular vectors, respectively, obtained through singular value decomposition of the matrix D.

$$D' = \sum_{i=1}^{L} \sigma_i U_i V_i^H \tag{D.8}$$

The first M values of $\tilde{d}$ constitute the estimated vector $\tilde{c}$.

After obtaining the solution for $\tilde{c}$, the zeros of the following polynomial $\psi(z)$ are solved whose roots are the unknown exponents z_k:

$$\psi(z) = z^M + c_1 z^{M-1} + \cdots + c_M \tag{D.9}$$

Now, the unknown values of h_k are obtained by solving the linear Equations in Equation D.10 and subsequently the amplitudes A_k corresponding to the frequencies of interest are extracted.

$$\begin{pmatrix} z_1^0 & z_2^0 & \cdots & z_M^0 \\ z_1^1 & z_2^1 & \cdots & z_M^1 \\ \vdots & \vdots & \ddots & \vdots \\ z_1^{M-1} & z_2^{M-1} & \cdots & z_M^{M-1} \end{pmatrix} \begin{pmatrix} h_1 \\ h_2 \\ \vdots \\ h_M \end{pmatrix} = \begin{pmatrix} y[1] \\ y[2] \\ \vdots \\ y[M] \end{pmatrix} \tag{D.10}$$